

INSTITUTE OF THEORETICAL PHYSICS AND ASTRONOMY  
OF VILNIUS UNIVERSITY

Miglius Alaburda

**POINT PROCESSES MODELING OF  $1/f$  NOISE**

Doctoral dissertation

Physical sciences, Physics (02 P), Mathematical and general theoretical physics, classical mechanics, quantum mechanics, relativity, gravitation, statistical physics, thermodynamics (190 P)

Vilnius, 2005

Doctoral dissertation prepared 1999 – 2004 at Institute of Theoretical Physics and Astronomy of Vilnius University.

Scientific supervisor:

Prof. Habil. Dr. Bronislovas Kaulakys (Institute of Theoretical Physics and Astronomy of Vilnius University, physical sciences, physics – 02 P, mathematical and general theoretical physics, classical mechanics, quantum mechanics, relativity, gravitation, statistical physics, thermodynamics – 190 P)

VILNIAUS UNIVERSITETO  
TEORINĖS FIZIKOS IR ASTRONOMIJOS INSTITUTAS

Miglius Alaburda

**TAŠKINIŲ PROCESŲ  $1/f$  TRIUKŠMO  
MODELIAVIMAS**

Daktaro disertacija

Fiziniai mokslai, fizika (02 P), matematinė ir bendroji teorinė fizika,  
klasikinė mechanika, kvantinė mechanika, reliatyvizmas, gravitacija,  
statistinė fizika, termodinamika (190 P)

Vilnius, 2005

Disertacija rengta 1999 – 2004 metais Vilniaus universiteto Teorinės fizikos ir astronomijos institute.

Mokslinis vadovas:

prof. habil. dr. Bronislovas Kaulakys (Vilniaus universiteto Teorinės fizikos ir astronomijos institutas, fiziniai mokslai, fizika – 02 P, matematinė ir bendroji teorinė fizika, klasikinė mechanika, kvantinė mechanika, reliatyvizmas, gravitacija, statistinė fizika, termodinamika – 190 P)

# Contents

<b>1</b>	<b>INTRODUCTION</b>	<b>7</b>
<b>2</b>	<b>1/f NOISE OVERVIEW</b>	<b>10</b>
2.1	History . . . . .	10
2.2	1/f <sup>β</sup> noise from the superposition of relaxation processes . . . . .	11
2.3	A random pulse train model of 1/f noise . . . . .	13
2.4	Distributed trapping model . . . . .	14
2.5	Fractal Renewal Processes generating 1/f noise . . . . .	15
2.6	1/f noise in deterministic dynamical systems . . . . .	20
2.7	Self-organized criticality . . . . .	21
2.8	Earthquakes . . . . .	23
2.9	1/f noise in meteorology . . . . .	24
2.10	1/f fluctuations in traffic . . . . .	25
2.11	Examples from biophysics . . . . .	25
2.12	Scaling of heartbeat intervals . . . . .	26
2.13	Statistical properties of stock price fluctuations . . . . .	27
2.14	1/f noise in computer networks and the Internet . . . . .	28
<b>3</b>	<b>POINT PROCESS MODEL</b>	<b>30</b>
3.1	Point processes . . . . .	30
3.2	Power spectral density . . . . .	32
3.3	Distribution density of the interpulse time $\tau_k$ . . . . .	35
3.4	Non-Gaussian perturbations and numerical analysis . . . . .	37
3.5	Multifractality of the point process . . . . .	38
3.6	Generalization of the point process model . . . . .	40
3.7	Correlation function . . . . .	45
<b>4</b>	<b>SUPERPOSITION OF SIGNALS WITH LINEAR RELAXATIONS</b>	<b>47</b>
4.1	Lorentzian spectrum . . . . .	47
4.2	Superposition of the Lorentzian spectra . . . . .	49
4.3	Monofractality of signals with linear relaxations . . . . .	51
4.4	Different slopes of power spectral density . . . . .	52
4.5	Conclusions of Sections 3 and 4 . . . . .	53
<b>5</b>	<b>STOCHASTIC SIGNAL MODEL</b>	<b>55</b>
5.1	Signal as a sequence of pulses of finite duration . . . . .	55
5.2	Stationary process . . . . .	55
5.3	Fixed shape pulses . . . . .	56
5.4	Transition from the point process to the continuous signal using the Gaussian pulses . . . . .	56
5.5	Transition from the point process to the stochastic signal using rectangular pulses . . . . .	58
5.6	Uncorrelated pulses . . . . .	60
5.7	Pulses of variable duration . . . . .	61
5.8	Spectrum at small frequencies . . . . .	61
5.9	Power-law distribution of the pulse duration . . . . .	62

5.10	Rectangular constant area pulses distributed according to the Poisson process . . . . .	63
5.11	Transition from the discrete point process to the continuous signal by counting pulses . . . . .	64
5.12	Transition from the stochastic signal to the point process . . . . .	65
5.13	Signals represented by the fluctuating intensity . . . . .	66
5.14	Stochastic nonlinear differential equation generating $1/f$ noise . . . . .	68
5.15	Generalization for class of stochastic equations . . . . .	71
<b>6</b>	<b>HAMILTONIAN SYSTEMS AND <math>1/f</math> NOISE</b>	<b>73</b>
6.1	Standard map . . . . .	73
6.2	Rotor affected by the periodic kicks . . . . .	75
6.3	Numerical simulation of the rotor's dynamics . . . . .	77
6.4	One-dimensional classical hydrogen atom in a monochromatic field . . .	78
6.5	Two-dimensional atom in a monochromatic field . . . . .	81
	6.5.1 Approximation for high relative frequency $s$ . . . . .	85
	6.5.2 Approximation for very extended orbits . . . . .	86
	6.5.3 Approximation for almost circular orbits . . . . .	87
6.6	Two-dimensional atom in a circular polarized field . . . . .	89
<b>7</b>	<b>PROGRAMS FOR NUMERICAL SIMULATIONS AND CALCULATIONS</b>	<b>91</b>
<b>8</b>	<b>SUMMARY OF THE RESULTS AND CONCLUSIONS</b>	<b>94</b>
<b>9</b>	<b>LIST OF PUBLICATIONS</b>	<b>96</b>
9.1	Publications . . . . .	96
9.2	Presentations at Conferences . . . . .	96
	<b>References</b>	<b>99</b>

# 1 INTRODUCTION

The power spectra of a large variety of systems ranging widely from astrophysics and technology to sociology and psychology at low frequencies have  $1/f$  behavior, i.e., the power spectral density  $S(f)$  is inversely proportional to the frequency  $f$ . Both time – dependent phenomena and spatial series may show such characteristics against the frequency. Great efforts have been made to explain and model the universal presence of  $1/f$  noise.

$1/f$  noise, also known as flicker noise, is intermediate between white noise [no correlation in time,  $S(f) \sim 1/f^0$ ] and the Brownian motion [no correlations between increments,  $S(f) \sim 1/f^2$ ]. Simple procedures of integration or differentiation of such fluctuating signals do not yield the signal exhibiting  $1/f$  noise.

Usually  $1/f$  noise theories are formulated for the intensity of the currents or signals. In such cases one starts from the systems of sufficiently complicated, as a rule nonlinear, differential equations with partial derivatives or from the system of equations with a wide and specific distribution of times of the linear relaxations of the signal components. In such a way the obtained signals are, as a rule, Gaussian. However, not all signals exhibiting  $1/f$  noise are Gaussian. Some of them are non-Gaussian, exhibiting power-law or even fractal distributions.

Some mathematical analyses, models and algorithms for the generation of processes with  $1/f$  noise also expose some shortcomings: they are very specific, formal (like “fractional Brownian motion”) or unphysical. They cannot usually be solved analytically, and they do not reveal either the origin or the necessary and sufficient conditions for the appearance of  $1/f$ -type fluctuations.

This makes the problem of omnipresence  $1/f$  noise one of the oldest problems and puzzles in the contemporary physics. In contrast to the Brownian motion generated by the linear stochastic equation, the simple systems of differential, even linear stochastic equations generating signals with  $1/f$  noise are not known.

Most of  $1/f$  noise physical models in some physical systems are special or complicated and they do not explain the omnipresence of the processes with  $1/f^\beta$  power spectral density.

Some random phenomena, however, occur at discrete times or locations, with the individual events largely identical. A stochastic point process is a mathematical construction which represents these events as random points in space or time. Point processes arise in different fields, such as physics, economics, cosmology, ecology, neurology, the Internet, signaling and telecom networks, and seismology, i.e., in a large variety of systems with the flow of point objects (electrons, photons, cars, pulses, events, and so on) or subsequent actions, like seismic events, neural action potentials, transactions in the financial markets, human heart beats, biological ion-channel openings, burst errors in many communication systems, the Internet network packets, etc.

The point process is completely described by the set of event times  $\{t_k\}$ , or equivalently by the set of interevent (interpulse) intervals  $\tau_k = t_{k+1} - t_k$ . Such point processes might be called fractal if some relevant statistics display scaling, characterized by a power-law behavior, with related scaling coefficients indicating that the phenomena contain clusters of points over a relatively large set of time scales.

The complete characterization of a stochastic process involves a description of all possible joint probabilities of various events occurring in the process. Different statistics provide complementary views of the process. One single statistics cannot in general

describe a stochastic process completely. Fractal stochastic processes exhibit scaling in their statistics. Fractal stochastic point processes exhibit scaling in all statistics, while the fractal-rate stochastic point processes are endowed with rate functions that are either themselves fractal or their increments are fractal.

The power-law distribution of the interpulse time of the point process results in the power-law distribution of the intensity of the stochastic signal – the phenomenon observable in a large variety of processes, ranging from earthquakes, Internetquakes, the behavior of physical systems in the vicinity of a critical point up to the financial time series, networks and growth of complex organizations. Power-law distributions are counter intuitive because they lack a characteristic scale. Examples of random variables with infinite variances were treated as paradoxes before the work of Lévy. Today power-law distributions are used in the description of open systems. Stochastic processes with power-law distributions, although well defined mathematically, are difficult to use and raise fundamental questions when applied to the real systems. A stochastic process with finite variance characterized by scaling relations in a large but finite interval is the truncated Lévy flight process, which is a bit artificial and not very well-founded.

The key result in recent findings is that a lot of power-law distributions are well outside the stable Lévy regime – they are neither Lévy stable nor invariant under addition. Therefore, new stochastic models with long-range correlations and power-law asymptotic behavior are of great interest.

Stochastic models for the time intervals between events of point processes may be characterised by the distributions which were mentioned above. Such models of time series have only a few parameters defining the statistical properties of the system, i.e., the power-law behavior of the distribution functions and the scaled power spectral density of the signal. The ability of the models to simulate power-law noise and produce signals with the values of power spectral density slope between 0.5 and 1.5, promises a wide variety of applications of the models in different fields.

**Main goals of the research are:**

- Generalization of the point process model for generation of signals with different slopes  $\beta$  of the power spectral density of  $S(f) \sim 1/f^\beta$  noise and power-law distributions of the signal intensity.
- Analysis of the relation of the point process models with the Bernamont-Surdin-McWorter model, representing the signal as a sum of the appropriate signals with a wide-range distributions of times of the linear relaxation of signal components and analysis of fractality of the generated signals.
- Relation of the point processes generating  $1/f$  noise with the stochastic signals represented by fluctuating intensity of the signal and derivation of stochastic non-linear difference and differential equations generating signals with  $1/f$  noise.
- Modeling and analysis of  $1/f$  noise processes by sequences of stochastic pulses of different duration, transition from the point processes to the continuous signals and generation of the point processes from the rate functions.
- Search of  $1/f$  noise in chaotic Hamiltonian systems, like a rotor affected by the periodic strikes and classical hydrogen atom in an electromagnetic field, dynamics of which represented by the appropriate mapping equations of motion.

## Scientific statements

1. The generalized point process model of  $1/f$  noise generates time series of the signals with different slopes  $0.5 \lesssim \beta \lesssim 1.5$  of the power spectral density  $S(f) \sim 1/f^\beta$  and results in the power-law distribution of the stochastic signals, i.e., the phenomenon observable in a large variety of processes, ranging from earthquakes and the Internet up to the financial markets.
2. The autoregressive point process model of  $1/f^\beta$  noise, representing the signal as consisting of pulses with the Brownian motion of the interpulse time is complementary to the model based on the sum of signals with a wide-range distribution of times of the linear relaxation. In contrast to the Gaussian distribution of the signal intensity of the sum of the uncorrelated components, the intensity of the point process exhibits asymptotically a power-law distribution.
3. The generated signals of the point processes are multifractal, in contrast to the monofractality of the signals, consisting of the sum of the uncorrelated components with a wide-range distribution of times of the linear relaxation.
4. The proposed and analysed transformations of the point process models with the stochastic dynamics of the interpulse time to the signals, represented by fluctuating intensity, preserve the power spectral density of the signals at low frequencies.
5. The derived mapping expressions for the energy and angular momentum changes of the classical hydrogen atom in an electromagnetic field may be used for analysis of transition to chaotic behavior while the fluctuations of the period of the trajectories of the nonlinear Hamiltonian systems in the transition from regular to chaotic motion exhibit  $1/f^\beta$  noise.

## Approbation of the results

The main results of the research described in this dissertation have been published in 7 scientific papers and 9 presentations made at scientific conferences.

## Personal contribution of the author

The author of the thesis has performed all numerical simulations presented in this dissertation. He has been involved in derivations of most of the analytical results, especially in deriving complicated expressions for the chaotic dynamics in Hamiltonian systems and analysis of numerical simulations conformity with according analytical approaches. The author has created a set of programs, which can simulate various point and stochastic signals, investigate their distributions, spectral densities, fractality, and other statistical properties.

## 2 $1/f$ NOISE OVERVIEW

### 2.1 History

The triode was invented by Lee de Forest in 1907, and soon afterwards the first amplifiers were built. By 1921 the “thermionic tube” amplifiers were developed to such an extent that C. A. Hartmann [1] made the first courageous experiment to verify Schottky’s formula for the shot noise spectral density [2]. Hartmann’s attempt failed, and finally it was J. B. Johnson who successfully measured the predicted white noise spectrum [3]. However, Johnson also measured an unexpected “flicker noise” at low frequency, and shortly thereafter W. Schottky tried to provide a theoretical explanation [4].

Schottky’s explanation was based on the physics of electron transport inside the vacuum tube, but in the years that followed Johnson’s discovery of flicker noise, it was discovered that this strange noise appeared again and again in many different electrical devices. The observed spectral density of flicker noise is actually quite variable: it behaves like  $1/f^\beta$ , where  $\beta$  is in the range  $0.5 \div 1.5$ , and usually this behavior extends over several frequency decades. The appearance of power laws in the theory of critical phenomena and above all the work of B. Mandelbrot on fractals in the 1970’s [5], seemed to indicate that something deeper was hidden in those ubiquitous spectra. Power laws and  $1/f$  spectra were most unexpectedly found in many different phenomena.

The work of Voss and Clarke on  $1/f$  noise in resistors also spawned an interesting study of  $1/f$  noise in music, which became widely known thanks to an excellent popularization made by M. Gardner in *Scientific American* [6]. Voss and Clarke found that both voice and music broadcasts have  $1/f$  spectra [7], and they even devised an algorithm to compose “fractal” music [8].

By then many physicists were convinced that there had to be a reason for the ubiquity of this kind of power-law noises, that there might be something akin to the universality of exponents in critical phenomena, and therefore many people set out to find an all-encompassing explanation.

$1/f$  fluctuations are widely found in nature, i.e., the power spectra of a large variety of physical [9, 10, 11, 12, 13, 14, 15, 16, 17, 18, 19, 20], biological [21, 22, 23], geophysical [24, 25, 26, 27], astronomical [28, 29, 30], fractals [31, 32], traffic [33, 34, 35], financial [36, 37, 38, 39, 40, 41, 42, 43, 44, 45] and other systems at low frequencies  $f$  have  $1/f^\beta$  (with  $\beta \approx 1$ ) behavior.

Investigation of fluctuations and noise processes, including  $1/f$  noise problem, in Lithuania has long-lasting and deep-rooted traditions (see, e.g., [46, 47, 48, 49, 50, 51, 52, 53, 54, 55, 56, 57, 58, 59, 60, 61, 62, 63, 64, 65, 66, 67] and references herein). Most of the investigations stemmed from semiconductor, solid state and discharge studies; fluctuations and noise processes have been related with the correlations and relaxation processes in the specific materials and systems.

The research presented in this dissertation is, however, mostly originated from the analytically solvable point process model of  $1/f$  noise proposed and analysed in Refs. [57, 60, 61, 62, 63]. The main objectives of the dissertation have been further generalizations, analytical and numerical analysis and comparison of the point process model of  $1/f$  noise with other approaches and search for  $1/f$  fluctuations in the chaotic Hamiltonian systems.

## 2.2 $1/f^\beta$ noise from the superposition of relaxation processes

An early and simple explanation of the appearance of  $1/f^\beta$  noise in vacuum tubes was implicit in some comments made by Johnson [3], and was mathematically stated by Schottky [4]: there was a contribution to the vacuum tube current from cathode surface trapping sites, which released the electrons according to a simple exponential relaxation law  $N(t) = N_0 e^{-\lambda t}$  for  $t \geq 0$  and  $N(t) = 0$  for  $t < 0$ . The Fourier transform of a single exponential relaxation process is

$$F(f) = \int_{-\infty}^{+\infty} N(t) e^{-i\omega t} dt = N_0 \int_0^{+\infty} e^{-(\lambda+i\omega)t} dt = \frac{N_0}{\lambda + i\omega}, \quad \omega = 2\pi f. \quad (1)$$

Therefore for a train of such pulses  $N(t, t_k) = N_0 e^{-\lambda(t-t_k)}$  for  $t \geq t_k$  and  $N(t, t_k) = 0$  for  $t < t_k$ , we find

$$F(f) = \int_{-\infty}^{+\infty} \sum_k N(t, t_k) e^{-i\omega t} dt = N_0 \sum_k e^{i\omega t_k} \int_0^{+\infty} e^{-(\lambda+i\omega)t} dt = \frac{N_0}{\lambda + i\omega} \sum_k e^{i\omega t_k} \quad (2)$$

and the spectrum is

$$S(f) = \lim_{T \rightarrow \infty} \frac{2}{T} \langle |F(f)|^2 \rangle = \frac{N_0^2}{\lambda^2 + \omega^2} \lim_{T \rightarrow \infty} \frac{2}{T} \left\langle \left| \sum_k e^{i\omega t_k} \right|^2 \right\rangle = \frac{2N_0^2 \bar{\nu}}{\lambda^2 + \omega^2}, \quad (3)$$

where  $\bar{\nu}$  is the average pulse rate and the triangle brackets denote an ensemble average. This spectrum is nearly flat near the origin, and after a transition region it becomes proportional to  $1/\omega^2$  at high frequency. This was sufficient for Schottky who found such a dependence in Johnson's data, but later it became clear that a single relaxation process was not enough, and that there had to be a superposition of such processes, with a distribution of relaxation rates  $\lambda$  [68, 69, 70, 71, 72, 73, 53]. If the relaxation rate is uniformly distributed between two values  $\lambda_1$  and  $\lambda_2$ , and the amplitude of each pulse remains constant, we find the spectrum

$$S(f) = \frac{2N_0^2 \bar{\nu}}{\lambda_2 - \lambda_1} \int_{\lambda_1}^{\lambda_2} \frac{1}{\lambda^2 + \omega^2} d\lambda = \frac{N_0^2 \bar{\nu}}{\pi f (\lambda_2 - \lambda_1)} \left[ \arctan \left( \frac{\lambda_2}{\omega} \right) - \arctan \left( \frac{\lambda_1}{\omega} \right) \right] \\ \approx \begin{cases} 2N_0^2 \bar{\nu}, & 0 < \omega \ll \lambda_1 \ll \lambda_2, \\ \frac{N_0^2 \bar{\nu}}{2f(\lambda_2 - \lambda_1)}, & \lambda_1 \ll \omega \ll \lambda_2, \\ \frac{2N_0^2 \bar{\nu}}{\omega^2}, & \lambda_1 \ll \lambda_2 \ll \omega. \end{cases} \quad (4)$$

Relaxation rates may be distributed according to different distributions, for instance we may have

$$dP(\lambda) = \frac{A}{\lambda^\alpha} d\lambda \quad (5)$$

in the range  $\lambda_1 < \lambda < \lambda_2$ : in this case it is still possible to integrate the spectrum exactly [74, 75] and we obtain

$$S(f) \propto \int_{\lambda_1}^{\lambda_2} \frac{1}{\lambda^2 + \omega^2} \frac{d\lambda}{\lambda^\alpha} = \begin{cases} \frac{1}{\omega^2} \ln \frac{\lambda}{\sqrt{\lambda^2 + \omega^2}} \Big|_{\lambda_1}^{\lambda_2}, & \alpha = 1, \\ \frac{\lambda^{1-\alpha}}{(1-\alpha)\omega^2}, F\left(\frac{1-\alpha}{2}, 1; 1 + \frac{1-\alpha}{2}; -\frac{\lambda^2}{\omega^2}\right) \Big|_{\lambda_1}^{\lambda_2}, & \alpha \neq 1, \end{cases} \quad (6)$$

where

$$F(a, b; c; z) = \sum_{k=0}^{\infty} \frac{(a)_k (b)_k}{(c)_k} \frac{z^k}{k!} = \frac{\Gamma(c)}{\Gamma(b)\Gamma(c-b)} \int_0^1 t^{b-1} (1-t)^{c-b-1} (1-tz)^{-a} dt \quad (7)$$

is the usual hyper-geometric function. However, we do not have to use the exact expression (6) to find the behavior of the spectral density in the range  $\lambda_1 \ll \omega \ll \lambda_2$ , since we can approximate the exact integral as follows:

$$S(f) \propto \int_{\lambda_1}^{\lambda_2} \frac{1}{\lambda^2 + \omega^2} \frac{d\lambda}{\lambda^\alpha} = \frac{1}{\omega^{1+\alpha}} \int_{\lambda_1/\omega}^{\lambda_2/\omega} \frac{1}{(1+x^2)} \frac{dx}{x^\alpha} \approx \frac{1}{\omega^{1+\alpha}} \int_0^\infty \frac{1}{(1+x^2)} \frac{dx}{x^\alpha} \propto \frac{1}{\omega^{1+\alpha}} \quad (8)$$

and thus we obtain a whole class of flicker noises with different exponents.

From the previous discussion one may argue that it is important to find experimentally the actual limiting values  $\lambda_1$  and  $\lambda_2$ , in order to characterize the noise process. Unfortunately, this is seldom possible, and in most cases it seems that the  $1/f$  behavior continues as far as one can see: according to the good data of Pellegrini, Saletti, Terreni and Prudenziati [76] the  $1/f$  behavior extends over more than 6 frequency decades and there seems to be still no noise power flattening at low frequency.

Caloyannides did a very long data-taking run using operational amplifiers as noise sources and extended his measurements down to  $10^{-6.3}$  Hz: he observed a  $1/f^{1.23}$  spectrum with no flattening at low frequency [77].

What if this behavior were real, and it continued indeed down to zero frequency? Then we would meet with a disaster, because the integrated fluctuation would be

$$\int_0^\infty S(f) df \propto \lim_{f_1 \rightarrow 0, f_2 \rightarrow \infty} \int_{f_1}^{f_2} \frac{1}{f^\beta} df = \begin{cases} \lim_{f_1 \rightarrow 0, f_2 \rightarrow \infty} \ln \frac{f_2}{f_1}, & \beta = 1, \\ \lim_{f_1 \rightarrow 0, f_2 \rightarrow \infty} \left( \frac{f_2^{1-\beta}}{1-\beta} - \frac{f_1^{1-\beta}}{1-\beta} \right), & \beta \neq 1 \end{cases} \quad (9)$$

and this expression always diverges, either at the low-frequency limit (for  $\beta > 1$ ) or at the high frequency limit (for  $\beta < 1$ ) or both (for  $\beta = 1$ ), so that low frequency fluctuations are arbitrarily large. But is this divergence real? Flinn [78] produced a simple argument which showed that we should not worry about it, even if it were there. Indeed for a true  $1/f$  spectrum we know that

$$\int_{f_1}^{f_2} \frac{df}{f} = \ln \frac{f_2}{f_1}, \quad (10)$$

so that the integrated fluctuation per decade is always the same. Moreover, the lowest observable frequency is given by the inverse of the life of the Universe  $\approx 2 \cdot 10^9$  years  $\approx 6 \cdot 10^{16}$  s, and therefore it should be approximately  $10^{-17}$  Hz. On the other hand it takes  $\lambda_C/c \approx (4 \cdot 10^{-13} \text{ m}) / (3 \cdot 10^8 \text{ m/s}) \approx 1.3 \cdot 10^{-21}$  s to go through an electron Compton wavelength at the speed of light, and this might be taken as the smallest observable time, which would correspond to a high frequency limit of  $10^{21}$  Hz. There are 38 frequency decades between these two extremes, so that the highest possible total fluctuation can be only 38 times the total fluctuation between 1 Hz and 10 Hz! Even if we extend slightly Finn's argument, and take Planck's time as the smallest observable

time  $t_p = l_p/c = \sqrt{G\hbar/c^5} \approx 10^{-43}s$ , we get a high frequency limit of  $10^{43}Hz$  which yields a total of 59 frequency decades, the conclusion remains the same, and we should not worry too much about the mathematical divergences.

Consider a  $1/f$  noise,  $x(t)$ , has the band-pass filtered power spectral density,

$$S(f) = \begin{cases} B/f, & \omega_1 \leq \omega \leq \omega_2, \\ 0, & \text{otherwise.} \end{cases} \quad (11)$$

The auto correlation function of  $x(t)$  is obtained by using the Wiener-Khintchine theorem [79, 80],

$$C(\tau) = B \int_{\omega_1}^{\omega_2} \frac{\cos(\omega\tau)}{\omega} d\omega = B[C_i(\omega_2\tau) - C_i(\omega_1\tau)], \quad (12)$$

where

$$C_i(z) = \int_{-\infty}^z \frac{\cos y}{y} dy \quad (13)$$

is the cosine integral. The series expansion of  $C_i(z)$  is

$$C_i(z) = \gamma + \ln(z) + \sum_{k=1}^{\infty} \frac{(-1)^k z^{2k}}{(2k)!2k}, \quad (14)$$

where  $\gamma = 0.5772\dots$  is Euler's constant. Thus, in the limit of  $z \rightarrow 0$ , the cosine integral reduces to  $C_i(z) \simeq \ln(z)$ . The mean-square of  $x(t)$  is thus given by

$$C(\tau = 0) = B \ln \left( \frac{\omega_2}{\omega_1} \right). \quad (15)$$

It is evident from the above argument that the band-pass filtered  $1/f$  noise is statistically stationary because it has the second-order quantities depending only on the delay time and not on the absolute time at which the ensemble average is performed.

### 2.3 A random pulse train model of $1/f$ noise

The power spectral density of a random pulse train,  $x(t)$ , is given by Carson's theorem [11, 81, 82],

$$S(f) = 2\bar{\nu}\bar{a}^2 |F(\omega)|^2, \quad (16)$$

where  $F(\omega)$  is the Fourier transform of the pulse shape function  $A(t)$ ,  $\bar{\nu}$  is the mean rate of the pulses and  $\bar{a}^2$  is the mean-square value of the pulse height. Thus, the frequency dependence of  $S(\omega)$  is entirely determined by  $A(t)$ . Consider the fictitious pulse shape function,

$$A(t) = \theta(t)t^{-(1-\frac{\beta}{2})}e^{-\omega_x t}, \quad (17)$$

where  $\beta$  and  $\omega_x$  are positive and independent of time, and  $\theta(t)$  is the unit step function. The Fourier transform of  $A(t)$  is

$$F(\omega) = \int_0^{\infty} t^{-(1-\frac{\beta}{2})} e^{-(\omega_x + i\omega)t} dt = \frac{\Gamma\left(\frac{\beta}{2}\right)}{(\omega_x + i\omega)^{\frac{\beta}{2}}}, \quad (18)$$

where  $\Gamma(x)$  is the gamma function. Using (18) in (16), we obtain

$$S(f) = \frac{2\bar{\nu}a^2\Gamma^2\left(\frac{\beta}{2}\right)}{(\omega_x^2 + \omega^2)^{\frac{\beta}{2}}}. \quad (19)$$

It shows the approximate  $1/f$  noise characteristic at  $\omega \gg \omega_x$ ,

$$S(f) \simeq B/f^\beta, \quad (20)$$

when  $\beta \simeq 1$ . Here  $B = 2\bar{\nu}a^2\Gamma^2\left(\frac{\beta}{2}\right)$ . In spite of how small  $\omega_x$  may be, provided it is non-zero,  $S(f)$  has the flat spectrum at  $\omega \leq \omega_x$ , which indicates that such a random pulse train is statistically stationary.

The auto correlation function of this random pulse train is given by

$$C(\tau) = \int_0^\infty S(f) \cos(\omega\tau) df = BK_0(\omega_x\tau), \quad (21)$$

where  $\beta = 1$  and  $K_0(z)$  is the modified Bessel function of the second kind of zero order. The series expansion of  $K_0(z)$  is

$$K_0(z) = -\gamma + \ln 2 - \ln(z) + \dots \quad (22)$$

For small  $\omega_x\tau$ ,  $C(\tau)$  varies as  $\ln(\omega_x\tau)$  and takes a finite value except at the origin  $\tau = 0$ . This logarithmic infinity is associated with the infinite extension of the  $1/f$  noise spectrum to high frequencies, which is of course unrealistic because any finite response time in a system introduces a cut-out characteristic beyond the certain frequency and the spectrum usually rolls off with a  $1/\omega^2$  dependence.

It is clear from the above argument that a random pulse train in which the pulse shape varies as  $t^{-1/2}$  shows the  $1/f$  noise behavior [83]. However, the physical origin of such a pulse shape is not clear [84].

## 2.4 Distributed trapping model

The most popular model of  $1/f$  noise is the trapping model with a wide spread of time constants. If a free carrier is immobilized by falling into a trap, it is no longer available for current transport. The modulation of carrier numbers has the form of random telegraph signal with a Poisson distribution of the occurrence times. The probability of observing  $n$  telegraphic signals in the time interval  $T$  is given by

$$P(n, T) = \frac{(\bar{\nu}T)^n}{n!} e^{-\bar{\nu}T}, \quad (23)$$

where  $\bar{\nu}$  is the mean rate of transitions per second. If  $\tau_+$  and  $\tau_-$  are the average times spent in the upper and lower states, respectively, the probability distributions of the upper and lower state times,  $t_+$  and  $t_-$ , are

$$P(t_\pm) = \tau_\pm^{-1} \exp\left\{-\frac{t_\pm}{\tau_\pm}\right\}. \quad (24)$$

The product  $x(t)x(t + \tau)$  is equal to  $+a^2$  if an even number of transitions occurs in the interval  $(t, t + \tau)$  and to  $-a^2$  if an odd number of transitions occurs in the same interval. Therefore, the auto correlation function is

$$\begin{aligned} C(\tau) &= a^2[P(0, \tau) + P(2, \tau) + \dots] - a^2[P(1, \tau) + P(3, \tau) + \dots] \\ &= a^2 e^{-\bar{\nu}\tau} \left[ 1 - \bar{\nu}\tau + \frac{(\bar{\nu}\tau)^2}{2!} - \frac{(\bar{\nu}\tau)^3}{3!} + \dots \right] = a^2 e^{-2\bar{\nu}\tau}. \end{aligned} \quad (25)$$

The power spectrum is thus calculated by the Wiener-Khintchine theorem,

$$S(f) = 4 \int_0^{\infty} C(\tau) \cos(\omega\tau) d\tau = \frac{2a^2/\bar{\nu}}{1 + \omega^2/4\bar{\nu}^2} = a^2 \frac{4\tau_z}{1 + \omega^2\tau_z^2}. \quad (26)$$

Here  $\tau_z = 1/2\bar{\nu}$  is the time constant of the trap. If  $\tau_z$  is distributed according to the function  $P(\tau_z)$ , the power spectral density of the total carrier number fluctuation is

$$S(f) = 4C(\tau = 0) \int_0^{\infty} \frac{\tau_z P(\tau_z)}{1 + \omega^2\tau_z^2} d\tau_z. \quad (27)$$

Here it is assumed  $\int_0^{\infty} P(\tau_z) dz = 1$ .

Suppose the carrier trap occurs by the tunneling of carriers from semiconductors to the traps inside the oxide layer at depth  $\omega$ , the time constant obeys

$$\tau_z = \tau_0 e^{\gamma\omega}, \quad (28)$$

where  $\tau_0$  and  $\gamma$  are constants. If the traps are homogeneously distributed between the depths  $\omega_1$  and  $\omega_2$ , corresponding to the time constants  $\tau_1$  and  $\tau_2$ , we obtain

$$P(\tau_z) d\tau_z = \begin{cases} \frac{d\tau_z/\tau_z}{\ln(\tau_2/\tau_1)}, & \tau_1 \leq \tau_z \leq \tau_2, \\ 0 & \text{otherwise.} \end{cases} \quad (29)$$

Using (29) in (27), the power spectral density of the total carrier number fluctuation is given by

$$S(f) = \frac{4C(0)}{\ln(\tau_2/\tau_1)} \int_{\tau_1}^{\tau_2} \frac{d\tau_z}{1 + \omega^2\tau_z^2} = \frac{4C(0)[\arctan(\omega\tau_2) - \arctan(\omega\tau_1)]}{\omega \ln(\tau_2/\tau_1)}. \quad (30)$$

Eq. (30) shows  $1/f$  power law in the frequency range of  $\omega\tau_2 \gg 1$  and  $0 \leq \omega\tau_1 \ll 1$ .

The above argument also applies to the intrinsic bulk transport property of the hopping conduction. The essential requirement to obtain the  $1/f$  power law is the Poissonian telegraphic event with a distributed time constant, which obeys  $1/\tau_z$  distribution function.

## 2.5 Fractal Renewal Processes generating $1/f$ noise

Fractals are distinguished by power-law scaling behavior. We also define fractal random variables as random variables with a power-law decay in their associated probability density functions.

Lévy-stable variables are a class of continuously distributed random variables that contain Gaussian random variables as a subset [85, 86, 87, 88, 39, 89, 90]. They are the only random variables with a property that the sum of any two drawn from the same Lévy-stable density will have a density differing from the original only by a scaling factor. Lévy-stable densities may be centered at any finite value, and thus the sum will differ from the original one by a constant shift term in addition to the scaling factor. In particular, if the random variables  $X$  and  $Y$  have the same Lévy-stable density, then for any positive numbers  $a$  and  $b$ , the random variable  $Z$  will have the same density as  $X$  and  $Y$  if and only if

$$cZ = aX + bY, \quad (31)$$

where

$$c^D = a^D + b^D \quad (32)$$

for some exponent  $D$  (sometimes called the Lévy index) depending only on the Lévy-stable density of  $X$  and  $Y$ .

The Gaussian density

$$P(x) = \frac{1}{\sqrt{2\pi\sigma^2}} \exp\left\{-\frac{x^2}{2\sigma^2}\right\} \quad (33)$$

(with  $\sigma$  a constant) has an exponent  $D = 2$ , while the Cauchy density

$$P(x) = \frac{k/\pi}{k^2 + x^2} \quad (34)$$

(with  $k$  a constant) corresponds to  $D = 1$ . Since renewal processes are usually defined to have positive interevent times, we only consider the sub-class of Lévy-stable densities which are positive only on the positive ordinate. Such one-sided Lévy-stable densities exist only within the range  $0 < D < 1$ . Closed-form analytical expressions for these densities do not exist, except for  $D = 1/2$ , in which case [91]

$$P(x) = \sqrt{\frac{k}{4\pi x^3}} \exp\left\{-\frac{k}{4x}\right\}. \quad (35)$$

Therefore, we define instead the family of one-sided Lévy-stable densities implicitly by their Fourier transforms [91]

$$Q_s(D; -i\theta) \equiv \mathcal{F}\{P_s(D; x)\} = \int_0^\infty P_s(D; x) e^{-i\theta x} dx = \exp[-(i\theta)^D], \quad (36)$$

where the index  $D$  refers to the associated exponent as defined in Eq. (32). These probability density functions  $P_s(D; x)$  have tails that decay as  $x^{-(D+1)}$  for large values of the independent variable  $x$ .

The Lévy-stable density defined by Eq. (36) has infinite moments of all orders [91]. Particularly, when a mean value of the interevent time  $\langle T \rangle = \infty$ , and a renewal process constructed with this density has a mean rate  $\bar{\nu}$  of zero at equilibrium. One method for ensuring a positive rate is to impose an upper exponential cutoff on the density, which results in

$$P(t) = A^{-1} \exp[(A/B)^D] P_s(D; t/A) e^{-t/B}, \quad (37)$$

where  $B$  is the upper cutoff value, and the factor constants in  $P(t)$  are normalizing constants ensuring unit area of the density. The resulting density has finite moments of all orders. The Fourier transform of the probability density function (37) (which is the complex conjugate of the characteristic function) has the simple form

$$Q(-i\omega) \equiv \mathcal{F}\{P(t)\} = \int_0^{\infty} P(t)e^{-i\omega t} dt = \exp[(A/B)^D - (i\omega A + A/B)^D]. \quad (38)$$

Successive derivatives of the characteristic function evaluated at  $\omega = 0$  yield the moments of the density  $P(t)$  [92]. The second characteristic function or the cumulant characteristic function is defined as the natural logarithm of the characteristic function, and its successive derivatives define the cumulants

$$C_n = D(A/B)^D \frac{\Gamma(n-D)}{\Gamma(1-D)} B^n, \quad (39)$$

for  $n \geq 1$ , where

$$\Gamma(x) \equiv \int_0^{\infty} t^{x-1} e^{-t} dt \quad (40)$$

is the Euler gamma function.

The modified Lévy-stable probability functions defined by Eqs. (36) and (37) vary as  $P(t) \sim t^{-(D+1)}$  for  $A \ll t \ll B$ , and it is this power-law dependence in the interevent time density which leads to fractal behavior in renewal point processes. Possibly the simplest interevent time density with this power-law form is the abrupt-cutoff power-law density

$$P(t) = \frac{D}{A^{-D} - B^{-D}} \times \begin{cases} t^{-(D+1)}, & A < t < B, \\ 0, & \text{otherwise.} \end{cases} \quad (41)$$

The associated moments are given by

$$\langle T^n \rangle = \frac{D}{n-D} (A/B)^D B^n \frac{1 - (A/B)^{n-D}}{1 - (A/B)^D}, \quad (42)$$

and the Fourier transform of the interevent time density is

$$Q(-i\omega) = \frac{D}{A^{-D} - B^{-D}} \int_A^B e^{-i\omega t} t^{-(D+1)} dt = \frac{D(i\omega)^D}{A^{-D} - B^{-D}} \int_{i\omega A}^{i\omega B} e^x x^{-(D+1)} dx. \quad (43)$$

In a case  $B^{-1} \ll \omega \ll A^{-1}$

$$1 - Q(-i\omega) \approx (i\omega A)^D \Gamma(1-D). \quad (44)$$

A standard (non-alternating) renewal process (SRP)  $N(t)$  is a point process in which the interevent times are independent random variables drawn from the same probability density, denoted  $P(t)$ . We require that  $P(t) = 0$  when  $t \leq 0$ . This density has an associated mean value  $\langle T \rangle$ , and we define  $\bar{\nu} \equiv \langle T \rangle^{-1}$  to be the average rate of events, where the angle brackets represent the expectation taken over the distribution of interevent times. We require that the mean dwell time  $\langle T \rangle$  is finite.

The coincidence rate  $G_N(\tau)$  is a measure of the correlation between the events with a specified time delay between them, regardless of intervening events. Assuming the point process  $N(t)$  to be stationary, the coincidence rate is defined as [93,31]

$$G_N(\tau) \equiv \lim_{\Delta \rightarrow 0} \frac{\Pr\{\mathcal{E}(t, t + \Delta) \text{ and } \mathcal{E}(t + \tau, t + \tau + \Delta)\}}{\Delta^2}, \quad (45)$$

where  $\mathcal{E}(x, y)$  represents the occurrence of at least one event in the interval  $(x, y)$ . The coincidence rate has units of frequency squared. Treating the events  $dN(t)$  as Dirac delta functions (pulses) distributed along the time axis, a power spectral density might be defined. It is equal to the Fourier transform of the coincidence rate by the Wiener-Khintchine theorem.

The interevent time density may be viewed as a conditional rate; that is, given an event at time  $t$ ,  $P(t)$  is the density of an event occurring at time  $t + \tau$  with no intervening events. If we define

$$P^{*2}(t) \equiv P \star P(t) = \int_0^t P(t - v)P(v)dv, \quad (46)$$

where  $\star$  represents the convolution operation, then  $P^{*2}(t)$  is the density of an event occurring at  $t + \tau$  with one intervening event. Continuing this process, we define

$$P^{*n}(t) \equiv P \star P \star \dots \star P(t), \quad (47)$$

with  $P(t)$  appearing  $n$  times, which corresponds to  $n - 1$  intervening events. The total interevent time density, also called the renewal function, is the sum over all possible numbers of intervening events, which can now be expressed as a function of  $P(t)$ . Therefore

$$u(t) = \sum_{n=0}^{\infty} P^{*n}(t), \quad (48)$$

where we define  $P^{*0} \equiv \delta(t)$ , the Dirac delta function for completeness. To remove the condition when an event occurred in the interval  $(t, t + \Delta)$ , we multiply by the rate of events  $\bar{\nu}$ , and thus the coincidence rate is given by

$$G_N(\tau) = \bar{\nu} \sum_{n=0}^{\infty} P^{*n}(|\tau|). \quad (49)$$

The power spectral density  $S_N(f)$  is the Fourier transform of the coincidence rate if both are defined, in which case

$$S_N(f) \equiv 2\mathcal{F}\{G_N(\tau)\} = 2 \int_{-\infty}^{\infty} e^{-i\omega\tau} \bar{\nu} \sum_{n=0}^{\infty} P^{*n}(|\tau|) d\tau = 2\bar{\nu}^2 \delta(f) + 2\bar{\nu} \operatorname{Re} \left\{ \frac{1 + Q(-i\omega)}{1 - Q(-i\omega)} \right\}, \quad (50)$$

where

$$Q(-i\omega) \equiv \mathcal{F}\{P(t)\} = \int_0^{\infty} e^{-i\omega t} P(t) dt \quad (51)$$

is the Fourier transform of the density  $P(t)$ , and  $Q(+i\omega)$  is the corresponding characteristic function of the interevent time  $T$ . The constant term in the coincidence rate  $\bar{\nu}^2$  leads to an impulsive term in the power spectral density

$$2\bar{\nu}^2\delta(f) = 2\bar{\nu}^2\delta(\omega/2\pi) = 4\pi\bar{\nu}^2\delta(\omega). \quad (52)$$

For low frequencies, in the range  $\omega \ll B^{-1}$ , the power spectral density approaches a constant value which depends on the moments of  $T$ . In the limit  $\omega \rightarrow 0$  the resulting form for the power spectral density is indeterminate, so we perform the substitution

$$Q(-i\omega) = 1 - i\omega\langle T \rangle - \omega^2\langle T^2 \rangle/2 + O(\omega^2), \quad (53)$$

where  $O(x)$  is some function satisfying

$$\lim_{x \rightarrow 0} O(x)/x = 0. \quad (54)$$

This yields

$$\lim_{\omega \rightarrow 0} S_N(f) = 2\bar{\nu} \lim_{\omega \rightarrow 0} \operatorname{Re} \left\{ \frac{1 + Q(-i\omega)}{1 - Q(-i\omega)} \right\} = 2\bar{\nu}^3 \operatorname{Var}\{T\}. \quad (55)$$

For the unmodified Lévy-stable densities the coincidence rate  $G_N(\tau)$  is zero for all nonzero delays  $\tau$ , so, the power spectral density  $S_N(f)$  is zero for all finite frequencies  $\omega$ . However, for the modified Lévy-stable densities, the resulting power spectral density may be obtained from Eqs. (38), (39) and (50), and is given by

$$S_N(f) = 2D^{-2}(B/A)^{2D}B^{-2}\delta(f) + 2D^{-1}(B/A)^DB^{-1}\operatorname{Re} \left\{ \frac{\exp[(i\omega A + A/B)^D] + \exp[(A/B)^D]}{\exp[(i\omega A + A/B)^D] - \exp[(A/B)^D]} \right\}. \quad (56)$$

In the limit  $B^{-1} \ll \omega \ll A^{-1}$  we obtain

$$\langle T \rangle S_N(\omega)(\omega A)^D \approx 2 \cos(\pi D/2), \quad (57)$$

so that

$$S_N(f) \approx 4D^{-1}(B/A)^DB^{-1} \cos(\pi D/2)(\omega A)^{-D}. \quad (58)$$

Thus the power spectral density varies as  $1/f^D$  over a substantial range of frequencies, where  $D$  corresponds to the exponent in the original Lévy-stable density.

Outside the range  $B^{-1} \ll \omega \ll A^{-1}$ , the power spectral density exhibits little change with frequency. For low frequencies, in the range  $\omega \ll B^{-1}$ , we have directly from (55)

$$\lim_{\omega \rightarrow 0} S_N(f) = 2D^{-2}(1 - D)(B/A)^{2D}B^{-1}. \quad (59)$$

In the range  $\omega \gg A^{-1}$ , we have  $|Q(-i\omega)| \ll 1$ , so that the power spectral density approaches a constant value

$$\lim_{\omega \rightarrow \infty} S_N(f) \approx 2\bar{\nu} = D^{-1}(B/A)^DB^{-1}. \quad (60)$$

This limiting value is the same as that obtained for the Poisson process; for these high frequencies the contributions of the individual events are essentially uncorrelated, thus, the Poisson limit is recovered.

## 2.6 $1/f$ noise in deterministic dynamical systems

One explanation of the occurrence of  $1/f$  noise in resistors is that the charge carriers get trapped in capture sites and are released with variable rates (this is essentially the extension of Schottky's original explanation of  $1/f$  noise in vacuum tubes), and in search for a "universal" explanation of  $1/f$  noise one may wonder if the same mechanism may act in more general dynamical systems. Geisel, Zacherl and Radons (GRZ) [94] devised just one such mechanism: it is well known that if we are given a particular Hamiltonian, its phase space splits in chaotic regions where the system point follows pseudo-orbits, and in ordered regions where the system point follows periodic orbits (this is the essence of the KAM theorem). The ordered regions are often surrounded by a hierarchy of cantori, and the conjecture of GRZ is that the system point gets temporarily trapped in these cantori and is released with variable rates, just as the charge carriers in an ordinary conductor with trapping sites. GRZ is considered, in particular, a classical particle in a periodic two-dimensional potential

$$V(x, y) = A + B[\cos(x) + \cos(y)] + C \cos(x) \cos(y), \quad (61)$$

and solved numerically the coupled equations of motion

$$\begin{cases} \dot{x} = [B + C \cos(y)] \sin(x), \\ \dot{y} = [B + C \cos(x)] \sin(y). \end{cases} \quad (62)$$

The particle performs a complex motion amid the many peaks of the potential, which looks like a sort of random walk, while the velocity of the particle looks like a periodic signal plus noise.  $1/f^\beta$  noise of velocity fluctuations with  $0.7 \leq \beta \leq 1.1$  was observed.

The dynamical system of GRZ is a Hamiltonian system, i.e. it belongs to a specific subclass, however in physics there are non-Hamiltonian systems as well, like the celebrated Lorentz system

$$\begin{cases} \dot{x} = \sigma(y - x), \\ \dot{y} = -xz + rx - y, \\ \dot{z} = xy - bz, \end{cases} \quad (63)$$

which has been extensively studied since its first appearance in 1963 [95, 96]. Systems, such as this, have many interesting features: stable limit cycles, strange attractors, intermittency and  $1/f$  noise. Intermittent behavior is characterized by a seemingly stationary signal, interrupted by bursts of activity [97, 98, 99, 100, 101, 102].

The fundamental work of Feigenbaum on the transition to chaos in the logistic map has shown that simple functions may be used as representatives of a much wider class of functions [103]: the function

$$f(x) = x + ux^2(\text{mod}1), \quad (64)$$

which maps the  $(0, 1)$  interval into itself has been used to study both intermittence and power-law noise in dynamical systems [98, 104, 105]. Repeated iteration of the map (64) yields a sequence

$$x_{n+1} = f(x_n) = x_n + ux_n^2(\text{mod}1), \quad (65)$$

which has both, an intermittent behavior and a very clean  $1/f$  spectral density. Schuster and Procaccia have [103] shown theoretically that it is a real  $1/f$  spectral density using

the Feigenbaum renormalization group method in function space [103]. It is important to note that the fluctuations produced by the dynamical systems, discussed in this section, are far from Gaussian, and therefore the spectral densities are not sufficient to characterize the processes.

## 2.7 Self-organized criticality

The outstanding feature of  $1/f$  noise is that it is scale invariant, i.e. it looks the same for any choice of frequency or time unit, and for this reason it has been widely considered to be a prominent manifestation of the fractal character of many natural phenomena. Since many nonlinear processes have complex phase spaces with fractal attractors, several physicists have looked into nonlinear processes as sources of  $1/f$  noise.

In 1987 Bak, Tang and Wiesenfeld (BTW) introduced a nonlinear model system that was met with wide interest and had since generated spates of scientific papers, the so-called “Sandpile Model” [106, 107]. The title of the original paper was *Self-Organized Criticality: An Explanation of  $1/f$  Noise*, and it put forward a very ambitious program, as it described a nonlinear process that had fractal characteristics, a complex behavior that mimicked a noise process, a spectral density that the authors claimed to be  $1/f$ , and displayed a limiting behavior that was called “self-organized criticality”.

The sandpile model is closely related to an earlier classical model developed to describe the charge-density waves observed in some special conductors like  $\text{NbSe}_3$  or  $\text{K}_{0.3}\text{MoO}_3$  (see [108] and [109] for very readable reviews or [110] for a more technical one): in this model a charge density wave may be viewed as a single particle (or an array of particles) in a periodic or quasi-periodic potential.

BTW introduced a coupled-pendula model of self-organized criticality but the analogy with sand proved to be so suggestive, that shortly only the sandpile paradigm survived in the literature. The two-dimensional version of the model is described mathematically by the discrete evolution equations

$$\begin{cases} z_{j,k} \rightarrow z_{j,k}, & z_{j,k} \leq K, \\ \begin{cases} z_{j,k} \rightarrow z_{j,k} - 4, \\ z_{j\pm 1,k} \rightarrow z_{j\pm 1,k} + 1, \\ z_{j,k\pm 1} \rightarrow z_{j,k\pm 1} + 1, \end{cases} & z_{j,k} > K, \end{cases} \quad (66)$$

where  $z_{j,k}$  is an integer variable that may be taken to represent the height differences between adjacent nodes in a two-dimensional lattice, and  $K$  is a threshold value. From equation (66) we see that the dynamics described by (66) represents a discrete, nonlinear diffusion process.

Being discrete and nonlinear, the sandpile model is very hard to study with the help of the usual analytical tools, but it can easily be adapted to large scale numerical calculations and in [107] BTW reported  $1/f^\beta$  spectral densities obtained from their numerical simulations, with  $\beta$  near 1.

BTW also argued that the sandpile model exhibits a form of self-organization as the slope of the sandpile approaches a limiting value, just as in real sandpiles (in plain words, the diffusion process cannot proceed until the threshold  $K$  is reached) and they dubbed it “Self Organized Criticality” (SOC).

Papers [106] and [107] initiated a flurry of activity as many physicists tried to replicate BTW's results, either with their own numerical simulations or with direct simulations of sand flows, and sometimes also with more sophisticated analytical tools such as the renormalization group approach. However, most of these studies have widened the scope of applications of SOC but have not led to a deeper understanding of the behavior of the model, which remains controversial. For instance, there are applications of SOC to the fields as diverse as fire propagation [111] or evolutionary biology [112, 113], but alongside the enthusiastic attitudes of some physicists (see, e.g. [114]) there is an increasing number of papers that raise doubts on the validity and actual applicability of the model.

The study of  $1/f$  noise started in electronics, and we have already seen that electrical  $1/f$  noise seems to be stationary and Gaussian, but the pulses of sandpiles are not Gaussian, and the other statistical properties, too, differ from those of the observed electrical  $1/f$  noise [115]; moreover, electrical  $1/f$  noise exists at equilibrium while all SOC models require an external driving process. Another point that remains highly controversial is the reality of the claimed  $1/f$  spectra: are they  $1/f^\beta$  spectra (with  $\beta \approx 1$ ) or are they trivial  $1/f^2$  spectra? If they were just  $1/f^2$  spectra, then SOC would not be essentially different from a simple Brownian process, and therefore it was essential to establish the numerical value of the exponent. Jaeger, Liu and Nagel performed an experiment with a real sandpile in 1988 [116, 117] and their results contradicted BTW's claims, they did not observe a  $1/f^\beta$  spectrum, but rather a white noise plateau modified at low frequency by grain size effects followed by a  $1/f^2$  tail.

Jensen, Christensen and Fogedby added mathematical substance to the measurements of Jaeger, Liu and Nagel [117], and they demonstrated that the spectra in real sandpiles were actually  $1/f^2$  [118]. The problem of establishing the exponent has been aggravated by serious errors in the literature, as in ref. [119], where the authors claimed to have found a sandpile model with a  $1/f$  spectrum, whereas they actually found a  $1/f^2$  spectrum and forgot to square the Fourier coefficients.

The importance of finding  $1/f^\beta$  spectra with  $\beta \neq 2$  seemed to have escaped the attention of some authors, such as Dalton and Corcoran, who recently performed another experiment on a granular system [120], found a trivial  $1/f^2$  spectrum and concluded that this was in accordance with SOC.

Skokov and Koverda investigated system near to the critical phase transition [121], which could be described by system of two non linear stochastic equations

$$\begin{aligned}\dot{\phi} &= -\phi\psi^2 + \psi + \xi_1(t), \\ \dot{\psi} &= -\psi\phi^2 + \gamma\phi + \xi_2(t),\end{aligned}\tag{67}$$

where  $\gamma$  is some parameter,  $\xi_1(t)$  and  $\xi_2(t)$  are white noise sources and, in their paper [121] they showed that equations (67) transformed white noise into two stochastic processes with power spectral densities proportional to  $1/f$  and  $1/f^2$ .

In general, the SOC does not seem to adequately describe  $1/f$  noise, neither does it aspire to the universality that its supporters claim. Moreover, the studies [122, 123, 124] on SOC systems show that the power laws of the spatial and timporal sizes are fingerprints of the SOC.

## 2.8 Earthquakes

After Mandelbrot's work,  $1/f$  noise has often been associated with fractal phenomena and other power laws, and the physics of earthquakes is just one of those fields where the features of scaling which lead to the power laws, seem to be applicable. The mainstay of this field is the celebrated Gutenberg-Richter law [125] which states that  $N(M)$ , the number of earthquakes with magnitude greater than  $M$ , is proportional to  $10^{-bM}$ , i.e.  $\log_{10}N(M) = A - bM$  where the slope  $b$  is found to be a number near 1. There is also a classical earthquake model with dissipative nonlinear dynamics, the Burridge-Knopoff model [126], so the challenge lies in solving the Burridge-Knopoff model or another similar model to retrieve the Gutenberg-Richter law, and other earthquake statistics. The Burridge-Knopoff model is a simple block-and-spring model of a crustal fault originally introduced in 1967, and it has been extensively studied [127], especially by Carlson and his collaborators [128, 129].

Milotti in [130] showed that there was indeed a magnitude range where a power law was held, while there was a low magnitude region where the power law broke down. Earthquakes are complex phenomena, and the restricted power law range may come from some fundamental difference in physics between small and large magnitude earthquakes [131].

Telesca, Cuomo, and Lappena (TCL) analysed seismic data from National Institute of Geophysics and Vulcanology catalogue, covering the period from 1986 to 2001 and analysed three different seismic zones located in northern, central and southern Italy [132]. They mathematically expressed a sequence of earthquakes by finite sum of Dirac's delta functions centered on the occurrence times  $t_i$  with amplitude  $A_i$  proportional to the magnitude  $M_i$  of the  $i$ -th event

$$x(t) = \sum_{i=1}^n A_i \delta(t - t_i). \quad (68)$$

They divided the time axis into equally spaced contiguous counting windows of duration  $\tau$ , and produced a sequence of counts  $\{N_k(\tau)\}$ , with  $N_k(\tau)$  denoting the number of earthquakes in the  $k$ -th window

$$N_k(\tau) = \int_{T_{k-1}}^{T_k} \sum_{i=1}^n \delta(t - t_i) dt. \quad (69)$$

Using representation (69) TCL calculated three different statistics. The Fano Factor is a measure of correlation over different time scales

$$FF(\tau) = \frac{\langle N_k^2(\tau) \rangle - \langle N_k(\tau) \rangle^2}{\langle N_k(\tau) \rangle}, \quad (70)$$

where  $\langle \dots \rangle$  denotes the expectation value. The Allan Factor is in relation with the variability of successive counts

$$AF(\tau) = \frac{\langle [N_{k+1}(\tau) - N_k(\tau)]^2 \rangle}{2\langle N_k(\tau) \rangle}, \quad (71)$$

and the Count-based Periodogram, which is the periodogram of the sequence of the counts  $N_k$  and allows estimating the exponent of the power spectral density  $\beta$ .

The calculations of this statistics showed the existence of  $1/f^\beta$  temporal fluctuations of seismicity at higher timescales and the sequences of Italian earthquakes demonstrated a clear clustering effect. These allow to detect correlation properties in the point processes [132].

## 2.9 $1/f$ noise in meteorology

Approximate  $1/f$  noise behavior was found by Yano, Fraedrich, and Zebiak (YFZ) in tropical surface temperature, moisture, and wind speed for periods of 1 hour to beyond 10 days and in oceanic wind stress up to 2 year periods [133]. They showed that the origin of the  $1/f$  noise can be closely tied to pulse-like events with a highly intermittent nature of the time series. Examples for such pulse-like events include the cumulus convection events leading to convecting downdraughts and intra seasonal westerly wind events associated with the Madden-Julian oscillations.

YFZ have used Tropical Ocean and Global Atmosphere, Coupled Ocean-Atmosphere Response Experiment (TOGA-COARE) collected data for analysis, which consisted of data intervals of 6–12 hours. In the following paper [134] longer (more than a month’s) time scales were analysed.

Yano introduced a method for objectively extracting the pulse-like events of particular scales from the original time series based on wavelets [135, 136]. Wavelets were expected to work effectively for this purpose with their highly localized structures. Specifically, the discrete Meyer wavelets were adopted by taking advantage of their completeness and orthogonality.

A discrete wavelet mode  $\psi_{i,j}(t)$  is characterized by the time scale (“duration”)  $\Delta t \equiv T/2^{j-1}$  and the timing  $t = (i - 1/2)\Delta t$  when the localized individual mode takes its maximum, where  $j = 1, \dots, \log_2 N$  and  $i = 1, \dots, 2^{j-1}$  for a time series of length  $T$  with  $N$  measurements in equal interval.

A time series  $x(t)$  was decomposed by the wavelets as

$$x(t) = \sum_{j=1}^{\log_2 N} \sum_{i=1}^{2^{j-1}} \hat{x}_{i,j} \psi_{i,j}(t) + \bar{x}, \quad (72)$$

with the expansion coefficients  $\hat{x}_{i,j}$ , where  $\bar{x}$  is the time mean. Orthogonality and completeness of the wavelets make this decomposition unique. Normalization

$$\langle \psi_{i,j}^2(t) \rangle = 1/2^{j-1} \quad (73)$$

was used, making the maximum values of wavelets approximately invariant with the scale, so the coefficients  $\hat{x}_{i,j}$  present the amplitudes of the corresponding localized signal. Total number of measurements  $N$  must be a power of two.

The resulting wavelet spectrum is two-dimensional, where  $i$ -axis graphically indicates the timing of events, whereas the  $j$ -axis indicates the characteristic scales. When a pulse-like event is found in a time series, it is expected that such an event is represented by a local maximum in absolute values of coefficients in this wavelets space, because the spatially localized nature of wavelets allows the event to be represented by its characteristic scale (“duration”) and timing. Thus, an extraction of such an event can be performed by extracting the modes clustered around this peak.

Temperature, moisture mixing ratio, wind speed, and precipitation rates consist of  $1/f$ -noise spectrum slope down to 1-hour scale and up to the intra seasonal time-scale (30–60 days).

## 2.10 $1/f$ fluctuations in traffic

In 1976 Musha and Higuchi (MH) decided to measure car current on an ordinary highway and calculate power spectral density [137]. They stayed on a bridge over a three-lane part of the chosen highway and recorded transit times of the cars on a magnetic tape. 11080 cars were recorded in four hours. By substituting each vehicle with delta function, they obtained a series of interevent transit times.

To eliminate  $1/f^2$  term at low frequencies, which was present regardless of the detailed structure of the sequence, MH divided the whole observation time  $T$  into 20 pieces of equal length and they took the differences between delta functions in different pieces. This led to a white noise at high frequencies and  $1/f$  noise at a small scale.

Furthermore, they wrote continuity equation for the local mean concentrations of the cars  $n(x, t)$  and local mean car current along  $x$  axis  $J(x, t)$  and found the diffusion current

$$J = nv - D \frac{\partial n}{\partial x}, \quad (74)$$

where  $v$  is local mean velocity and  $D$  is effective diffusion coefficient.

Greenberg [138] observed that the car velocity decreased with the increase of the car concentration and MH assumed linear relationship between them

$$v = v_0 \left(1 - \frac{n}{n_s}\right), \quad (75)$$

where  $v_0$  was the drift velocity when  $n$  approached zero and the constant  $n_s$  was usually much larger than the mean concentration.

Changing coordinates to  $x = -x' + v_0 t'$  and  $t = t'$  MH obtained Navier-Stokes' equation with the pressure term being ignored

$$\frac{\partial n}{\partial t'} + an \frac{\partial n}{\partial x'} = D \frac{\partial^2 n}{\partial x'^2}, \quad (76)$$

where  $a = 2v_0/n_s$ .

Car currents flowing into and leaving out of the main current at ramps were regarded as external disturbance continuously given to the main car current, and the uniform stationary car current on the highway was considered as a superposition of non stationary car currents at ramps. Introducing wave number  $k'$  and frequency  $f'$  in the frames of reference  $(x', t')$  and  $k = -k'$ ,  $f = f' - v_0 k'/(2\pi)$  in the original frame of reference  $(x, t)$  and taking into account that fluctuations are small, leads to power spectral density

$$S(f) \propto v_0^2/f. \quad (77)$$

As we can see MH derived a  $1/f$  power spectrum, which agreed with the observation data.

## 2.11 Examples from biophysics

As an example of a biophysical system in which  $1/f$  noise is actually observed, we can mention the fluctuations of the electrical dipole moment of an important enzyme – lysozyme.

It is a very interesting physical system in as much as it provides the information on the structure of water and on its interaction with biological molecules [139]. The

fluctuations have been studied by Careri and Consolini [140] and the spectral density is once again a  $1/f^\alpha$  spectrum, with  $\alpha = 1.5$ .

Milotti [130] believes that the electrical dipole fluctuations are due to the migration of free protons on the molecule surface, and to test this model he has set up a Monte Carlo simulation. The first results obtained with this approach are encouraging, as Milotti has found good values for the noise exponent and reasonable dependencies on the other physical parameters. It is found that the distribution of transition rates between different proton states follows a power law, and therefore produces a  $1/f^\alpha$  spectral density. The individual signals are non-Gaussian, but the macroscopic signal is a superposition of many such signals, and thus it is Gaussian.

Takano, Takahashi, and Nagayama (TTN) simulated molecular dynamics of the helix-coil transition of a polypeptide [141]. The simulated transition was two-state-like and similar to the solid-liquid-like transition that has been observed in computer simulations of an atomic cluster. At the transition temperature, the polypeptide chain fluctuated between a helical and a random-coil state, and TTN observed  $1/f$  fluctuation through potential-energy fluctuations.

## 2.12 Scaling of heartbeat intervals

Scale-invariant properties in biological systems have recently received much attention. Kobayashi and Musha investigated human heartbeat and found a  $1/f$  behavior of power spectra [142]. Peng, Mietus, Hausdorff, Havlin, Stanley, and Goldberger (PMHSG) showed that the power spectra of the human heartbeat intervals from healthy individuals exhibits a scale invariant  $1/f$  pattern in the low frequency range ( $f < 0.1$  Hz) [143]. They analysed the digitized electrocardiograms of beat-to-beat heart rate fluctuations over very long time intervals (up to 24 h  $\approx 10^5$  beats), recorded with an ambulatory monitor. Time series, obtained by plotting the sequential intervals between beat  $n$  and  $n + 1$ , typically reveal a complex type of variability related to competing neuroautonomic inputs. PMHSG passed the time series through a digital filter that removed fluctuations of frequencies  $> 0.005$  beat $^{-1}$ . They observed a more complex pattern of fluctuations for a representative healthy adult compared to the “smoother” pattern of interbeat intervals for a subject with severe heart disease and came to a conclusion that loss of  $1/f$  slope in power spectra is closely related to the prognosis and severity of heart disease.

Heart failure can predict other parameters as well. Ivanov, Amaral, Goldberger, Havlin, Rosenblum, Stanley, Struzik (IAGHRSS) investigated multifractality in heartbeat dynamics [144]. They measured a time series for 18 healthy subjects and for 12 patients with congestive heart failure. Investigation of the shape of fractal dimensions  $D(h)$  for the healthy people indicated multifractal behavior, however,  $D(h)$  for the heart failure group was very narrow, indicating the loss of multifractality. IAGHRSS assumed that a different form of fractal dimensions may reflect perturbation of the cardiac neuroautonomic control mechanisms associated with this pathology.

Though the characteristics of a point process are often studied via the sequence of intervals between successive events, in some cases it is advantageous to examine the sequence of event numbers (counts)  $\{N_k\}$  observed in successive counting times  $\tau$ . Teich introduced a wavelet-based version of the Allan factor (71) generated by replacing Haar-function counting windows of duration  $\tau$  by wavelet and scaling functions, denoted  $\psi(t)$  and  $\varphi(t)$  respectively, in an arbitrary wavelet basis [145]. Wavelet and scaling

coefficients,  $d(\tau, k)$  and  $c(\tau, k)$  respectively, can then be constructed from the point process  $N(t)$ ,

$$d(\tau, k) = \frac{1}{\sqrt{\tau}} \int_{-\infty}^{\infty} [\psi(u/\tau - k)]^* dN(u), \quad (78)$$

$$c(\tau, k) = \frac{1}{\sqrt{\tau}} \int_{-\infty}^{\infty} [\varphi(u/\tau - k)]^* dN(u), \quad (79)$$

where  $*$  denotes complex conjugation. The wavelet Allan factor is then defined as

$$A_W(\tau) = \sqrt{\tau} \frac{\langle |d(\tau, k)|^2 \rangle}{\langle |c(\tau, k)| \rangle}, \quad (80)$$

where the average is over  $k$ . Teich computed wavelet Allan factor for 12 normal and 15 heart-failure patients and showed that the threshold value for wavelet Allan factor can be chosen in such a way, that all heart-failure and normal patients can be properly identified.

### 2.13 Statistical properties of stock price fluctuations

Economic time series, such as stock market indices or currency exchange rates, depend on the evolution of a large number of interacting systems and are examples of complex evolving systems widely studied in physics [36, 37, 38, 39, 40, 41]. The recent availability of large amounts of data allows the study of economic time series with high accuracy on a wide range of time scales varying from  $\approx 1$  minute up to  $\approx 1$  year.

Liu, Gopikrishnan, Cizeau, Meyer, Peng, and Stanley (LGCMPs) analysed S&P 500 index  $Z(t)$  from the New York Stock Exchange historical data for the 13-year period January 1984 to December 1996 with a recording frequency of 15 s interval [146]. LGCMPs introduced the price change  $G(t)$  as the change in the logarithm of the index

$$G(t) \equiv \ln Z(t + \Delta t) - \ln Z(t) \cong \frac{Z(t + \Delta t) - Z(t)}{Z(t)}, \quad (81)$$

where  $\Delta t$  is the sampling time interval. Only the time during the opening hours of the stock market was counted, whereas, nights, weekends and holidays were removed from the data set and the closing as well as the opening of the market were considered to be continuous. LGCMPs defined the volatility as the average of  $|G(t)|$  over a time window  $T = n\Delta t$ , i.e.,

$$V_T(t) \equiv \frac{1}{n} \sum_{t'=t}^{t+n-1} |G(t')|, \quad (82)$$

where  $n$  is an integer. The central part of volatility pdf exhibits a log-normal behavior, however, tail of the cumulative distribution of the volatility is consistent with a power-law asymptotic behavior

$$P(V_T > x) \sim \frac{1}{x^\mu}, \quad (83)$$

where  $\mu \approx 3$ , is well outside the stable Lévy range  $0 < \mu < 2$ .

LGCMPs calculated the power spectral density of the price change  $G(t)$  and found that it would be fitted by two separate power laws  $S(f) \sim 1/f^{\beta_1}$  for  $f > f_x$  and  $S(f) \sim 1/f^{\beta_2}$  for  $f < f_x$ , where condition  $0 < \beta_1 < \beta_2 < 1$  is met.

Gontis and Kaulakys (GK) assumed transactions in the financial markets as point events and introduced a multiplicative stochastic model for the time intervals between events of point process [44, 45]. Their model of time series has only a few parameters defining the statistical properties of the system, i.e., the power-law behavior of the distribution function and the scaled power spectral density with the slope  $\beta$  ranging between 0.5 and 1.5. GK showed numerical results confirming that the multiplicative stochastic model of the time intervals between the trades in the financial markets is able to reproduce the main statistical properties of the trading activity and its power spectral density.

## 2.14 $1/f$ noise in computer networks and the Internet

The statistical characteristics of network traffic have been of interest to researchers for many years in order to obtain a better understanding of the factors that effect the performance and scalability of a large system, such as the Internet. Early studies of the Internet traffic proved particularly interesting, as they exposed self-similar characteristics that were not previously commonplace [147].

Field, Harder and Harrison (FHH) analysed the switched Ethernet system in a University Computing department at Imperial College, London [148]. They collected a huge amount of network traffic data, logged in files from different sources – web servers and routers. Time stamp and size of each packet were logged. Using this data they obtained a point process of network packets, and later divided the time scale into equal intervals and formed an aggregated time series by calculating number of packets sent or received in each particular time interval.

FFH observed that the power spectrum of both the incoming and outgoing traffic time series, aggregated over different time intervals exhibit a  $1/f$  behavior [148]. Furthermore, they investigated the changes in the observed packet rates and found out that they were extremely well approximated by a Cauchy distribution

$$P(x) = \frac{2}{\pi} \frac{s}{s^2 + x^2}, \quad (84)$$

where  $s > 0$  is some parameter. FFH generated network traffic packets with different, Cauchy and Poisson time distribution and feeded them to a web server. Power spectral density of outgoing packets from the server proved to be a power-law.

Csabai performed measurements on the speed of the network between two points. He measured round-trip times (RTT) between a workstation at Eötvös University, Hungary, and a distant ftp site, located in Finland [149]. There were 15 gateways between the two hosts. Csabai found no simple low dimensional chaotic attractor in the analysis of time series, but the power spectrum of data showed a  $1/f$ -like behavior in the whole time domain (see Figure 1).

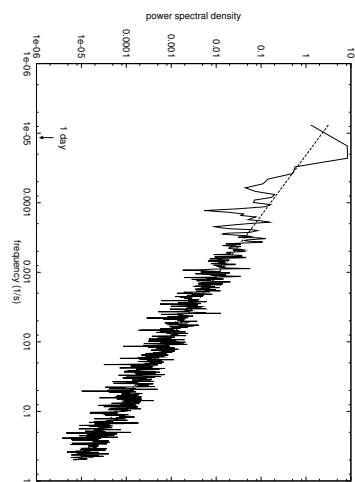


**Figure 1.** Power spectral density of the RTT, obtained by Csabai [149].

### 3 POINT PROCESS MODEL

#### 3.1 Point processes

In many cases the intensity of some signal or current can be represented by a sequence of random (however, as a rule, mutually correlated) pulses or elementary events  $A_k(t-t_k)$ . Here the function  $A_k(\phi)$  represents the shape of the  $k$  pulse having an influence on the signal  $I(t)$  in the region of transit time  $t_k$  [57]. The signal of intensity of the current of particles in some space cross section may, therefore, be expressed as

$$I(t) = \sum_k A_k(t-t_k). \quad (85)$$

It is easy to show that the shapes of the pulses mainly influence the high frequency,  $f \geq \Delta t_p$ , with  $\Delta t_p$  being the characteristic pulse length, power spectral density, while fluctuations of the pulse amplitudes result, as a rule, in white or Lorentzian, but not  $1/f$ , noise [150, 151, 152]. Therefore, we restrict our analysis to noise due to correlations between the transit times  $t_k$ . In such an approach we can replace the function  $A_k(t-t_k)$  by the Dirac delta function  $\delta(t-t_k)$  and the signal express as

$$I(t) = \bar{a} \sum_k \delta(t-t_k), \quad (86)$$

with  $\bar{a}$  being an average contribution to the signal of one pulse. This model also corresponds to the flow of identical objects: electrons, photons, cars, and so on, when they cross the section of observation and it is called the point process model. Point processes arise in different fields, such as physics, economics, cosmology, ecology, neurology, seismology, traffic flow, signaling and telecom networks, audio streams, and the Internet (e.g., [152, 137, 153, 154, 155, 149, 31, 156, 132, 157, 148] and references herein). On the other hand, fluctuations of the amplitudes  $A_k$  may result in additional noise but cannot reduce  $1/f$  noise we are looking for.

The power spectral density of current (86) is

$$\begin{aligned} S(f) &= \lim_{T \rightarrow \infty} \left\langle \frac{2}{T} \left| \int_{t_i}^{t_f} I(t) e^{-i2\pi ft} dt \right|^2 \right\rangle = \lim_{T \rightarrow \infty} \left\langle \frac{2\bar{a}^2}{T} \left| \sum_{k=k_{\min}}^{k_{\max}} e^{-i2\pi ft_k} \right|^2 \right\rangle \\ &= \lim_{T \rightarrow \infty} \left\langle \frac{2\bar{a}^2}{T} \sum_k \sum_{q=k_{\min}-k}^{k_{\max}-k} e^{i2\pi f \Delta(k;q)} \right\rangle, \quad (87) \end{aligned}$$

where  $t_i$  and  $t_f$  are initial and final observation times,  $T = t_f - t_i \gg \omega^{-1}$  is the whole observation time,  $\omega = 2\pi f$ ,

$$\Delta(k;q) \equiv t_{k+q} - t_k = \sum_{i=k}^{k+q-1} \tau_i \quad (88)$$

is the difference between the pulses occurrence times  $t_{k+q}$  and  $t_k$ , and  $\tau_k = t_k - t_{k-1}$  is the time intervals between pulses. Here  $k_{\min}$  and  $k_{\max}$  are minimal and maximal values of index  $k$  in the interval of observation  $T$  and the brackets  $\langle \dots \rangle$  denote the averaging over realizations of the process.

It should be stressed that the spectrum is related to the underlying process but not to a realization of the process [79, 80, 81, 82, 158]. Therefore, the averaging over realizations of the process is essential. Without the averaging over the realizations we obtain the squared modulus of the Fourier transform of the data, i.e., the periodogram which is fluctuating widely and its variance is almost independent of  $T$  [80, 158]. For calculation of the power spectrum of the actual signal one should use the well-known procedures of the smoothing for spectral estimations [80, 158, 82, 159].

Equation (87) may be rewritten as

$$S(f) = 2\bar{a}^2\bar{\nu} + \lim_{T \rightarrow \infty} \left\langle \frac{4\bar{a}^2}{T} \sum_{q=1}^N \sum_{k=k_{\min}}^{k_{\max}-q} \cos[2\pi f \Delta(k; q)] \right\rangle \quad (89)$$

where  $N = k_{\max} - k_{\min}$  and

$$\bar{\nu} = \left\langle \lim_{T \rightarrow \infty} \frac{N+1}{T} \right\rangle \quad (90)$$

is the mean number of pulses per unit time. The first term in the right-hand-side of Eq. (89) represents the shot noise,

$$S_{\text{shot}}(f) = 2\bar{a}^2\bar{\nu} = 2\bar{a}\bar{I}, \quad (91)$$

with  $\bar{I} = \bar{a}\bar{\nu}$  being the average signal.

Eqs. (87) – (91) may be modified as

$$S(f) = 2\bar{a}^2 \sum_{q=-N}^N \left( \bar{\nu} - \frac{|q|}{T} \right) \chi_{\Delta(q)}(\omega) \quad (92)$$

and used for evaluation of the power spectral density of the non-stationary process or for the process of finite duration, as well. Here

$$\chi_{\Delta(q)}(\omega) = \overline{\langle e^{i\omega\Delta(q)} \rangle} = \int_{-\infty}^{+\infty} e^{i\omega\Delta(q)} \Psi_q[\Delta(q)] d\Delta(q) \quad (93)$$

is the characteristic function of the distribution density  $\Psi_q[\Delta(q)]$  of  $\Delta(q)$ , a definition  $\Delta(q) = -\Delta(-q) = \Delta(k; q)$  is introduced, and the brackets  $\langle \dots \rangle$  denote the averaging over realizations of the process and over the time (index  $k$ ) [57, 61, 62]. For the non-stationary process or the process of the finite duration one should use the real distribution  $\Psi_q[\Delta(q)]$  with the finite interval of the variation of  $\Delta(q)$  or calculate the power spectra directly according to Eq. (87).

When the second sum of Eq. (92) in the limit  $T \rightarrow \infty$ , due to the decrease of the characteristic function  $\chi_{\Delta(q)}(\omega)$  for finite  $\omega$  and large  $q$ , approaches to zero,

$$\lim_{T \rightarrow \infty} \frac{1}{T} \sum_{q=-N}^N |q| \chi_{\Delta(q)}(\omega) \rightarrow 0, \quad (94)$$

we have from Eq. (92) the power spectrum in the form

$$S(f) = \lim_{T \rightarrow \infty} \left\langle \frac{2\bar{a}^2}{T} \sum_{k,q} e^{i\omega\Delta(k;q)} \right\rangle = 2\bar{a}\bar{I} \sum_{q=-N}^N \chi_{\Delta(q)}(\omega). \quad (95)$$

According to the above analysis, the power spectral density of the signal depends on the statistics and correlations of the transit times  $t_k$  only. It is well known that a sequence of random, Poisson transit times generates white (shot) noise [150, 151, 152]. The sequence of transit times  $t_k$  with random increments  $t_k = t_{k-1} + \bar{\tau} + \sigma\varepsilon_k$  (where  $\bar{\tau}$  is the average interpulse time between pulses,  $\{\varepsilon_k\}$  denotes the sequence of uncorrelated normally distributed random variables with zero expectation and unit variance, i.e., the white noise source, and  $\sigma$  is the standard deviation of white noise) results in a Lorentzian spectra [37, 73]. Here we will consider sequences of transit times with random increments of the time intervals between pulses,  $\tau_k = \tau_{k-1} + \sigma\varepsilon_k$ , where  $\tau_k = t_k - t_{k-1}$ . It is natural to restrict in some way infinite Brownian increase or decrease of the interpulse times  $\tau_k$ , e.g., by the introduction of relaxation to the average interpulse time  $\bar{\tau}$  rate  $\gamma$ . So, we have recurrent equations for the transit times:

$$\begin{aligned} t_k &= t_{k-1} + \tau_k, \\ \tau_k &= \tau_{k-1} - \gamma(\tau_{k-1} - \bar{\tau}) + \sigma\varepsilon_k. \end{aligned} \quad (96)$$

### 3.2 Power spectral density

An advantage of model (96) is that it may be solved analytically. So, an iterative solution of Eqs. (96) results in an expression for the interpulse time,

$$\tau_k = \bar{\tau} + (\tau_0 - \bar{\tau})(1 - \gamma)^k + \sigma \sum_{j=1}^k (1 - \gamma)^{k-j} \varepsilon_j, \quad (97)$$

where  $\tau_0$  is the initial interpulse time. The dispersion of the interpulse time  $\tau_k$  is

$$\sigma_\tau^2(k) \equiv \langle \tau_k^2 \rangle - \langle \tau_k \rangle^2 = \frac{\sigma^2[1 - (1 - \gamma)^{2k}]}{2\gamma(1 - \gamma/2)} \simeq \begin{cases} \sigma^2 k, & 2k\gamma \ll 1, \\ \sigma^2/2\gamma, & 2k\gamma \gg 1. \end{cases} \quad (98)$$

Therefore, after a characteristic transition to the stationary process time,  $t_{\text{tr}} = \bar{\tau}/\gamma$ , the dispersion of the interpulse time approaches the limiting value  $\sigma_\tau^2 = \sigma^2/2\gamma$ .

After some algebra we can also obtain an explicit expression for the transit times  $t_k$  ( $k \geq 1$ ),

$$t_k = t_0 + k\bar{\tau} + \frac{1 - \gamma}{\gamma} [1 - (1 - \gamma)^k] (\tau_0 - \bar{\tau}) + \frac{\sigma}{\gamma} \sum_{l=1}^k [1 - (1 - \gamma)^{k+1-l}] \varepsilon_l, \quad (99)$$

where  $t_0$  is the initial time. The dispersion of the transit time

$$\begin{aligned} \sigma_t^2(k) \equiv \langle t_k^2 \rangle - \langle t_k \rangle^2 &= \frac{\sigma^2}{\gamma^2} \left\{ k - 2 \frac{1 - \gamma}{\gamma} [1 - (1 - \gamma)^k] + (1 - \gamma)^2 \frac{1 - (1 - \gamma)^{2k}}{1 - (1 - \gamma)^k} \right\} \\ &= \begin{cases} \sigma^2(k/6 + k^2/2 + k^3/3 + \dots), & 2\gamma k \ll 1, \\ (\sigma/\gamma)^2(k - 3/(2\gamma) + 5/4 \pm \dots), & 2\gamma k \gg 1. \end{cases} \end{aligned} \quad (100)$$

At  $k \gg \gamma^{-1}$ , Eq. (99) generates a stationary time series. The difference of the transit

times  $t_{k+q}$  and  $t_k$  in Eq. (87), for  $\tau_0 = \bar{\tau}$  or  $2\gamma k \gg 1$ , is

$$\Delta(k; q) = \bar{\tau}q + \frac{\sigma}{\gamma} \left\{ [1 - (1 - \gamma)^q] \sum_{l=1}^k (1 - \gamma)^{k+1-l} \varepsilon_l + \sum_{l=k+1}^{k+q} [1 - (1 - \gamma)^{k+q+1-l}] \varepsilon_l \right\}, \quad q \geq 0. \quad (101)$$

The dispersion of these times' differences equals

$$\langle \Delta(k; q)^2 \rangle - \bar{\tau}^2 q^2 = \frac{\sigma^2}{2} g(q), \quad (102)$$

where

$$g(q) = \frac{2}{\gamma^2} \left\{ [1 - (1 - \gamma)^q]^2 \sum_{l=1}^k (1 - \gamma)^{2l} + \sum_{l=1}^q [1 - (1 - \gamma)^l]^2 \right\}, \quad q \geq 0. \quad (103)$$

Summation in Eq. (103) results in

$$g(q) = \frac{2}{\gamma^2} \left\{ q - \frac{(1 - \gamma)[1 - (1 - \gamma)^q]}{1 - (1 - \gamma)^2} \{2 + [1 - (1 - \gamma)^q](1 - \gamma)^{2k+1}\} \right\}. \quad (104)$$

At  $\gamma q \ll 1$ ,

$$g(q) = \begin{cases} (2k + 1)q^2 + q/3 + 2q^3/3, & 2\gamma k \ll 1, \\ \left(\frac{1}{\gamma} + \frac{1}{2}\right) q^2 + \frac{1}{3}q - \frac{1}{3}q^3, & 2\gamma k \gg 1, \end{cases} \quad (105)$$

while for  $2\gamma q \gg 1$  we have

$$g(q) = \frac{2}{\gamma^2} \left[ q - 2 \frac{(1 - \gamma)[1 - (1 - \gamma)^q]}{1 - (1 - \gamma)^2} \right] \simeq \begin{cases} \left(\frac{1}{\gamma} + \frac{1}{2}\right) q^2 + \frac{1}{3}q - \frac{1}{3}q^3, & \gamma k \ll 1, \\ \frac{2}{\gamma^2} \left(q + \frac{1}{2}\right) - \frac{2}{\gamma^3} + \dots, & q \gg \gamma^{-1} \gg 1. \end{cases} \quad (106)$$

Note that for  $q < 0$  we should replace  $q$  in Eqs. (101) – (106) by  $|q|$  and  $k$  by  $k - |q|$ . Therefore, the function  $g(q)$  at  $k - |q| \gg \gamma^{-1}$  is even, i.e,  $g(-q) = g(q)$ .

Substituting Eq. (101) into Eq. (87), and replacing the summations in the exponents by the multiplications of the exponents, we have the following expression for the power spectral density of the current

$$S(f) = \lim_{T \rightarrow \infty} \left\langle \frac{2\bar{a}^2}{T} \sum_k \sum_{q=k_{\min}-k}^{k_{\max}-k} e^{i2\pi f \bar{\tau} q} \times \prod_{l=1}^k \exp \left\{ i \frac{2\pi f \sigma}{\gamma} [1 - (1 - \gamma)^q] (1 - \gamma)^{k+1-l} \varepsilon_l \right\} \times \prod_{l=k+1}^{k+q} \exp \left\{ i \frac{2\pi f \sigma}{\gamma} [1 - (1 - \gamma)^{k+q+1-l}] \varepsilon_l \right\} \right\rangle. \quad (107)$$

The average over realizations of the process coincides with the average over the distribution of the random variables  $\varepsilon_l$ . Using the fact that random variables  $\varepsilon_l$  are

independent and mutually uncorrelated, we can fulfill the averaging over every random variable  $\varepsilon_l$  independently. Therefore, Eq. (107) may be rewritten in the form

$$S(f) = \lim_{T \rightarrow \infty} \frac{2\bar{a}^2}{T} \sum_{k,q} e^{i2\pi f\bar{\tau}q} \prod_{l=1}^k \left\langle \exp \left\{ i \frac{2\pi f\sigma}{\gamma} [1 - (1-\gamma)^q] (1-\gamma)^{k+1-l} \varepsilon_l \right\} \right\rangle \\ \times \prod_{l=k+1}^{k+q} \left\langle \exp \left\{ i \frac{2\pi f\sigma}{\gamma} [1 - (1-\gamma)^{k+q+1-l}] \varepsilon_l \right\} \right\rangle. \quad (108)$$

The result of the averaging of the exponent  $\exp\{ic\varepsilon_l\}$  (with  $c$  being a constant) over the normally distributed random variable  $\varepsilon_l$  with zero expectation and unit variance is

$$\langle e^{ic\varepsilon_l} \rangle = \int_{-\infty}^{+\infty} e^{ic\varepsilon_l} \frac{1}{\sqrt{2\pi}} e^{-\varepsilon_l^2/2} d\varepsilon_l = e^{-c^2/2}. \quad (109)$$

Therefore, after the averaging over the normal distribution of the random variables  $\varepsilon_l$ , Eq. (108) takes the form

$$S(f) = \lim_{T \rightarrow \infty} \frac{2\bar{a}^2}{T} \sum_{k,q} e^{i2\pi f\bar{\tau}q} \prod_{l=1}^k \exp \left\{ -\frac{2\pi^2 f^2 \sigma^2}{\gamma^2} [1 - (1-\gamma)^q]^2 (1-\gamma)^{2(k+1-l)} \right\} \\ \times \prod_{l=k+1}^{k+q} \exp \left\{ -\frac{2\pi^2 f^2 \sigma^2}{\gamma^2} [1 - (1-\gamma)^{k+q+1-l}]^2 \right\} \quad (110)$$

The transition in Eq. (110) from the multiplications of the exponents to the summations in the exponents and transformations, in analogy with Eq. (103) of the two sums' summation indexes  $l \rightarrow k+1-l$  and  $l \rightarrow k+q+1-l$ , respectively, yield, according to Eq. (103), the final expression for the power spectral density:

$$S(f) = \lim_{T \rightarrow \infty} \frac{2\bar{a}^2}{T} \sum_{k,q} e^{i2\pi f\bar{\tau}q - \pi^2 f^2 \sigma^2 g(q)}. \quad (111)$$

Since the expansion of the function  $g(q)$  in powers of  $\gamma|q| \ll 1$  at  $2\gamma k \gg 1$ , according to Eq. (104) and Eq. (105), is

$$g(q) = \frac{1}{\gamma} q^2 - \frac{1}{3} |q|^3 + \frac{1}{2} q^2 \pm \dots \quad (112)$$

for  $f \ll f_\tau = (2\pi\bar{\tau})^{-1}$  and  $f < f_2 = 2\sqrt{\gamma}/\pi\sigma$ , we can replace the summation in Eq. (111) by the integration

$$S(f) = 2\bar{a}\bar{I} \int_{-\infty}^{+\infty} e^{i2\pi f\bar{\tau}q - \pi^2 f^2 \sigma^2 g(q)} dq \quad (113)$$

where  $\bar{I} = \lim_{T \rightarrow \infty} (k_{\max} - k_{\min} + 1)\bar{a}/T = (\bar{\tau})^{-1}$  is the averaged current.

Furthermore, at  $f \gg f_1 = \gamma^{3/2}/\pi\sigma$ , it is sufficient to take into account only the first term of expansion (112),  $g(q) = q^2/\gamma$ . Integration in Eq. (113) hence yields the  $1/f$  spectrum

$$S(f) = 2\bar{a}\bar{I} \int_{-\infty}^{+\infty} \exp \left[ i2\pi f\bar{\tau}q - \frac{(\pi f\sigma)^2}{\gamma} q^2 \right] dq = \bar{I}^2 \frac{\alpha_H}{f}, \quad f_1 < f < f_2, f_\tau \quad (114)$$

where  $\alpha_H$  is a dimensionless constant (the Hooke parameter)

$$\alpha_H = \frac{2}{\sqrt{\pi}} K e^{-K^2}, \quad K = \frac{\bar{\tau}}{\sqrt{2}\sigma_\tau} = \frac{\bar{\tau}\sqrt{\gamma}}{\sigma}. \quad (115)$$

Using an expansion of the function  $g(q)$  at  $\gamma q \gg 1$  according to expansion (105),  $g(q) = 2q/\gamma^2$ , from Eq. (113) we obtain the Lorentzian power spectrum density for  $f < f_1$ :

$$S(f) = 2\bar{a}\bar{I} \frac{\sigma^2}{\bar{\tau}^2\gamma^2} \frac{1}{1 + (\pi f\sigma^2/\bar{\tau}\gamma^2)^2} = \bar{I}^2 \frac{4\tau_{\text{rel}}}{1 + \tau_{\text{rel}}^2\omega^2}. \quad (116)$$

Here  $\omega = 2\pi f$ , and  $\tau_{\text{rel}} = D_t = \sigma^2/2\bar{\tau}\gamma^2$  is the ‘‘diffusion’’ coefficient of the time  $t_k$  according to Eqs. (99) and (100). The model is, therefore, free from the unphysical divergence of the spectrum at  $f \rightarrow 0$ ; for  $f \ll f_0 = \bar{\tau}\gamma^2/\pi\sigma^2 = 1/2\pi\tau_{\text{rel}}$ , we have, from Eq. (116), the white noise

$$S(f) = \bar{I}^2(2\sigma^2/\bar{\tau}\gamma^2). \quad (117)$$

Therefore, the model containing only one relaxation rate  $\gamma$  for a sufficiently small parameter  $\gamma$  can produce an exact  $1/f$ -like spectrum in any desirably wide range of frequency,  $f_1 < f < f_2, f_\tau$ . Furthermore, due to the contribution to the transit times  $t_k$  of the large number of rather separated in time random variables,  $\varepsilon_l$  ( $l = 1, 2, \dots, k$ ), our model represents a ‘‘long-memory’’ random process.

### 3.3 Distribution density of the interpulse time $\tau_k$

Recurrent equation for stochastic increments between pulses  $\tau_k$  (96) can be written as one variable differential Langevin equation in Itô form [160]

$$d\tau_k = h(\tau_k)dk + g(\tau_k)dW, \quad (118)$$

where function  $h(\tau_k)$  corresponds to the drift and function  $g(\tau_k)$  to the diffusion of the interevent time  $\tau_k$ , and  $W(k)$  is a realization of the Wiener process  $W(k) = \int_0^k \xi(k')dk'$ , where  $\xi(t)$  is the white noise source with zero expectation and unit variance [161]. In our model both functions  $h(\tau_k)$  and  $g(\tau_k)$  do not change with time and their expressions are  $h(\tau_k) = -\gamma(\tau_k - \bar{\tau})$  and  $g(\tau_k) = \sigma$ , accordingly. Finally we have differential equation for increments between pulses

$$d\tau_k = -\gamma(\tau_k - \bar{\tau})dk + \sigma dW. \quad (119)$$

The process described by the Langevin equation (118) or (119) with  $\delta$ -correlated random variables  $\langle \xi(t)\xi(t') \rangle = \delta(t - t')$  is a Markov process, i.e., its conditional probability at time  $t_k$  depends only on the value  $\tau_{k-1}$  at the next earlier time. This follows from the fact that a first-order differential equation is uniquely determined by its initial value

and that the  $\delta$ -correlated random variable  $\xi(t)$  at a former time  $t < t_{k-1}$  cannot change the condition probability at a later time  $t > t_{k-1}$ .

From the differential equations (118) and (119) we can write a Fokker-Planck equation for the distribution density  $P_k(\tau_k, t)$  of  $\tau_k$  [161]

$$\begin{aligned} \frac{\partial P_k(\tau_k, t)}{\partial t} &= -\frac{\partial}{\partial \tau_k} [h(\tau_k)P_k(\tau_k, t)] + \frac{1}{2} \frac{\partial^2}{\partial^2 \tau_k} [g^2(\tau_k)P_k(\tau_k, t)] \\ &= \frac{\partial}{\partial \tau_k} [\gamma(\tau_k - \bar{\tau})P_k(\tau_k, t)] + \frac{1}{2} \frac{\partial^2}{\partial^2 \tau_k} [\sigma^2 P_k(\tau_k, t)] \end{aligned} \quad (120)$$

The steady-state solution of (120) does not depend on time,  $P_k(\tau_k, t) = P_k(\tau_k)$ , and, therefore,  $\partial P_k(\tau_k, t)/\partial t = 0$ . In the stationary case we can integrate differential equation (120) analytically, and, taking into account normalization condition  $\int_{-\infty}^{+\infty} P_k(\tau_k) d\tau_k = 1$ , we find the distribution density

$$P_k(\tau_k) = \frac{1}{\sqrt{2\pi}\sigma_\tau} \exp \left\{ -\frac{(\tau_k - \bar{\tau})^2}{2\sigma_\tau^2} \right\}, \quad (121)$$

which is the Gaussian distribution with the mean value  $\bar{\tau}$  and deviation  $\sigma_\tau = \sigma/\sqrt{2\gamma}$ .

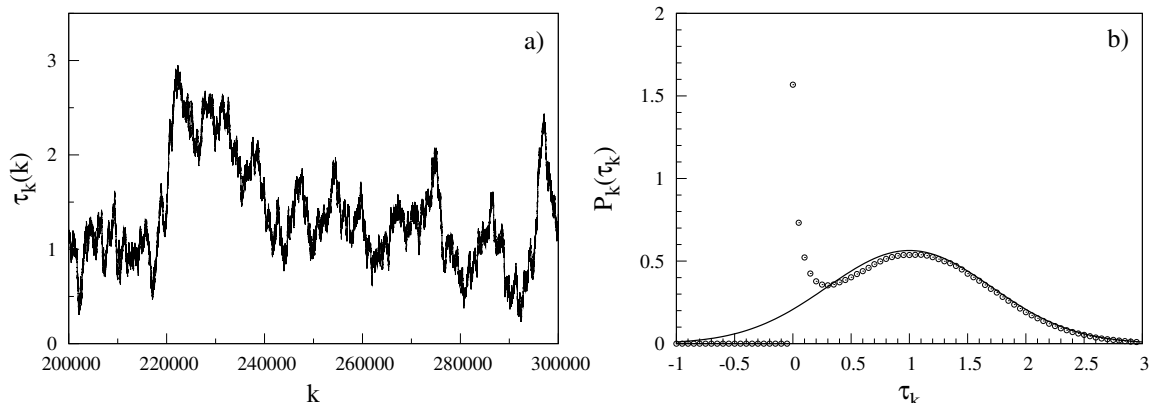


**Figure 2.** Interpulse time  $\tau_k$  of the recurrent sequence (96) a); and the distribution density  $P_k(\tau_k)$  b). Open circles represent numerical simulations of  $N_\tau = 10^6$  points, averaged over  $n = 100$  realizations with parameters  $\bar{\tau} = 1$ ,  $\sigma = 0.01$  and  $\gamma = 0.0001$ ; solid line corresponds to the analytical distribution density, calculated according to Eq. (121).

In Figure 2 we compare distribution density for  $\tau_k$  (121) with the numerical calculation, obtained by generating  $\tau_k$  sequence according to Eq. (96) and calculating distribution density numerically. As we can see, the right hand side of numerically calculated  $\tau_k$  distribution density is in good agreement with the analytically calculated Gaussian distribution. However left hand side of the numerically calculated distribution density is not Gaussian, because while generating time intervals between pulses, we made physical assumption and considered that the time difference  $\tau_k$  cannot be negative. If  $\tau_k = t_k - t_{k-1} < 0$ , it means that event at time  $t_k$  occurred before event at time  $t_{k-1}$ . In order to avoid negative  $\tau_k$  values we constructed a time sequence  $\{t_k\}$  from the sequence of  $\{\tau_k\}$  according to Eq. (96) and rearranged it in increasing order to a new time sequence  $\{t'_k\}$ , where  $t'_{k+1} \geq t'_k$  for all  $k$ . From  $\{t'_k\}$  we calculated new, positive in all points, sequence  $\tau'_k = t'_k - t'_{k-1}$ . Distribution density for  $\tau'_k$  is shown in Figure 2

as open circles. Had we not followed the assumption that all  $\tau_k$  must be positive, we would have had a good agreement with analytical curve on the left hand side of the picture as well.

### 3.4 Non-Gaussian perturbations and numerical analysis

This model may also be generalized for non-Gaussian and for continuous perturbations of the systems' parameters, resulting in the fluctuations of the interpulse time  $\tau$ . So, for perturbations by the non-Gaussian sequence of random impacts  $\{\varepsilon_k\}$  with zero expectations, Eqs. (85) – (106) remain valid. It is only Eq. (111) which describes the averaging over realizations of the process in the case of non-Gaussian perturbations may have a different form. We now consider such situation in greater detail.

The power spectral density (87) may be rewritten in the form

$$S(f) = 2\bar{a}\bar{I} \left\langle \sum_q e^{i2\pi f\tau_k(q)q} \right\rangle, \quad (122)$$

where the difference between the transit times  $t_{k+q}$  and  $t_k$  is expressed as

$$\Delta(k; q) = \sum_{l=k+1}^{k+q} \tau_l = \tau_k(q)q, \quad q \geq 0, \quad (123)$$

and the brackets denote the averaging over the time (index  $k$ ) and over the realizations of the process. Here  $\tau_k(q) \equiv \Delta(k; q)/q$  is the averaged interpulse time between the subsequent transit times in the time interval  $\Delta(k; q)$ . Note that for the slow (diffusive-like) fluctuations of the averaged interval  $\tau_k(q)$  with the change of the index  $k$ , Eq. (123) is valid also when  $q < 0$ , i.e.,  $\Delta(k; q) = \tau_{k+q}(q)q \simeq \tau_k(q)q$ ,  $q < 0$ . The variance  $\sigma_\Delta^2$  of the time difference  $\Delta(k; q)$  for  $|q| \ll \gamma^{-1}$  is a quadratic function of the time difference and, consequently, of the difference  $q$  of the pulse serial numbers  $k$ , i.e.,

$$\sigma_\Delta^2 = \sigma_\tau^2(k)q^2. \quad (124)$$

At  $2\pi f\tau_k(q) \ll 1$  we may replace the summation in Eq. (122) by the integration, and do not take into account the dependence of  $\tau_k(q)$  on  $q$ . In such case Eq. (122) yields

$$S(f) = 2\bar{a}\bar{I} \left\langle \int_{-\infty}^{+\infty} e^{i2\pi f\tau_k q} dq \right\rangle = 2\bar{a}\bar{I} \int_{-\infty}^{+\infty} \langle e^{i2\pi f\tau_k q} \rangle dq. \quad (125)$$

Here, the averaging over  $k$  and over the realizations of the process coincides with the averaging over the distribution of the interpulse times  $\tau_k$ , i.e.,

$$\langle e^{i2\pi f q \tau_k} \rangle = \int_{-\infty}^{+\infty} e^{i2\pi f q \tau_k} P_k(\tau_k) d\tau_k = \chi_\tau(2\pi f q), \quad (126)$$

where  $P_k(\tau_k)$  is a distribution density of interpulse times  $\tau_k$ , and  $\chi_\tau(\vartheta)$  is a characteristic function of the distribution  $P_k(\tau_k)$ . Taking into account the property of the characteristic function,

$$\int_{-\infty}^{+\infty} \chi_\tau(\vartheta) d\vartheta = 2\pi P_k(0), \quad (127)$$

we have from Eqs. (126) and (127), the final expression for the power spectral density:

$$S(f) = 2\bar{a}\bar{I}P_k(0)/f. \quad (128)$$

Substituting into Eq. (128) the value  $P_k(0) = \exp(-\bar{\tau}^2/2\sigma_\tau^2)/\sqrt{2\pi}\sigma_\tau$  for the Gaussian distribution of the interpulse times  $\tau_k$ , we recover results (114) and (115).

Since different processes result in the Gaussian distribution, it is likely that perturbations by non-Gaussian impacts  $\{\varepsilon_k\}$  in Eq. (96) nevertheless yield the Gaussian distribution of the interpulse times  $\tau_k$ .

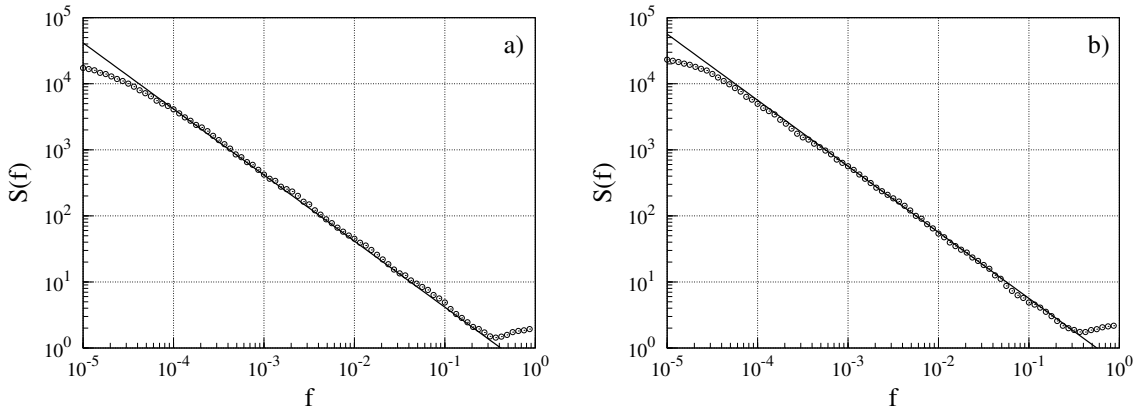


**Figure 3.** Power spectral density vs frequency of the current generated by Eqs. (86) – (96) for  $\bar{\tau} = 1$ ,  $\sigma = 0.01$ ,  $\gamma = 0.0001$  and  $\bar{a} = 1$  with the Gaussian distribution of the random increments  $\{\varepsilon_k\}$  a); and uniform distribution of the  $\{\varepsilon_k\}$  in the interval  $(-0.02, 0.02)$  b). Open circles represent the results of numerical simulations of  $N_\tau = 10^6$  points, averaged over  $n = 100$  realizations, and the solid lines represent the analytical spectra according to Eqs. (114), (115), and (128), respectively.

As an illustrative example, in Figure 3, the numerically calculated power spectral densities of the process (96) with Gaussian and uniform distributions of the random increments  $\{\varepsilon_k\}$  are compared with the analytical calculations according to Eqs. (113) – (117) and (128), respectively. The analytical results are in good agreement with the numerical simulations. For the non-Gaussian distribution of the random perturbations we have no explicit expression analogous to Eq. (113) for the integral representation of the noise power spectral density. Note that analytical results predict not only the slope and intensity of  $1/f$  noise, but the frequency range  $f_1 - f_2$ ,  $f_\tau$  of  $1/f$  noise and the intensity of the very low frequency  $f \ll f_0$  white noise (117) as well.

The proposed point process model (86) – (128) can be modified and useful for the modeling and analysis of self-organized systems [18, 24], atmospheric variability [133, 25, 27, 134, 26], large flares from Gamma-ray Repeaters in astronomy [162], particles moving in viscous fluid [163], dynamical percolation [164],  $1/f$  noise observed in cortical neurons and earthquake data [22], financial markets [42, 165, 44, 45], cognitive experiments [21, 166], the Parkinsonian tremors [23], and time intervals production in tapping and oscillatory motion of the hand [167].

### 3.5 Multifractality of the point process

Multifractality of the point process can be investigated by transition from the point process to the stochastic signal  $I(t)$ , using rectangular pulses (as shown in Section

5.5). Stochastic signal will have the same fractal properties as the origin point process. We calculate a generalized  $q$ th order height-height correlation function (GHCF)  $F_q(t)$  defined as

$$F_q(t) = \langle |I(t' + t) - I(t')|^q \rangle^{1/q}, \quad (129)$$

where the angular brackets denote a time average. The GHCF  $F_q(t)$  characterizes the correlation properties of the signal  $I(t)$ , and for a multiaffine signal a power-law behavior like

$$F_q(t) \sim t^{H_q} \quad (130)$$

is expected, where  $H_q$  is the generalized  $q$ th order Hurst exponent [168]. If  $H_q$  is independent on  $q$ , a single scaling exponent  $H_q$  is involved and the signal  $I(t)$  is said to be monofractal [169, 170, 171]. If  $H_q$  depends on  $q$ , the signal is considered to be multifractal.

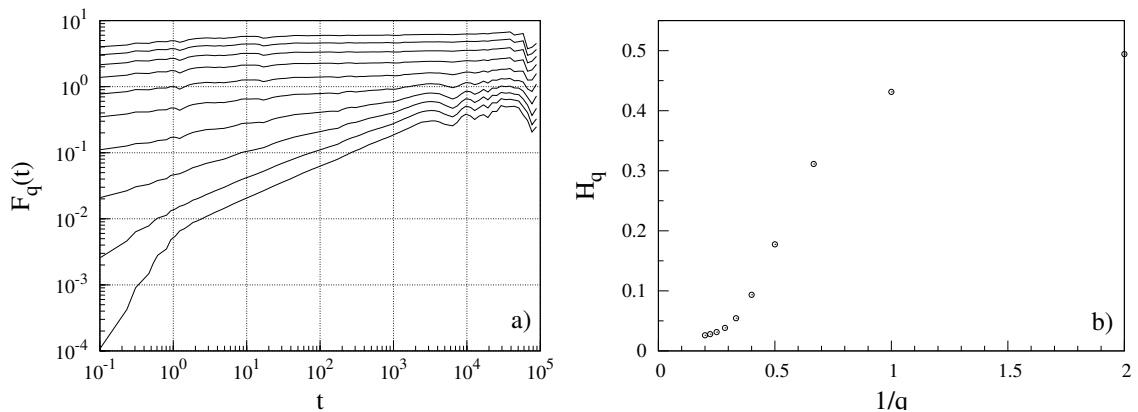


**Figure 4.** a) Generalized height-height correlation function  $F_q(t)$  versus time  $t$  for the signal (86) with  $q = 0.5, 1, 1.5, \dots, 5$  from bottom to top. The signal of  $N_I = 10^6$  points was generated from  $N_\tau = 10^5$  point process points with the parameters  $\bar{\tau} = 1$ ,  $\sigma = 0.01$  and  $\gamma = 0.0001$ . b) The generalized Hurst exponents  $H_q$  versus  $1/q$  for the corresponding GHCF in a) in the scaling regime  $1 < t < 1000$ .

In Figure 4 a) we present the GHCF as a function of the time interval  $t$ . We observe clear multifractal behavior since the slopes of the log-log plot depend on  $q$ . In Figure 4 b) we show a Hurst exponents calculated from GHCF using linear regression dependence on  $1/q$ . This, too, indicates to the multifractality of the point process.

Multifractal models have been used to account for scale invariance properties of various objects in very different domains ranging from the energy dissipation or the velocity field in turbulent flows [172] to financial data [173].

Healthy human heartbeat intervals, rather than being fractal, exhibit multifractal properties and for a life-threatening condition, known as congestive heart failure, there is a loss of multifractality [174]. Cerebral blood flow in healthy humans is also multifractal [175].

The analytically solvable model (86) – (128) and its generalizations contain, however, some shortage of generality, i.e., it results only in exact  $1/f$  (with  $\beta = 1$ ) noise and only if  $P_k(\tau_k) \simeq const$  when  $\tau_k \rightarrow 0$ . On the other hand, the numerical analysis of the generalized model with different restrictions for diffusion of the interpulse time  $\tau_k$  reveals  $1/f^\beta$  spectra with  $1 \lesssim \beta \lesssim 1.5$  [61, 62].

The aims of next sections 3.6 – 4.4 are to generalize the analytical model seeking to define the variety of time series, exhibiting the power spectral density  $S(f) \sim 1/f^\beta$  with  $0.5 \lesssim \beta \lesssim 2$  and to analyze the relation of the point process model with the Bernamont-Surdin-McWhorter model [68, 69, 70, 71, 53], representing the signal as a sum of the appropriate signals with the different rates of the linear relaxation.

### 3.6 Generalization of the point process model

In a point process the power spectrum of the signal is completely described by the set of the interevent intervals  $\tau_k$ . Moreover, the low frequency noise is defined by the statistical properties of the signal at a large-time-scale, i.e., by the fluctuations of the time difference  $\Delta(k; q)$  at large  $q$ , determined by the slow dynamics of the average interpulse time  $\tau_k(q) = \Delta(k; q)/q$  between the occurrence of pulses  $k$  and  $k + q$ . In such case quite generally the dependence of the average interevent time  $\tau_k$  on the occurrence number  $k$  may be described by the general Langevin equation with the drift coefficient  $h(\tau_k)$  and a multiplicative noise  $g(\tau_k)\xi(k)$ , Eq. (118) [44, 45],

$$\frac{d\tau_k}{dk} = h(\tau_k) + g(\tau_k)\xi(k). \quad (131)$$

Here we interpret  $k$  as a continuous variable while the white Gaussian noise  $\xi(k)$  satisfies the standard condition

$$\langle \xi(k)\xi(k') \rangle = \delta(k - k') \quad (132)$$

with the brackets  $\langle \dots \rangle$ , denoting the averaging over the realizations of the process. We understand the equation (131) in Itô interpretation.

Perturbative solution of Eq. (131) in the vicinity of  $\tau_k$  yields

$$\tau_{k+j} \simeq \tau_k + h(\tau_k)j + g(\tau_k) \int_k^{k+j} \xi(l)dl, \quad (133)$$

$$\Delta(k; q) = \sum_{i=k}^{k+q-1} \tau_i \simeq \int_0^q \tau_{k+j}dj \simeq \tau_k q + h(\tau_k) \frac{q^2}{2} + g(\tau_k) \int_0^q dj \int_k^{k+j} \xi(l)dl. \quad (134)$$

After integration by parts we have

$$\Delta(k; q) = \tau_k q + h(\tau_k) \frac{q^2}{2} + g(\tau_k) \int_k^{k+q} (k + q - l)\xi(l)dl, \quad (135)$$

$$\langle \Delta(k; q) \rangle = \tau_k q + h(\tau_k) \frac{q^2}{2}. \quad (136)$$

Analogously, in the same approximation we can also obtain the variance  $\sigma_\Delta^2(k; q) = \langle \Delta(k; q)^2 \rangle - \langle \Delta(k; q) \rangle^2$  of the time difference  $\Delta(k; q)$ ,

$$\sigma_\Delta^2(k; q) = g^2(\tau_k) \frac{q^3}{3}. \quad (137)$$

Substituting Eqs. (135) and (136) into Eq. (87) and replacing the averaging over  $k$  by the averaging over the distribution of the interevent times  $\tau_k$  we have

$$S(f) = 4\bar{I}^2\bar{\tau} \int_0^\infty d\tau_k P_k(\tau_k) \operatorname{Re} \int_0^\infty dq \exp \left\{ i2\pi f \left[ \tau_k q + h(\tau_k) \frac{q^2}{2} \right] \right\} \\ = \frac{2\bar{I}^2\bar{\tau}}{\sqrt{\pi}f} \int_0^\infty P_k(\tau_k) \operatorname{Re} \left[ e^{-i(x-\frac{\pi}{4})} \operatorname{erfc}\sqrt{-ix} \right] \frac{\sqrt{x}}{\tau_k} d\tau_k \quad (138)$$

where  $x = \pi f \tau_k^2 / h(\tau_k)$ .

Approach (138) is the improvement of the simplest model of the pure  $1/f$  noise (96) taking into account the second, drift, term  $h(\tau_k)q^2/2$  in expression for  $\Delta(k; q)$ . Note, that for  $h(\tau_k) \rightarrow 0$  from Eq. (138) we recover result (128).

According to Eqs. (128) and (138) the small interevent times and the clustering of the pulses make the greatest contribution to  $1/f^\beta$  noise. The power-law spectral density is frequently related with the power-law behavior of other characteristics of the signal, such as an autocorrelation function, probability densities and other statistics, and with the fractality of the signals, in general [31, 38, 32, 39, 43]. Therefore, we investigate the power-law dependences of the drift coefficient and of the distribution density on the time  $\tau_k$  in some interval of the small interevent times, i.e.,

$$h(\tau_k) = \gamma\tau_k^\delta, \quad P_k(\tau_k) = C\tau_k^\alpha, \quad \tau_{\min} \leq \tau_k \leq \tau_{\max} \quad (139)$$

where the coefficient  $\gamma$  represents the rate of the signal relaxation and  $C$  has to be defined from the normalization.

The power-law distribution of the interpulse, interevent, interarrival, recurrence or waiting time is observable in different systems ranging from physics, astronomy and seismology to the Internet, financial markets and neural spikes (see, e.g., [31, 176, 149, 148, 177, 178, 18, 24] and references herein).

Because of the divergence of the power-law distribution and requirement of the stationarity of the process, the stochastic diffusion may be realized over a certain range of the variable  $\tau_k$  only. Therefore, we restrict the diffusion of  $\tau_k$  in the interval  $[\tau_{\min}, \tau_{\max}]$  with the appropriate boundary conditions. Then, the steady state solution of the stationary Fokker-Planck equation (120) with a zero flow corresponding to Eq. (131) is [161]

$$P_k(\tau_k) = \frac{C}{g^2(\tau_k)} \exp \left\{ 2 \int_{\tau_{\min}}^{\tau_k} \frac{h(\tau)}{g^2(\tau)} d\tau \right\}. \quad (140)$$

Then equations (138) and (139) yield the power spectra with different slopes  $\beta$ , i.e.,

$$S(f) = \frac{2\bar{I}^2}{\sqrt{\pi}(2-\delta)f} \left( \frac{f_0}{f} \right)^{\frac{\alpha}{2-\delta}} I_\kappa(x_{\min}, x_{\max}), \quad (141)$$

$$I_\kappa(x_{\min}, x_{\max}) = \operatorname{Re} \int_{x_{\min}}^{x_{\max}} e^{-i(x-\frac{\pi}{4})} \operatorname{erfc}(\sqrt{-ix}) x^\kappa dx. \quad (142)$$

Here  $\bar{I}$  is the average signal,  $\kappa = \frac{\alpha}{2-\delta} - \frac{1}{2}$ ,  $x_{\min} = f/f_2$ ,  $x_{\max} = f/f_1$ ,

$$f_0 = \frac{\gamma}{\pi} (C\bar{\tau})^{\frac{2-\delta}{\alpha}}, \quad f_1 = \frac{\gamma}{\pi\tau_{\max}^{2-\delta}}, \quad f_2 = \frac{\gamma}{\pi\tau_{\min}^{2-\delta}}. \quad (143)$$

Note that  $f_0$  is indefinite when  $\alpha \rightarrow 0$ , however,  $f_0^{\frac{\alpha}{2-\delta}}$  is definite and converges to  $C\bar{\tau}$  in this limit.

We note the special cases of the power spectral density (141).

(i)  $f_1 \ll f \ll f_2$ ,  $-1 < \kappa < 1/2$ ,

$$S(f) = \frac{\Gamma(1+\kappa)\bar{I}^2}{\sqrt{\pi}(2-\delta)\cos[(\kappa/2+1/4)\pi]f} \left(\frac{f_0}{f}\right)^{\kappa+\frac{1}{2}}, \quad (144)$$

i.e.,  $S(f) \sim 1/f^{1+\frac{\alpha}{2-\delta}}$  and  $S(f) \sim 1/f$  for  $\alpha = 0$ , in accordance with Eq. (128).

(ii)  $f \ll f_1$ ,  $\kappa > -1$ ,

$$S(f) = \frac{\bar{I}^2}{(1+\alpha-\delta/2)} \left(\frac{f_0}{f_1}\right)^{\frac{\alpha}{2-\delta}} \sqrt{\frac{2}{\pi f_1 f}}, \quad (145)$$

i.e., for very low frequencies  $S(f) \sim 1/\sqrt{f}$ .

(iii)  $f \gg f_2$ ,  $\kappa < 1/2$ ,

$$S(f) = \frac{\bar{I}^2}{\sqrt{\pi}(2-\alpha-\delta)} \left(\frac{f_0}{f_2}\right)^{\frac{\alpha}{2-\delta}} \frac{f_2}{f^2}, \quad (146)$$

i.e., for high frequencies  $S(f) \sim 1/f^2$ .

For very high frequencies  $f \gg \tau_{\max}^{-1}$ , however, we cannot replace the summation in Eq. (87) by the integration. Then from Eq. (87) one gets the shot noise  $S(f) = 2\bar{a}\bar{I}$ .

Equations (141) and (144) – (146) reveal that the proposed model of the stochastic point process may result in the power-law spectra over several decades of low frequencies with the slope  $\beta$  between 0.5 and 2.

The simplest and well-known process generating the power-law probability distribution function for  $\tau_k$  is a multiplicative stochastic process with  $g(\tau_k) = \sigma\tau_k^\mu$  and  $\delta = 2\mu - 1$ , written as

$$\tau_{k+1} = \tau_k + \gamma\tau_k^{2\mu-1} + \sigma\tau_k^\mu\varepsilon_k. \quad (147)$$

Here  $\gamma$  represents the nonlinear relaxation of the signal, while  $\tau_k$  fluctuates due to the perturbation by normally distributed uncorrelated random variables  $\varepsilon_k$  with a zero expectation and unit variance and  $\sigma$  is a standard deviation of the white noise. According to Eq. (140), the steady state solution of the stationary Fokker-Planck equation with a zero flow, corresponding to Eq. (147), gives the power-law probability density function for  $\tau_k$  in the  $k$ -space,

$$P_k(\tau_k) = \frac{1+\alpha}{\tau_{\max}^{1+\alpha} - \tau_{\min}^{1+\alpha}} \tau_k^\alpha, \quad \alpha = \frac{2\gamma}{\sigma^2} - 2\mu. \quad (148)$$

The power spectrum for the intermediate  $f$ ,  $f_1 \ll f \ll f_2$ , according to Eq. (144) is

$$S(f) = \frac{(2+\alpha)(\beta-1)\bar{a}^2\Gamma(\beta-1/2)}{\sqrt{\pi}\alpha(\tau_{\max}^{2+\alpha} - \tau_{\min}^{2+\alpha})\sin(\pi\beta/2)} \left(\frac{\gamma}{\pi}\right)^{\beta-1} \frac{1}{f^\beta} \quad (149)$$

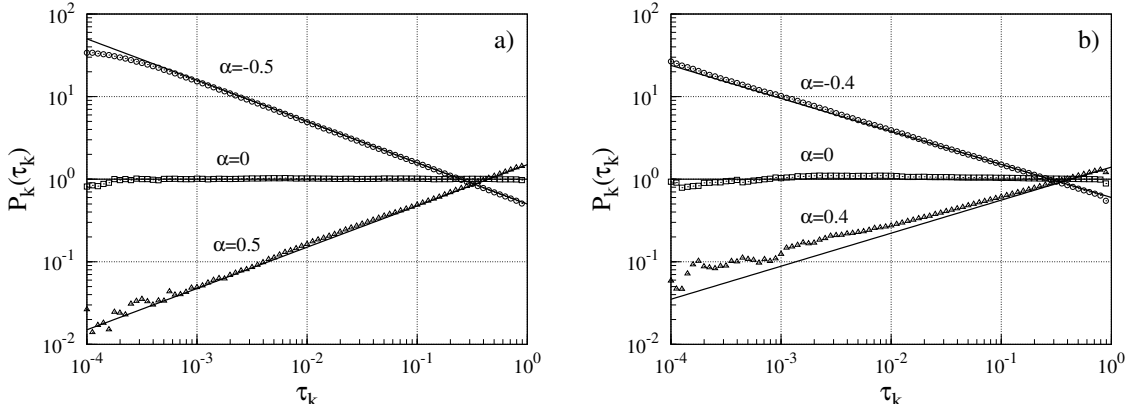


**Figure 5.** Distribution density  $P_k(\tau_k)$  of  $\tau_k$  generated according to Eqs. (147) with the parameters a)  $\mu = 0.5$ ,  $\sigma = 0.02$  and different relaxations of the signal  $\gamma = 0.0001$  (open circles),  $0.0002$  (open squares),  $0.0003$  (open triangles); and b)  $\mu = 1$ ,  $\sigma = 0.1$  and  $\gamma = 0.008$  (open circles),  $0.01$  (open squares),  $0.012$  (open triangles). We restrict the diffusion of the interevent time in the interval  $\tau_{\min} = 10^{-6}$ ,  $\tau_{\max} = 1$  with the reflective boundary condition at  $\tau_{\min}$  and transition to the white noise,  $\tau_{k+1} = \tau_{\max} + \sigma\varepsilon_k$ , for  $\tau_k > \tau_{\max}$  and  $n = 100$  realizations with  $N_\tau = 10^6$  points each were used. Solid lines represent distributions, calculated according to Eq. (148).

where

$$\beta = 1 + \frac{\alpha}{3 - 2\mu}, \quad \frac{1}{2} < \beta < 2. \quad (150)$$

For  $\mu = 1$  we have a completely multiplicative point process when the stochastic change of the interevent time is proportional to itself. Multiplicativity is an essential feature of the financial time series, economics, some natural and physical processes [179, 180].

Another case of interest concerns  $\mu = 1/2$ , when the Langevin equation in the actual time takes the form

$$\frac{d\tau}{dt} = \gamma \frac{1}{\tau} + \sigma\xi(t), \quad (151)$$

i.e., the Brownian motion of the interevent time with the linear relaxation of the signal  $I \simeq \bar{a}/\tau$ .

In Figure 5 we present the distribution density of  $\tau_k$ , generated according to (147) for different parameters. We can see that the distribution density exhibits a power-law distribution described by Eq. (148).

Figure 6 represents the spectral densities with the different slopes  $\beta$  of the signals generated numerically according to Eqs. (86), (87) and (147) for different parameters of the model. We see that the simple iterative equation (147) with the multiplicative noise produces the signals with the power spectral density of different slopes, depending on the parameters of the model. The agreement of the numerical results with the approximate theory is quite good, especially for the case with  $\mu = 1/2$ .

It should be noted that the low frequency noise is insensitive to the small additional fluctuations of the particular occurrence times  $t_k$ . Therefore, we can interpret that Eqs. (131), (147) and (149) describe the slow diffusive motion of the average interevent time, superimposed by some additional randomness.

On the other hand, the numerical investigations have shown that the proposed model is stable with respect to variation of dynamics of the interevent time  $\tau_k$ . The

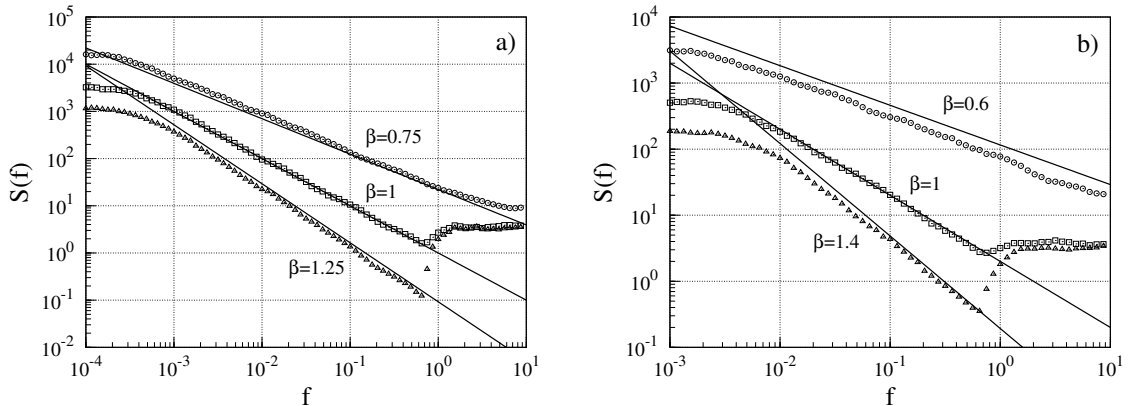


**Figure 6.** Power spectral density (87) vs frequency of the signal generated by Eqs. (86) and (147). The parameters used are the same as in Figure 5. The solid lines represent the analytical results according to Eq. (144).

substitution of the reflecting boundaries for  $\tau_k$  by an appropriate confining potential does not change the result.

The origin for appearance of  $1/f$  fluctuations in the point process model is related with the slow, Brownian fluctuations of the interpulse time  $\tau_k$  as a function of the pulse number  $k$ , when the average interpulse time  $\tau_k(q)$  is a slowly fluctuating function of the arguments  $k$  and  $q$ . In such case transition from the occurrence number  $k$  to the actual time  $t$  according to the relation  $dt = \tau_k dk$  yields the probability distribution density  $P_t(\tau_k)$  of  $\tau_k$  in the actual time  $t$ ,

$$P_t(\tau_k) = P_k(\tau_k)\tau_k/\bar{\tau}. \quad (152)$$

The signal averaged over the time interval  $\tau_k$  according to Eq. (86) is  $I = \bar{a}/\tau_k$ . Therefore, the distribution density of the intensity of the point process (86) averaged over the time interval  $\tau_k$  is

$$P(I) = \frac{\bar{a}\bar{I}}{\bar{I}^3} P_k\left(\frac{\bar{a}}{I}\right). \quad (153)$$

If  $P_k(\tau_k) \simeq \text{const}$  when  $\tau_k \rightarrow 0$  (the condition for the exhibition for the pure  $1/f$  noise in the point process model) the distribution density of the signal is

$$P(I) \sim I^{-3}. \quad (154)$$

For the generalized multiplicative processes (86), (131), and (139) we have from Eqs. (148) and (153) the power-law distribution density of the signal intensity

$$P(I) = \frac{\lambda - 1}{\tau_{\max}^{\lambda-1} - \tau_{\min}^{\lambda-1}} \frac{\bar{a}^{\lambda-1}}{I^\lambda}, \quad \lambda = 3 + \alpha. \quad (155)$$

The power-law distribution of the signals is observed in a large variety of systems, ranging from earthquakes to the financial time series ([31, 132, 157, 181, 182, 183, 184, 38, 32, 39, 43, 185, 186, 187, 124, 188, 189] and references herein).

In Figure 7 we present the distribution density of the signals, calculated from the point processes described by Eq. (147) with the transition from the point process to the stochastic signal using rectangular pulses (as in Section 5.5).

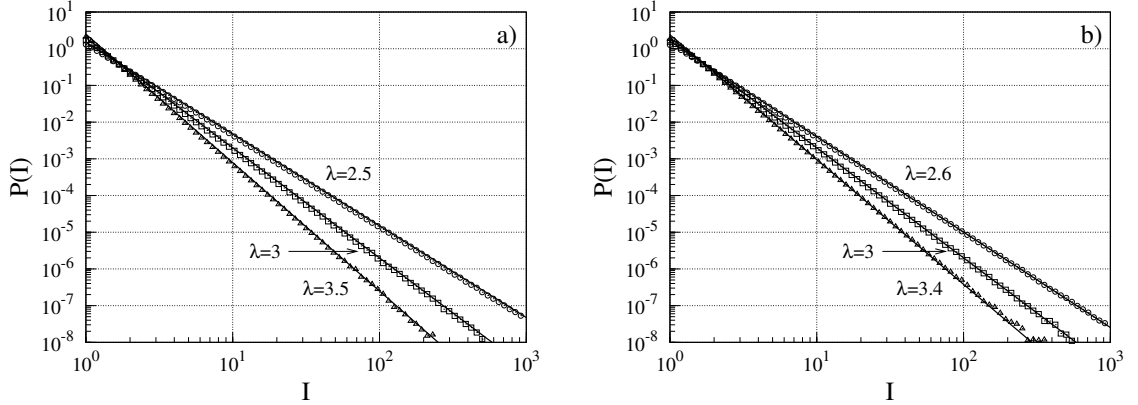


**Figure 7.** Distribution density  $P(I)$  of the signal (86). The parameters used are the same as in Fig 5. The solid lines represent the analytical results according to Eq. (155).

### 3.7 Correlation function

The correlation function  $C(s)$  of the point process (86) may be found from the Wiener-Khinchine relations or expressed as

$$\begin{aligned}
 C(s) &= \left\langle \frac{1}{T} \int_{t_i}^{t_f-s} I(t)I(t+s)dt \right\rangle = \left\langle \frac{\bar{a}^2}{T} \sum_{k,q} \delta(\Delta(k;q) - s) \right\rangle \\
 &= \bar{a}\bar{I} \sum_q \int_{-\infty}^{+\infty} \Psi_q[\Delta(q)]\delta(\Delta(q) - s)d\Delta(q) = \bar{a}\bar{I} \sum_q \Psi_q(s), \quad (156)
 \end{aligned}$$

where the brackets  $\langle \dots \rangle$  denote the averaging over the realizations of the process and over time (index  $k$ ) as well. Such averaging coincides with the averaging over the distribution of the time difference  $\Delta(q)$ ,  $\Psi_q[\Delta(q)]$ . For approximation (123) expression (156) for the correlation function is

$$C(s) \simeq \bar{a}\bar{I} \sum_q \langle \delta(\tau_k q - s) \rangle. \quad (157)$$

Averaging over realizations of the process  $\langle \dots \rangle$  coincidences with the averaging over the distribution of time differences  $\tau_k$ , i.e.,

$$C(s) \simeq \bar{a}\bar{I} \sum_q \int_{-\infty}^{\infty} P_k(\tau_k)\delta(\tau_k q - s)d\tau_k = \bar{a}\bar{I}\delta(s) + \bar{a}\bar{I} \sum_{q \neq 0} P_k\left(\frac{s}{q}\right) \frac{1}{|q|}. \quad (158)$$

Replacing the summation in Eq. (158) by the integration we have the approximate expression for the correlation function of the point processes (86) and (96) or (131)

$$C(s) \simeq \bar{a}\bar{I} \int_0^{\infty} P_k\left(\frac{s}{q}\right) \frac{dq}{q}, \quad s \geq 0, \quad C(-s) = C(s). \quad (159)$$

For the Gaussian distribution of the interevent time  $\tau_k$ , Eq. (121), the correlation function (158) reads as

$$C(s) = \frac{\bar{a}\bar{I}}{\sqrt{2\pi}\sigma_\tau} \sum_q \exp\left\{-\frac{(s - q\bar{\tau})^2}{2\sigma_\tau^2 q^2}\right\} \frac{1}{|q|}. \quad (160)$$

It should be noted that the deviation of the variance  $\sigma_{\Delta}^2$  for large  $q$  from the quadratic dependence (124) and the approach to the linear function  $\sigma_{\Delta}^2 = 2D_{t_k}|q|$  ensures the convergence of sums (158) and (160) and, consequently, results in the Lorentzian power spectrum at  $f \rightarrow 0$  [60, 57, 61]. Here  $D_{t_k}$  is the “diffusion” coefficient of the pulse occurrence time  $t_k$ , related with the variance  $\sigma_{\tau_k}^2$  of the pulse occurrence time as  $\sigma_{\tau_k}^2 = 2D_{\tau_k}k$ . For the model (96),  $D_{t_k} = \sigma^2/2\gamma^2$ .

## 4 SUPERPOSITION OF SIGNALS WITH LINEAR RELAXATIONS

### 4.1 Lorentzian spectrum

Consider a signal  $I_l(t)$  generated of the stochastic differential equation with the relaxation time  $\tau_l^{rel} = 1/\gamma_l$ ,

$$\dot{I}_l = -\gamma_l(I_l - \bar{I}_l) + \sigma_l \xi_l(t). \quad (161)$$

Here  $\bar{I}_l$  is the average value of the signal component  $I_l$ ,  $\xi_l(t)$  is the white noise source with zero expectation and unit variance, and  $\sigma_l$  is the intensity (standard deviation) of the white noise. Solution of differential equation (161) is

$$I_l(t) = \int_0^t e^{-\gamma_l(t-t')} [\gamma_l \bar{I}_l + \sigma_l \xi_l(t')] dt'. \quad (162)$$

When observation time  $T \rightarrow \infty$  Eq. (162) results in the expression for the correlation function of the signal

$$C_l(s) = \lim_{T \rightarrow \infty} \left\langle \frac{1}{T} \int_{t_i}^{t_f-s} I_l(t) I_l(t+s) dt \right\rangle = \frac{\sigma_l^2}{2\gamma_l} e^{-\gamma_l s} + \bar{I}_l^2, \quad s \geq 0. \quad (163)$$

According to Wiener-Khintchine relations the correlation function (163) yields the power spectrum of the signal  $I_l$

$$S_l(f) = 2 \lim_{T \rightarrow \infty} \int_{-T}^T C_l(s) e^{i2\pi f s} ds = \frac{2\sigma_l^2}{\gamma_l^2 + (2\pi f)^2} + 2\delta(f) \bar{I}_l^2. \quad (164)$$

The steady-state solution of the stationary Fokker-Planck equation corresponding to stochastic Eq. (161) yields distribution density of the signal  $I_l$

$$P_l(I_l) = \frac{1}{\sqrt{2\pi}\sigma_I^{(l)}} \exp \left\{ -\frac{(I_l - \bar{I}_l)^2}{2\sigma_I^{(l)2}} \right\}, \quad (165)$$

which is the Gaussian distribution with  $\sigma_I^{(l)} = \sigma_l/\sqrt{2\gamma_l}$ .

To generate a Lorentzian signal we can rewrite differential equation (161) in the recurrent form

$$I_l^{(k)} = I_l^{(k-1)} - \gamma_l(I_l^{(k-1)} - \bar{I}_l)\Delta t + \sigma_l \varepsilon_l^{(k)} \sqrt{\Delta t}. \quad (166)$$

Using the recurrent relation (166), we can generate signal  $I_l^{(k)}(k\Delta t)$ ,  $k = 1, \dots, N-1$ . We choose initial signal value equal to the signal average  $I_l^{(0)} = \bar{I}_l$  and the signal duration time then is  $T = N\Delta t$ .

In Figure 8 a sample signal, numerically generated according to Eq. (166), is presented and the signal's distribution density, calculated numerically from the signal and calculated from Eq. (165), are compared. As we can see, both distribution densities are in good agreement.

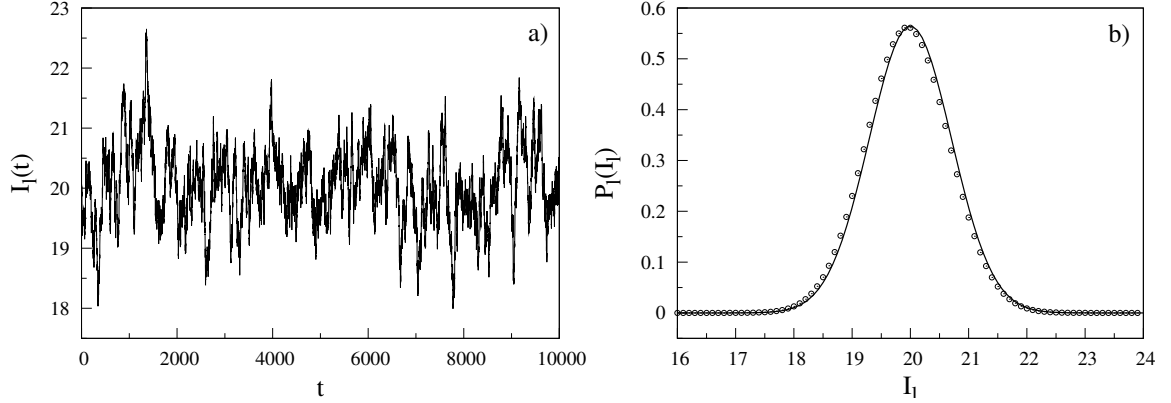


**Figure 8.** a) Signal (161) sample; and b) the signal (161) distribution density (open circles), numerically calculated according to Eq. (166) with parameters  $\sigma_l = 0.1$ ,  $\gamma = 0.01$ , and  $\bar{I} = 20$ . The signal was generated from  $N_I = 10^6$  points with  $\Delta t = 1$ . Solid line in b) represents distribution density according to Eq. (165).

When we have the generated signal in constant time intervals  $I_l^{(k)}(k\Delta t)$  we can calculate the power spectral density of the signal by replacing integration by the summation,

$$S_l(f) = \frac{2}{N\Delta t} \left| \int_0^{N\Delta t} I_l(t) e^{-i2\pi ft} dt \right|^2 = \frac{2\Delta t}{N} \left| \sum_{k=0}^{N-1} I_l^{(k)} e^{-i2\pi fk\Delta t} \right|^2. \quad (167)$$

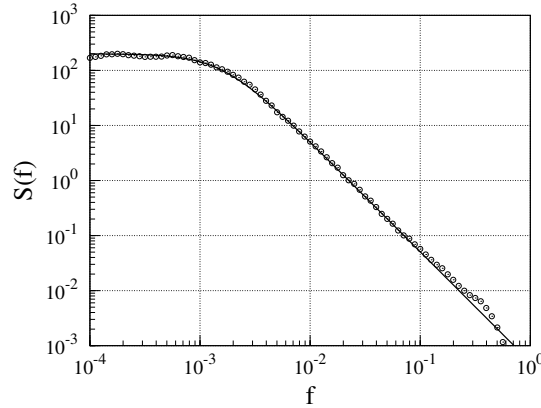


**Figure 9.** The power spectral density calculated for signal (166) using Fast Fourier Transform (167) – (169) and averaged over  $n = 100$  realizations (open circles). The solid line represents the power spectral density calculated according to Eq. (164).

For calculation of the sum in Eq. (167) we can use libraries for the Fast Fourier Transform for a complex variables calculation. Fast Fourier Transform

$$x_j = \sum_{k=0}^{N-1} z_k e^{-i2\pi jk/N} \quad (168)$$

calculates complex values  $\{x_j\}$  in discrete constant intervals from the sequence  $\{z_k\}$  of the stochastic variable  $z_k$ . Libraries allow to calculate the discrete power spectral

density  $S_l(f_j)$ ,

$$S_l(f_j) = \frac{2\Delta t}{N} \left| \sum_{k=0}^{N-1} I_l^{(k)} e^{-i2\pi jk/N} \right|^2, \quad (169)$$

at discrete points  $f_j = j\Delta f = j/N\Delta t$ , where  $j = 0, \dots, N/2$ .

In Figure 9 the comparison of power spectral density obtained by numerically generation of the signal according to Eq. (166) and applying Fast Fourier Transform (167) – (169) with the power spectral density calculated according to analytical Eq. (164) is shown.

## 4.2 Superposition of the Lorentzian spectra

$1/f$  noise is often modeled as the superposition of the Lorentzian spectra with the appropriate weights of a wide range distribution of the relaxation times  $\tau^{rel}$ . It should be noted that the summation of the spectra is allowed only if the processes with different relaxation times are isolated one from another [72, 68, 69, 70, 71, 53, 190, 83, 191, 192]. For construction of the signal  $I(t)$  with  $1/f$  noise spectrum from the stochastic equations with a wide range distribution of the relaxation times, one should express the signal as a sum of uncorrelated components [63]

$$I(t) = \sum_l I_l(t) \quad (170)$$

where every component  $I_l$  satisfies the stochastic equation (161).

The distribution density  $P(I)$  of the signal  $I(t)$ , Eq. (170), expressed as a sum of uncorrelated Gaussian components, is Gaussian as well,

$$P(I) = \frac{1}{\sqrt{2\pi}\sigma} \exp \left\{ -\frac{(I - \bar{I})^2}{2\sigma^2} \right\}, \quad (171)$$

with the average value  $\bar{I}$  and the variance  $\sigma^2$  expressed as

$$\bar{I} = \sum_l \bar{I}_l, \quad \sigma^2 = \sum_l \frac{\sigma_l^2}{2\gamma_l}. \quad (172)$$

Therefore, the Bernamont-Surdin-McWhorter model based on the sum of signals with a wide range distribution of the relaxation times, always results in the Gaussian distribution of the signal intensity. However, not all signals exhibiting  $1/f$  noise are Gaussian [13, 14, 16, 17]. Some of them are non-Gaussian, exhibiting power-law distribution or even fractal [31, 38, 32, 39, 43].

When observation time  $T \rightarrow \infty$  Eqs. (162) and (170) results in the expression for the correlation function of the signal:

$$C(s) = \lim_{T \rightarrow \infty} \left\langle \frac{1}{T} \int_{t_i}^{t_f-s} I(t)I(t+s)dt \right\rangle = \sum_l \left[ \frac{\sigma_l^2}{2\gamma_l} e^{-\gamma_l s} + \bar{I}_l^2 \right], \quad s \geq 0. \quad (173)$$

Introducing the distribution of the relaxations rates,  $g(\gamma)$ , we can replace the summation in Eq. (173) by the integration

$$C(s) = \int_{\gamma_{\min}}^{\gamma_{\max}} g(\gamma) \left[ \frac{\sigma^2(\gamma)}{2\gamma} e^{-\gamma s} + \bar{I}^2(\gamma) \right] d\gamma, \quad s \geq 0, \quad (174)$$

where  $\gamma_{\min}$  and  $\gamma_{\max}$  are minimal and maximal values of relaxation rate, respectively. Then the correlation function (174) yields the power spectral density of the signal (170)

$$S(f) = \int_{\gamma_{\min}}^{\gamma_{\max}} \frac{2\sigma^2(\gamma)g(\gamma)}{\gamma^2 + (\omega)^2} d\gamma = \frac{1}{\pi f} \int_{\gamma_{\min}/\omega}^{\gamma_{\max}/\omega} \frac{\sigma^2(\omega x)g(\omega x)}{1 + x^2} dx, \quad \omega = 2\pi f. \quad (175)$$

Eq. (175) yields the  $1/f$  power spectral density only in case when  $\sigma^2(\omega x)g(\omega x) = \sigma^2(\gamma)g(\gamma) = A = \text{const}$ . In such case we can integrate (175) and find approximate power spectral density

$$S(f) = \frac{A}{\pi f} \left[ \arctan\left(\frac{\gamma_{\max}}{\omega}\right) - \arctan\left(\frac{\gamma_{\min}}{\omega}\right) \right] \simeq \frac{A}{2f}, \quad \gamma_{\min} \ll \omega \ll \gamma_{\max}. \quad (176)$$

When condition  $\sigma^2(\omega x)g(\omega x) = \text{const}$  is met the correlation function (174) may be expressed as

$$C(s) \simeq \int_{\gamma_{\min}}^{\gamma_{\max}} e^{-\gamma s} \frac{d\gamma}{\gamma} = \int_{\tau_{\min}}^{\tau_{\max}} e^{-s/\tau^{rel}} \frac{d\tau^{rel}}{\tau^{rel}}, \quad (177)$$

were  $\tau_{\min} = 1/\gamma_{\min}$  and  $\tau_{\max} = 1/\gamma_{\max}$ .

On the other hand, after replacing the summation in Eq. (159) by the integration we have the expression for the correlation function of the point process (85)

$$C(s) \simeq \bar{a}\bar{I} \int_0^{\infty} P_k\left(\frac{s}{q}\right) \frac{dq}{q}, \quad s \geq 0. \quad (178)$$

We see the similarity of expressions (178) and (177) for the correlation function of the point process model and that of the sum of signals with different relaxation rates, respectively. In general, however, different distributions  $P_k(\tau_k)$  of the interpulse time  $\tau_k$  when  $P_k(0) \neq 0$ , e.g., exponential, the Gaussian and continuous distributions with the slowly fluctuating interpulse time  $\tau_k$  may result in  $1/f$  noise. Therefore, the point process model is, in some sense, more general than the model based on the sum of the Lorentzian spectra.

For the signal expressed not as a sum (170) but as an average of  $N$  uncorrelated components,

$$I_a(t) = \frac{1}{N} \sum_{l=1}^N I_l(t), \quad (179)$$

all characteristics (171) – (177) are similar, except that the average value  $\bar{I}_a$  of the averaged signal (179) is  $N$  times smaller than that according to Eq. (172), while the expressions for the correlation function  $C(s)$ , Eq. (177), for the power spectral density  $S(f)$ , Eqs. (175) and (176), and for the variance  $\sigma_a^2$ , Eq. (172), should be divided by  $N^2$ , i.e.,

$$\bar{I}_a = \frac{1}{N} \sum_l \bar{I}_l, \quad \sigma_a^2 = \frac{1}{N^2} \sum_l \frac{\sigma_l^2}{2\gamma_l}, \quad (180)$$

$$S_a(f) \simeq \frac{A}{2N^2 f}, \quad (181)$$

$$C_a(s) = \frac{1}{2N^2} \int_{\gamma_{\min}}^{\gamma_{\max}} \frac{e^{-\gamma s}}{\gamma} \sigma^2(\gamma) g(\gamma) d\gamma. \quad (182)$$

When replacing the summation in Eqs. (170), (172) – (175) and (179) – (182) by the integration, the distribution density of the relaxation rates,  $g(\gamma)$ , should be normalized to the number of uncorrelated components  $N$ ,

$$\int_{\gamma_{\min}}^{\gamma_{\max}} g(\gamma) d\gamma = N. \quad (183)$$

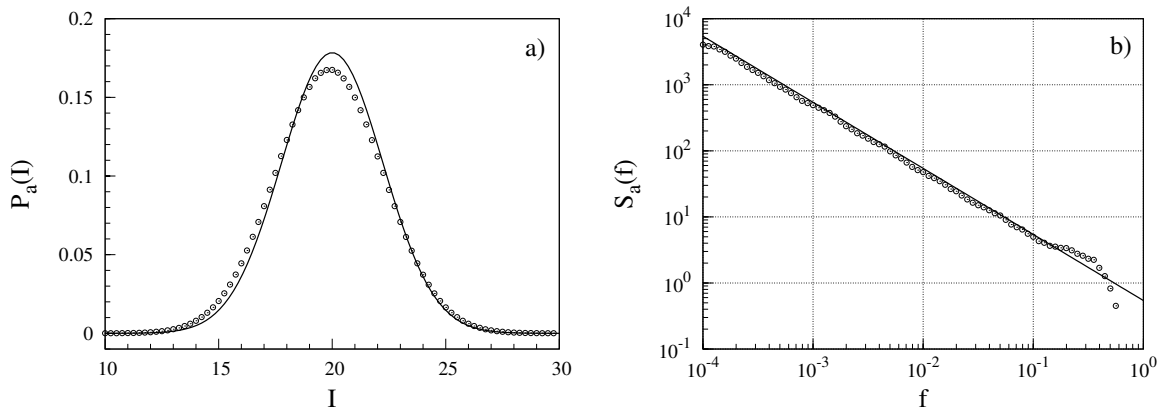


**Figure 10.** a) Signal distribution density; and b) power spectral density calculated for signal (179) from  $N = 10$  components with  $A = \sigma^2(\gamma)g(\gamma) = 10.8574$  and uniform distribution of  $\lg \gamma$  of  $\gamma$  values in the interval  $10^{-4} - 10$  with the parameter  $\bar{I} = 20$ , open circles. Signals were generated from  $N_I = 10^6$  points, averaged over  $n = 100$  realizations, and Fast Fourier Transformation was used for numerical calculation of the power spectral density. Solid lines represent the distribution density, calculated according Eqs. (171) and (180); and the power spectral density, calculated according to approximation (181).

In Figure 10 the example of the signal distribution density and of the power spectral density generated from the superposition of the averaged (179) Lorentzian signals (161) are presented. To create a resulting signal, we used 10 Lorentzian signals with  $\bar{I}_i = 20$  and different  $\gamma$  values, but we preserved condition  $\sigma^2(\gamma)g(\gamma) = \text{const}$ . We see the similarity of the spectra with the spectra of the point process Figure 3, but a very different distribution of the intensity of the signal: the signal of the sum of Lorentzians is Gaussian, while that of the point process is of the power-law type.

### 4.3 Monofractality of signals with linear relaxations

In this section we present numerical investigation of fractality of the signal  $I(t)$ , expressed as an average of uncorrelated components, Eq. (179). We numerically calculate the GHCF functions  $F_q(t)$ , Eq. (129) and Hurst exponents, Eq. (130).

In Figure 11 a) we present the GHCF as a function of the time interval  $t$ . In Figure 11 b) we show a Hurst exponents, calculated from GHCF, using linear regression dependence on  $1/q$ . From the picture we clearly see that Hurst exponent  $H_q$  does not depend on  $q$  and that the signal (179) is monofractal.

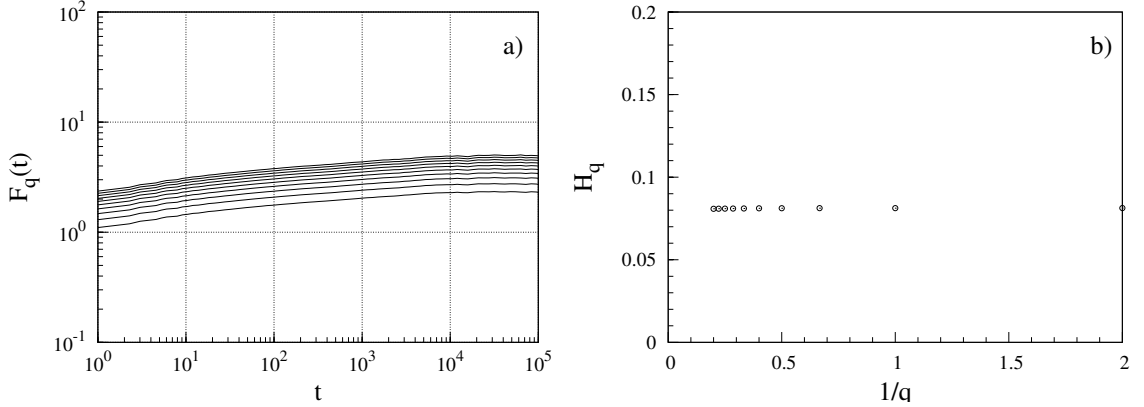


**Figure 11.** a) Generalized height-height correlation function  $F_q(t)$  versus time  $t$  for the signal (179) with  $q = 0.5, 1, 1.5, \dots, 5$  from bottom to top. The signal of  $N_I = 10^6$  points was generated from  $N = 10$  components. Parameters used are the same as in Figure 10. b) The generalized Hurst exponents  $H_q$  versus  $1/q$  for the corresponding GHCF in a) in the scaling regime  $1 < t < 1000$ .

#### 4.4 Different slopes of power spectral density

Using the sum of different Lorentzian signals we can generate not only a signal with the pure  $1/f$  spectrum but also the signal with any predefined slope  $\beta$  of  $1/f^\beta$  power spectral density. Indeed, let us investigate the case when

$$\sigma^2(\gamma)g(\gamma) = A\gamma^\eta, \quad (184)$$

where  $A$  and  $\eta$  are some parameters. Substitution of Eq. (184) into Eq. (175) yields the power spectral density

$$S(f) = \frac{A}{\pi f} \int_{\gamma_{\min}/\omega}^{\gamma_{\max}/\omega} \frac{(\omega y)^\eta}{1+y^2} dy = \frac{A}{\omega^{1-\eta}} \left\{ \left[ \frac{\gamma_{\max}}{\omega} \right]^{\eta+1} \Phi \left( - \left[ \frac{\gamma_{\max}}{\omega} \right]^2, 1, \frac{\eta+1}{2} \right) - \left[ \frac{\gamma_{\min}}{\omega} \right]^{\eta+1} \Phi \left( - \left[ \frac{\gamma_{\min}}{\omega} \right]^2, 1, \frac{\eta+1}{2} \right) \right\} \quad (185)$$

where  $\Phi(z, s, a)$  is a Lerch's Phi transcendent. In the limit when  $\gamma_{\min} \rightarrow 0$  and  $\gamma_{\max} \rightarrow \infty$  we can approximate the power spectral density (185) as

$$S(f) \simeq \frac{(2\pi)^\eta A}{2 \cos(\pi\eta/2)} \frac{1}{f^{1-\eta}}, \quad (186)$$

i.e., we have the generalization of the result (176).

For the average signal (179) we have

$$S_a(f) \simeq \frac{(2\pi)^\eta A}{2N^2 \cos(\pi\eta/2)} \frac{1}{f^{1-\eta}}. \quad (187)$$

In order to obtain an arbitrary  $\beta$  of the  $1/f^\beta$  power spectral density, we should choose in Eq. (184)  $\eta = 1 - \beta$ .

The distribution density  $P_a(I_a)$  of the average signal  $I_a(t)$  is Gaussian

$$P_a(I_a) = \frac{1}{\sqrt{2\pi}\sigma_a} \exp \left\{ -\frac{(I - \bar{I}_a)^2}{2\sigma_a^2} \right\} \quad (188)$$

with the variance  $\sigma_a^2$  expressed as

$$\sigma_a^2 = \frac{1}{2N^2} \int_{\gamma_{\min}}^{\gamma_{\max}} \frac{\sigma^2(\gamma)g(\gamma)}{\gamma} d\gamma = \frac{A(\gamma_{\max}^\eta - \gamma_{\min}^\eta)}{2N^2\eta}. \quad (189)$$

The correlation function in such a case according to Eq. 182 is

$$C_a(s) = \frac{A}{2N^2} \int_{\gamma_{\min}}^{\gamma_{\max}} e^{-\gamma s} \gamma^{\eta-1} d\gamma = \frac{A}{2N^2 s^\eta} [\Gamma(\eta, \gamma_{\min} s) - \Gamma(\eta, \gamma_{\max} s)] \quad (190)$$

where  $\Gamma(a, z)$  is an incomplete gamma function.

Figure 12 demonstrates the possibility to generate stochastic signals, exhibiting similar  $1/f^\beta$  power spectral densities with different slopes  $\beta$  by the summation of signals with different relaxation rates and according to the multiplicative point process model. The distribution densities of the corresponding signals are, however, completely different.

## 4.5 Conclusions of Sections 3 and 4

The generalized multiplicative point processes (86), (87), (131), and (147) may generate time series, exhibiting the power spectral density  $S(f) \sim 1/f^\beta$  with  $0.5 \lesssim \beta \lesssim 2$ , Eqs. (138), (141), (144), and (149), i.e., with the slope observable in a large variety of systems. Such spectral density is caused by the stochastic diffusion of the interpulse time, resulting in the power-law distribution. The power-law distribution of the interpulse, interevent, interarrival, recurrence or waiting times is observed in different systems ranging from physics, astronomy and seismology to the Internet, financial markets, neural spikes, and human cognition (e.g. [31, 176, 149, 148, 177, 178, 18, 24] and references herein).

Furthermore, the power-law distribution of the interpulse time results in the power-law distribution of the stochastic signal,  $P(I) \sim I^{-\lambda}$  with  $2 \lesssim \lambda \lesssim 4$ , i.e., the phenomenon observable in a large variety of processes, from earthquakes up to the financial time series.

The proposed model relates and connects the power-law autocorrelation and spectral density with the power-law distribution of the signal intensity into the consistent theoretical approach. The generated time series of the model are fractal since they jointly exhibit the power-law probability distribution and the power-law autocorrelation of the signal.

In addition, we have analysed the relation of the point process model with the Bernamont-Surdin-McWhorter model of  $1/f$  noise, representing the signal as a sum of the appropriate signals with the different rates of the linear relaxation. From the analysis performed we can conclude that the multiplicative point process model of  $1/f$  noise, when the signal, consisting of pulses with a stochastic motion of the interpulse time is more general and complementary to the model, based on the sum of signals with a

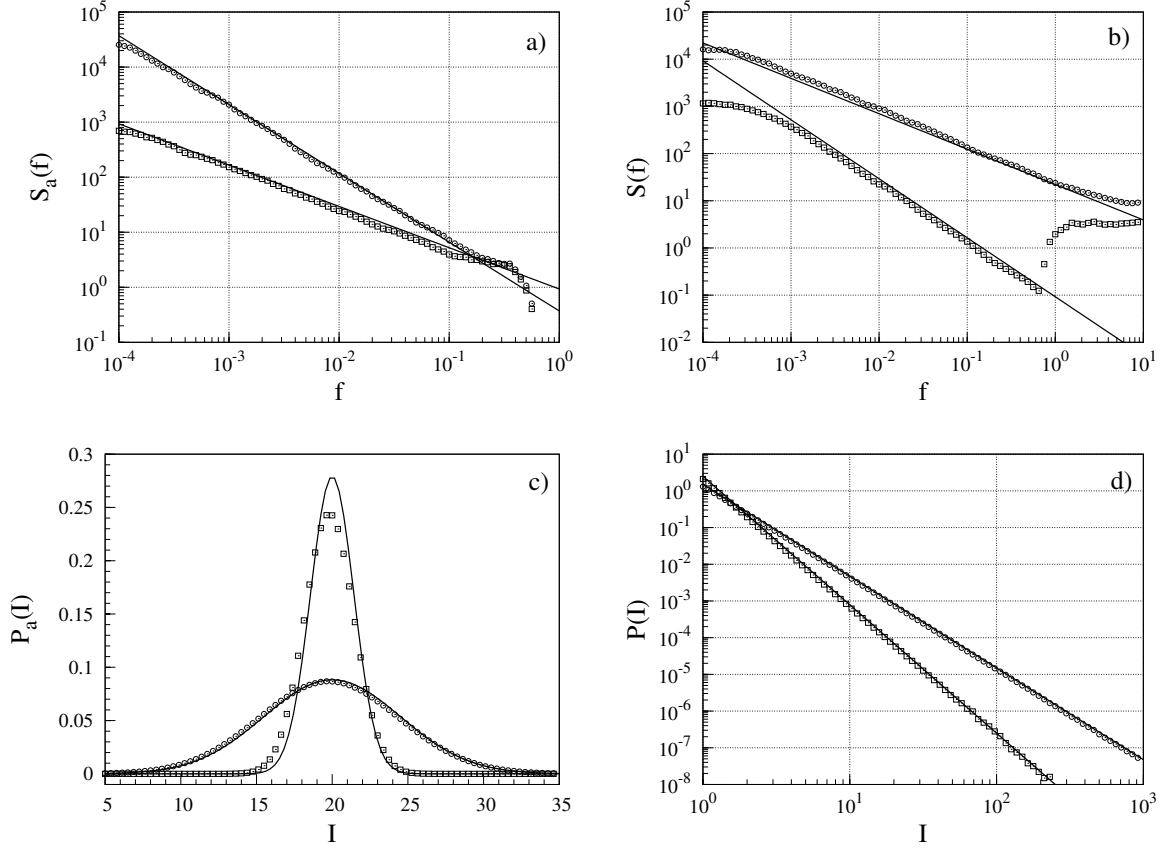


**Figure 12.** Power spectral density: a) numerically calculated for signal (161), (179) and (184) from  $N_I = 10^6$  points, averaged over  $n = 100$  realizations, consisting of  $N = 10$  components with  $\bar{I} = 20$ ,  $A = 10.8574$ ,  $\eta = -0.25$ , open circles, and  $\eta = 0.25$ , open squares, in comparison with theoretical results (187), solid line; b) for the point process (86), (87), and (147) with the parameters  $\bar{a} = 1$ ,  $\mu = 0.5$ ,  $\sigma = 0.02$ , and  $\gamma = 0.0001$ , open circles, and  $\gamma = 0.0003$ , open squares, averaged over  $n = 100$  realizations of  $N_\tau = 10^6$  pulse sequences in comparison with the theoretical results (149), solid lines. c) and d) show numerically calculated distribution densities of the corresponding signals in comparison with the theoretical results (188), (189), and (155), respectively, solid lines.

wide-range distribution of the relaxation times. In contrast to the Gaussian distribution of the intensity of the sum of the uncorrelated components, the point process model generating  $1/f$  noise exhibits the power-law distribution of the intensity of the signal. Moreover, it is free from the requirement of a wide-range distribution of the relaxation times. Obviously, the multiplicative point process model of  $1/f^\beta$  noise may be used for modeling and analysis of stochastic processes in different systems, exhibiting the pulsing signals.

## 5 STOCHASTIC SIGNAL MODEL

### 5.1 Signal as a sequence of pulses of finite duration

In real life we usually have to deal with signals in physical systems varying in time rather than with discrete point processes. In this section we will investigate a signal, consisting of a sequence of different pulses, Eq. (85). Thus, the power spectral density of the signal can be written as

$$S(f) = \lim_{T \rightarrow \infty} \left\langle \frac{2}{T} \sum_{k,k'} e^{i\omega(t_k - t_{k'})} \int_{t_i - t_k}^{t_f - t_k} du \int_{t_i - t_{k'}}^{t_f - t_{k'}} du' A_k(u) A_{k'}(u') e^{i\omega(u - u')} \right\rangle, \quad (191)$$

where  $\omega = 2\pi f$ . We assume that pulse shape functions  $A_k(u)$  decrease sufficiently fast when  $|u| \rightarrow \infty$ . Since  $T \rightarrow \infty$ , the bounds of the integration in Eq. (191) can be changed to  $\pm\infty$ . We also assume that time moments  $t_k$  are not correlated with the shape of the pulse  $A_k$ . Then the power spectrum is

$$S(f) = \lim_{T \rightarrow \infty} \frac{2}{T} \sum_{k,k'} \langle e^{i\omega(t_k - t_{k'})} \rangle \left\langle \int_{-\infty}^{+\infty} du \int_{-\infty}^{+\infty} du' A_k(u) A_{k'}(u') e^{i\omega(u - u')} \right\rangle. \quad (192)$$

After the introduction of the functions [193]

$$\Psi_{k,k'}(\omega) = \left\langle \int_{-\infty}^{+\infty} du A_k(u) e^{i\omega u} \int_{-\infty}^{+\infty} du' A_{k'}(u') e^{-i\omega u'} \right\rangle \quad (193)$$

and

$$\chi_{k,k'}(\omega) = \langle e^{i\omega(t_k - t_{k'})} \rangle \quad (194)$$

the spectrum can be written as

$$S(f) = \lim_{T \rightarrow \infty} \frac{2}{T} \sum_{k,k'} \chi_{k,k'}(\omega) \Psi_{k,k'}(\omega). \quad (195)$$

### 5.2 Stationary process

Equation (195) can be further simplified assuming that the process is stationary. In the stationary case all averages can depend only on  $k - k'$ . Then

$$\Psi_{k,k'}(\omega) \equiv \Psi_{k-k'}(\omega) \quad (196)$$

and

$$\chi_{k,k'}(\omega) \equiv \chi_{k-k'}(\omega). \quad (197)$$

Equation (195) then reads

$$S(f) = \lim_{T \rightarrow \infty} \frac{2}{T} \sum_{k,k'} \chi_{k-k'}(\omega) \Psi_{k-k'}(\omega). \quad (198)$$

Introducing a new variable  $q \equiv k - k'$  and changing the order of summation, yields

$$S(\omega) = \lim_{T \rightarrow \infty} \frac{2}{T} \sum_{q=1}^{k_{\max} - k_{\min}} \sum_{k=k_{\min}}^{k_{\max} - q} \chi_q(\omega) \Psi_q(\omega) + \lim_{T \rightarrow \infty} \frac{2}{T} \sum_{q=k_{\min} - k_{\max}}^{-1} \sum_{k=k_{\min} - q}^{k_{\max}} \chi_q(\omega) \Psi_q(\omega) + \lim_{T \rightarrow \infty} \frac{2}{T} \sum_{k=k_{\min}}^{k_{\max}} \Psi_0(\omega). \quad (199)$$

Now we can introduce  $N = k_{\max} - k_{\min}$ , then

$$S(f) = 2\Psi_0(\omega)\bar{\nu} + \lim_{T \rightarrow \infty} 4 \sum_{q=1}^N \left( \bar{\nu} - \frac{q}{T} \right) \operatorname{Re} \chi_q(\omega) \Psi_q(\omega) \quad (200)$$

where

$$\bar{\nu} = \lim_{T \rightarrow \infty} \left\langle \frac{N+1}{T} \right\rangle \quad (201)$$

is the mean number of pulses per unit time.

If the sum  $\frac{1}{T} \sum_{q=1}^N q \operatorname{Re} \chi_q(\omega) \Psi_q(\omega) \rightarrow 0$  when  $T \rightarrow \infty$ , then the second term in the sum (200) vanishes and the spectrum is

$$S(f) = 2\bar{\nu}\Psi_0(\omega) + 4\bar{\nu} \sum_{q=1}^{\infty} \operatorname{Re} \chi_q(\omega) \Psi_q(\omega) = 2\bar{\nu} \sum_{q=-\infty}^{\infty} \chi_q(\omega) \Psi_q(\omega). \quad (202)$$

### 5.3 Fixed shape pulses

When the shape of the pulses is fixed ( $k$ -independent) then the function  $\Psi_{k,k'}(\omega)$  does not depend on  $k$  and  $k'$  and, therefore,  $\Psi_{k,k'}(\omega) = \Psi_{0,0}(\omega)$ . Then equation (195) yields the power spectrum

$$S(f) = \Psi_{0,0}(\omega) \lim_{T \rightarrow \infty} \frac{2}{T} \sum_{k,k'} \chi_{k,k'}(\omega) \equiv \Psi_{0,0}(\omega) S_{\delta}(\omega). \quad (203)$$

This is the spectrum of one pulse, multiplied by the spectrum of the sequence (86) of  $\delta$ -shaped pulses  $S_{\delta}(\omega)$ .

### 5.4 Transition from the point process to the continuous signal using the Gaussian pulses

Let us construct a real time signal by substituting  $\delta$ -functions in (86) with some arbitrary shape equal pulses  $A_k(t - t_k)$ , for example, Gaussian-like pulses. In such case we can rewrite Eq. (86) as

$$I(t) = \bar{a} \sum_k \frac{1}{\sqrt{2\pi}\sigma_p} \exp \left\{ -\frac{(t - t_k)^2}{2\sigma_p^2} \right\}, \quad (204)$$

where  $\{t_k\}$  is calculated according to Eq. (96). Using (204) we can calculate power spectral density of the signal. After some algebra we derive

$$\begin{aligned} S(f) &= \lim_{T \rightarrow \infty} \left\langle \left| \frac{2}{T} \int_{t_i}^{t_f} I(t) e^{-i2\pi ft} dt \right|^2 \right\rangle = \lim_{T \rightarrow \infty} \left\langle \frac{2\bar{a}^2}{T} \left| \sum_k e^{-i2\pi ft_k} e^{-2\pi^2 f^2 \sigma_p^2} \right|^2 \right\rangle \\ &= \lim_{T \rightarrow \infty} \left\langle \frac{2\bar{a}^2}{T} \left| \sum_k e^{-i2\pi ft_k} \right|^2 \right\rangle e^{-(2\pi f \sigma_p)^2}. \end{aligned} \quad (205)$$

We can compare expression (205) with the power spectral density  $S_\delta(f)$  of the point process signal, constructed from the sum of the  $\delta$ -functions, Eq. (87), and notice that

$$S(f) = S_\delta(f) S_\sigma(f). \quad (206)$$

Here

$$S_\delta(f) = \lim_{T \rightarrow \infty} \left\langle \frac{2\bar{a}^2}{T} \left| \sum_k e^{-i2\pi ft_k} \right|^2 \right\rangle \quad (207)$$

and

$$S_\sigma(f) = \Psi_{0,0}(f) = e^{-(2\pi f \sigma_p)^2}. \quad (208)$$

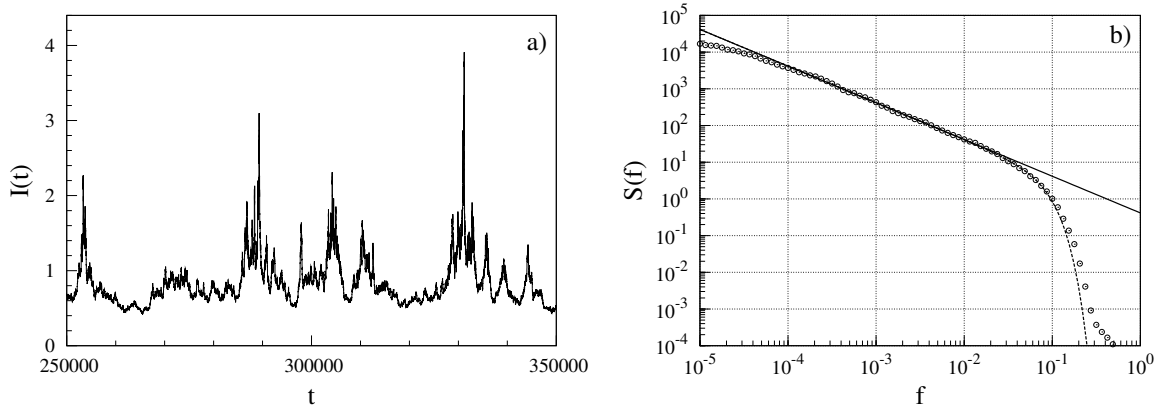


**Figure 13.** a) Sample signal  $I(t)$  generated according to Eqs. (96) and (204) from  $N_\tau = 10^6$   $\{\tau_k\}$  points with parameters  $\bar{\tau} = 1$ ,  $\sigma = 0.01$ ,  $\gamma = 0.0001$ ,  $\bar{a} = 1$  and  $\sigma_p = 2$ ; and b) the power spectral density. Open circles represent the power spectral density, calculated using Fast Fourier Transform from numerically generated signal (204) of  $N_I = 10^6$  points, averaged over  $n = 100$  realizations; the solid line corresponds to the numerical integration of Eq. (113) with  $g(q)$  from Eq. (106), dashed line represents the analytical result (206).

Figure 13 a) shows sample signal, generated from the point process, using the Gaussian pulses according to Eq. (204). As we see, the signal intensity has sharp peaks in some time points. In Figure 13 b) we compare the power spectral density of the point process, generated with  $\delta$ -functions, Eq. (96), and the signal, numerically generated using the same point process  $\{t_k\}$  values, but with the Gaussian pulses, Eq. (204). We see that the Gaussian pulses of finite duration influence the high frequency region and introduce the exponential cut-off according to the Eq. (206). However, the power spectral density at low frequency remains the same as in the point process.

## 5.5 Transition from the point process to the stochastic signal using rectangular pulses

We can construct continuous real time signal from the point process in a number of different ways. We should not restrict ourselves to the identical pulses  $A_k(t-t_k)$ , but we should require that the “contribution” of each pulse to the overall signal should remain constant. This could be achieved by requiring that areas of the pulses are equal,

$$\int_{-\infty}^{\infty} A_k(t, t_k) dt = A_c, \quad (209)$$

for each  $k$ , and  $A_c$  is some arbitrary constant. The simplest way to construct the signal would be to use rectangular pulses

$$A_k(t, t_k) = f_k(t_{k-1}, t_k)/\tau_k, \quad (210)$$

where function  $f_k(t_{k-1}, t_k)$  is a window function

$$f_k(t_{k-1}, t_k) = \begin{cases} 1, & t_{k-1} < t \leq t_k \\ 0, & \text{elsewhere} \end{cases} \quad (211)$$

and  $\tau_k = t_k - t_{k-1}$ . The corresponding signal can be written as a sum

$$I(t) = \bar{a} \sum_k f_k(t_{k-1}, t_k)/\tau_k. \quad (212)$$

Now we can calculate the distribution density of the signal intensity  $P(I)$ . From Eq. (212) we see that the signal at the arbitrary time  $t$ , except a discrete set of points  $\{t_k\}$ , equals  $I(t) = \bar{a}/\tau$ , where  $\tau = \tau(t) = \tau_k$  is a continuous time function, when  $t_{k-1} < t \leq t_k$ . At points  $t \neq t_k$  differential  $d\tau$  equals

$$d\tau = -\frac{\bar{a}}{I^2} dI. \quad (213)$$

The probability that  $\tau'$  is in the range  $\tau \leq \tau' < \tau + d\tau$  is equal to  $P(\tau)d\tau$ . Transition from the occurrence number  $k$  to the actual time  $t$  according to the relation  $dt = \tau_k dk$  yields the probability distribution density  $P_t(\tau_k)$  of  $\tau_k$  in the actual time  $t$ ,

$$P_t(\tau_k) = P_k(\tau_k)\tau_k/\bar{\tau}. \quad (214)$$

Taking into account that we already have found probability density  $P_k(\tau_k)$ , Eq. (121), from Eq. (214) we derive the signal probability density  $P(I)$ ,

$$P(I) = \frac{\bar{a}\bar{I}}{I^3} P_k\left(\frac{\bar{a}}{I}\right). \quad (215)$$

For a point process (96) the distribution density of the intensity of the signal according to Eqs. (115), (121) and (215) then is

$$P(I) = \frac{K\bar{I}^2}{\sqrt{\pi}I^3} \exp\left\{-\frac{\gamma\bar{a}^2}{\sigma^2} \left(\frac{1}{\bar{I}} - \frac{1}{I}\right)^2\right\}. \quad (216)$$

Restricting the diffusion of the interpulse time  $\tau_k$  by the reflective boundary condition at  $\tau_{\min} > 0$  and for  $\tau_{\min} \rightarrow 0$ , we have the truncated distribution density of the signal intensity

$$P_r(I) = \frac{2K\bar{I}^2}{\sqrt{\pi}[1 + \operatorname{erf}(K)]} \exp \left\{ -K^2 \left( 1 - \frac{\bar{I}}{I} \right)^2 \right\} \frac{1}{I^3}, \quad I > 0. \quad (217)$$

In the asymptotic  $I \gg \bar{I}$  and  $I \gg 2K^2\bar{I}$  from Eq. (217) we obtain

$$P_r(I) \simeq \alpha_H^r \frac{\bar{I}^2}{I^3} \sim \frac{1}{I^3}, \quad (218)$$

i.e., the power-law distribution density of the signal. Here

$$\alpha_H^r = \frac{\alpha_H}{1 + \operatorname{erf}(K)}. \quad (219)$$

The restriction of motion of  $\tau_k$  by the reflective boundary condition at  $\tau_k = 0$  reduces the effective (average) value of  $P_k(0) = \frac{1}{2}[P_k(\tau_k \rightarrow +0) + P_k(\tau_k \rightarrow -0)]$  in Eq. (128) and, consequently, the power spectral density approximately 2 times compared to the theoretical result (115), obtained without the restriction, because  $P_k(\tau_k \rightarrow -0) = 0$  for the restricted motion. To be more exact, in such case the power spectral density may be expressed by Eq. (115) with  $\alpha_H^r$  instead of  $\alpha_H$ , i.e.,

$$S_r(f) = \bar{I}^2 \frac{\alpha_H^r}{f}. \quad (220)$$

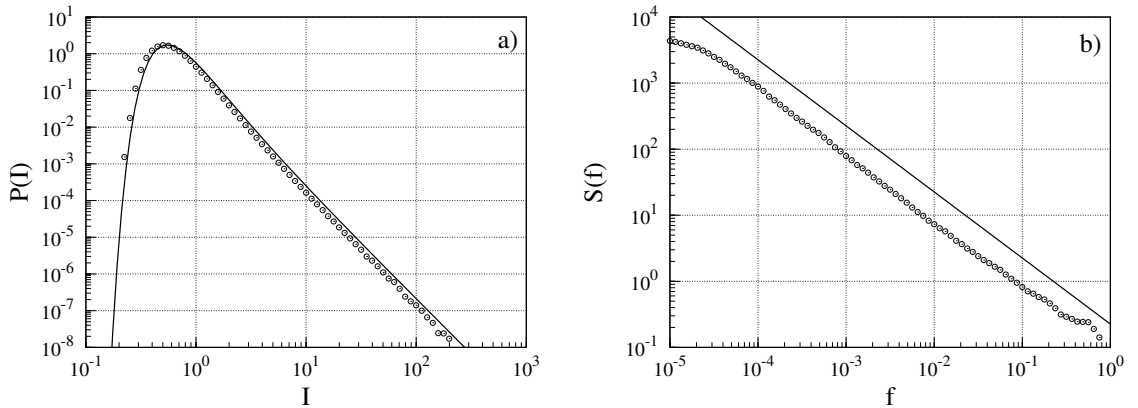


**Figure 14.** a) Distribution density of the signal, generated using rectangular pulses according to Eq. (212) from  $N_I = 10^6$  points, with  $\bar{a} = 1$  and  $\{\tau_k\}$  generated for  $N_\tau = 10^6$  points, according to Eq. (96) with parameters  $\bar{\tau} = 1$ ,  $\sigma = 0.01$  and  $\gamma = 0.0001$ , open circles, compared with the theoretical result (217), solid line; and b) the power spectral density of this signal calculated using Fast Fourier Transform and averaged over  $n = 100$  realizations, open circles, compared with power spectral density, calculated according to Eq. (220), solid line.

From Eqs. (215) and (121) we find that at  $I \gg \bar{a}$  distribution density  $P(I) \sim 1/I^3$ .

In Figure 14 we present a numerically calculated distribution density of the signal, generated using rectangular pulses. We can see that at higher signal amplitude  $I$  values,

$P(I)$  is proportional to power function  $1/I^3$  as expected from Eq. (218). In Figure 14 we compare power spectral density, calculated using Fast Fourier Transform for a signal (212) with the theoretical power spectral density of the original point process (86), calculated according to Eq. (220).

We can compare Figure 14 with Figure 10 and notice that signals with completely different signal distribution densities, i.e., Gaussian for the superposition of Lorentzian signals and power-law for a signal, generated using rectangular pulses on a point process result in the same  $1/f$  power spectral density.

## 5.6 Uncorrelated pulses

When the pulses are uncorrelated and  $k \neq k'$  then from Eq. (193)

$$\Psi_{k-k'}(\omega) = \left\langle \int_{-\infty}^{+\infty} A_k(u) e^{i\omega u} du \right\rangle \left\langle \int_{-\infty}^{+\infty} A_{k'}(u') e^{-i\omega u'} du' \right\rangle = |\langle F_k(\omega) \rangle|^2, \quad (221)$$

where

$$F_k(\omega) = \int_{-\infty}^{+\infty} A_k(u) e^{i\omega u} du. \quad (222)$$

is the Fourier transform of the pulse  $A_k$ . When  $k = k'$  then

$$\Psi_0(\omega) = \langle |F_k(\omega)|^2 \rangle. \quad (223)$$

From Eq. (202) we obtain the spectrum

$$S(f) = 2\bar{\nu} \langle |F_k(\omega)|^2 \rangle + 4\bar{\nu} |\langle F_k(\omega) \rangle|^2 \sum_{q=1}^{\infty} \text{Re} \chi_q(\omega). \quad (224)$$

When the interevent times  $\tau_k = t_k - t_{k-1}$  are random and uncorrelated then

$$\chi_q(\omega) = \langle e^{i\omega(t_{k+q} - t_k)} \rangle = \langle e^{i\omega\tau_k} \rangle^q \equiv \chi_\tau(\omega)^q. \quad (225)$$

From Eq. (224) we obtain

$$S(f) = 2\bar{\nu} \langle |F_k(\omega)|^2 \rangle + 4\bar{\nu} |\langle F_k(\omega) \rangle|^2 \text{Re} \frac{\chi_\tau(\omega)}{1 - \chi_\tau(\omega)}. \quad (226)$$

Here

$$\bar{\nu} = \left[ -i \frac{d\chi_\tau(\omega)}{d\omega} \Big|_{\omega=0} \right]^{-1}. \quad (227)$$

We assume that the pulse sequences are stationary and ergodic, while the interevent times and the shapes of different pulses are independent. If the occurrence times of the pulses  $t_k$  are distributed according to Poisson process, then the interevent time probability distribution is  $P(\tau) = \frac{1}{\bar{\tau}} \exp\{-\frac{\tau}{\bar{\tau}}\}$ . The characteristic function obeys the equality  $\text{Re} \frac{\chi_\tau(\omega)}{1 - \chi_\tau(\omega)} = 0$  and the spectrum is

$$S(f) = 2\bar{\nu} \langle |F_k(\omega)|^2 \rangle. \quad (228)$$

## 5.7 Pulses of variable duration

Let us assume that the only random parameter of the pulse is the duration. We take the form of the pulse as [193]

$$A_k(t) = T_k^\rho A\left(\frac{t}{T_k}\right), \quad (229)$$

where  $T_k$  is the characteristic duration of the pulse. The value  $\rho = 0$  corresponds to fixed height pulses;  $\rho = -1$  corresponds to constant area pulses. Differentiating the fixed area pulses we obtain  $\rho = -2$ . The Fourier transform of the pulse (229) is

$$F_k(\omega) = \int_{-\infty}^{+\infty} T_k^\rho A\left(\frac{t}{T_k}\right) e^{i\omega t} dt = T_k^{\rho+1} \int_{-\infty}^{+\infty} A(u) e^{i\omega T_k u} du \equiv T_k^{\rho+1} F(\omega T_k). \quad (230)$$

From Eq. (228) the power spectrum for the pulses, distributed according to Poisson process is

$$S(f) = 2\bar{\nu} \langle T_k^{2\rho+2} |F(\omega T_k)|^2 \rangle. \quad (231)$$

Introducing the probability density  $P(T_k)$  of the pulses durations  $T_k$  we can write

$$S(f) = 2\bar{\nu} \int_0^{\infty} T_k^{2\rho+2} |F(\omega T_k)|^2 P(T_k) dT_k. \quad (232)$$

If  $P(T_k)$  is a power-law distribution, then the expressions for the spectrum are similar for all  $\rho$ .

## 5.8 Spectrum at small frequencies

For small frequencies we expand the Fourier transform of the pulse into Taylor series. The first coefficients are

$$F(0) = \bar{a}, \quad \frac{dF(0)}{d\omega} = i\bar{a}\langle t \rangle, \quad \frac{d^2F(0)}{d\omega^2} = -\bar{a}\langle t^2 \rangle, \quad (233)$$

where

$$\bar{a} = \int_{-\infty}^{+\infty} A(t) dt \quad (234)$$

is the area of the pulse,

$$\langle t \rangle = \frac{1}{\bar{a}} \int_{-\infty}^{+\infty} t A(t) dt, \quad \langle t^2 \rangle = \frac{1}{\bar{a}} \int_{-\infty}^{+\infty} t^2 A(t) dt. \quad (235)$$

Then the spectrum from Eq. (232) is

$$S(f) \simeq 2\bar{\nu} \bar{a}^2 \int_0^{\infty} T_k^{2\rho+2} (1 - \Delta t^2 \omega^2 T_k^2) P(T_k) dT_k, \quad (236)$$

where  $\Delta t^2 = \langle t^2 \rangle - \langle t \rangle^2$ . We obtain

$$S(f) = 2\bar{\nu}\bar{a}^2 \langle T_k^{2\rho+2} \rangle (1 - \Delta t^2 \omega^2 \langle T_k^{2\rho+4} \rangle), \quad (237)$$

where

$$\langle T_k^\xi \rangle = \int_0^\infty T_k^\xi P(T_k) dT_k. \quad (238)$$

## 5.9 Power-law distribution of the pulse duration

We take the power-law distribution of pulse durations

$$P(T_k) = \begin{cases} \frac{\alpha+1}{T_{\max}^{\alpha+1} - T_{\min}^{\alpha+1}} T_k^\alpha, & T_{\min} \leq T_k \leq T_{\max}, \\ 0, & \text{otherwise.} \end{cases} \quad (239)$$

From Eq. (232) we have the spectrum

$$\begin{aligned} S(f) &= 2\bar{\nu} \frac{\alpha+1}{T_{\max}^{\alpha+1} - T_{\min}^{\alpha+1}} \int_0^\infty T_k^{\alpha+2\rho+2} |F(\omega T_k)|^2 dT_k \\ &= \frac{2\bar{\nu}(\alpha+1)}{\omega^{\alpha+2\rho+3} (T_{\max}^{\alpha+1} - T_{\min}^{\alpha+1})} \int_{\omega T_{\min}}^{\omega T_{\max}} u^{\alpha+2\rho+2} |F(u)|^2 du. \end{aligned} \quad (240)$$

When  $\alpha > -1$  and  $\frac{1}{T_{\max}} \ll \omega \ll \frac{1}{T_{\min}}$  then the expression for the spectrum can be approximated as

$$S(f) \approx \frac{2\bar{\nu}(\alpha+1)}{\omega^{\alpha+2\rho+3} (T_{\max}^{\alpha+1} - T_{\min}^{\alpha+1})} \int_0^\infty u^{\alpha+2\rho+2} |F(u)|^2 du. \quad (241)$$

If  $\alpha + 2\rho + 2 = 0$  then in the frequency domain  $\frac{1}{T_{\max}} \ll \omega \ll \frac{1}{T_{\min}}$  the spectrum is

$$S(f) \approx \frac{2\bar{\nu}(\alpha+1)}{\omega (T_{\max}^{\alpha+1} - T_{\min}^{\alpha+1})} \int_0^\infty |F(u)|^2 du. \quad (242)$$

We obtained  $1/f$  spectrum. The condition  $\alpha + 2\rho + 2 = 0$  is satisfied, e.g., for the fixed area pulses ( $\rho = -1$ ) and uniform distribution of pulse durations or for fixed height pulses ( $\rho = 0$ ) and uniform distribution of inverse durations  $\gamma = T_k^{-1}$ , i.e. for  $P(T_k) \propto T_k^{-2}$ .

If  $\alpha + 2\rho + 4 = 0$  then in the frequency domain  $\frac{1}{T_{\max}} \ll \omega \ll \frac{1}{T_{\min}}$  the spectrum is

$$S(f) \approx \frac{2\bar{\nu}(\alpha+1)\omega}{(T_{\max}^{\alpha+1} - T_{\min}^{\alpha+1})} \int_0^\infty |F(u)|^2 \frac{du}{u^2}. \quad (243)$$

Such a spectrum can be obtained after differentiation of the signal exhibiting  $1/f$  spectrum.

## 5.10 Rectangular constant area pulses distributed according to the Poisson process

As an example we will obtain the spectrum of rectangular constant area pulses. The duration of the pulse is  $T_k$ . The Fourier transform of the pulse is

$$F(\omega T_k) = \bar{a} \int_0^1 e^{i\omega T_k u} du = \bar{a} \frac{e^{i\omega T_k} - 1}{i\omega T_k} = \bar{a} e^{i\frac{\omega T_k}{2}} \frac{2 \sin\left(\frac{\omega T_k}{2}\right)}{\omega T_k}. \quad (244)$$

Then the spectrum according to Eqs. (232), (239) and (244) is

$$S(f) = \frac{4\bar{\nu}a^2(\alpha + 1)(T_{\max}^{\alpha-1} - T_{\min}^{\alpha-1})}{\omega^2(\alpha - 1)(T_{\max}^{\alpha+1} - T_{\min}^{\alpha+1})} + \frac{4\bar{\nu}a^2(\alpha + 1)}{\omega^{\alpha+1}(T_{\max}^{\alpha+1} - T_{\min}^{\alpha+1})} \times \text{Re} \left\{ i^{1-\alpha} [\Gamma(\alpha - 1, i\omega T_{\max}) - \Gamma(\alpha - 1, i\omega T_{\min})] \right\}, \quad (245)$$

where  $\Gamma(a, z)$  is an incomplete gamma function,  $\Gamma(a, z) = \int_z^\infty u^{a-1} e^{-u} du$ .

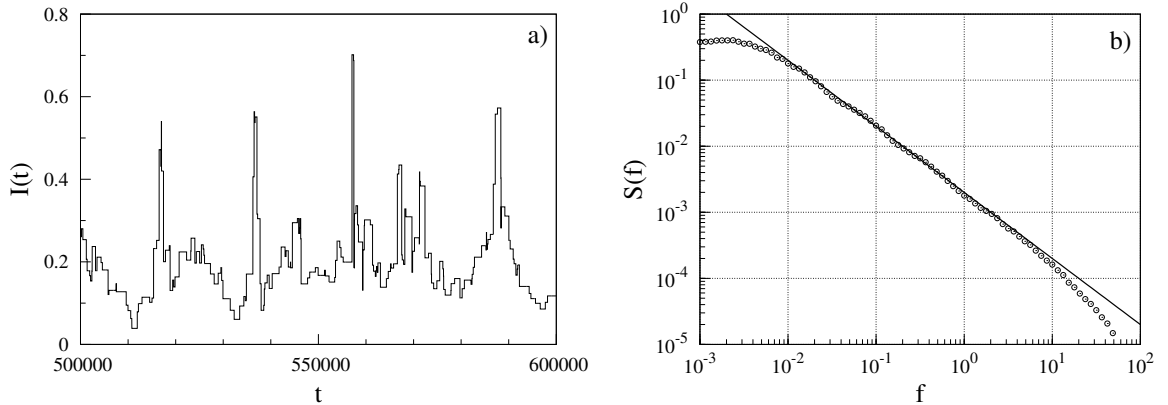


**Figure 15.** A typical signal  $I(t)$  a) and the power spectral density of the signal, calculated using Fast Fourier Transform b), open circles. The signal consists of the  $N_T = 10^3$  fixed area rectangular pulses ( $\rho = -1$ ) with uniformly distributed durations. The time intervals between the pulses are distributed according to the Poisson process with the average  $\bar{\tau} = 5$ . The used parameters are  $T_{\min} = 0.01$ ,  $T_{\max} = 100$ , and the signal was calculated from  $N_I = 10^6$  points. The solid line represents the power spectral density according to Eq. (248).

When  $-1 < \alpha < 1$  then the term with  $\Gamma(\alpha - 1, i\omega T_{\max})$  is small and can be neglected. We also assume that  $T_{\min} \ll T_{\max}$  and when  $\alpha > -1$  we neglect the term  $(T_{\min}/T_{\max})^{\alpha+1}$ . Then we have

$$S(f) \simeq -\frac{4\bar{\nu}a^2(\alpha + 1)}{\omega^{\alpha+1}T_{\max}^{\alpha+1}} \cos\left[\frac{\pi}{2}(\alpha - 1)\right] \Gamma(\alpha - 1). \quad (246)$$

For  $\alpha = 0$  we have the uniform distribution of the pulses duration. Using the result of the limit

$$\lim_{\alpha \rightarrow 0} \cos\left[\frac{\pi}{2}(\alpha - 1)\right] \Gamma(\alpha - 1) = -\frac{\pi}{2}, \quad (247)$$

we obtain  $1/f$  spectrum

$$S(f) \simeq \frac{\bar{\nu}a^2}{fT_{\max}}. \quad (248)$$

The spectrum was also obtained from numerical calculations. Typical signal of the rectangular fixed area pulses is shown in Figure 15 a) and the power spectral density in Fig. 15 b).

### 5.11 Transition from the discrete point process to the continuous signal by counting pulses

We can use even simpler method to construct continuous time signal from the discrete point process (96) by dividing total time  $T = \sum_k \tau_k$  into  $d$  constant length  $\Delta t_d$  intervals

$$\Delta t_d = T/d. \quad (249)$$

and defining signal values to be constant in equal time intervals ( $[k-1]\Delta t_d, k\Delta t_d$ ), where  $k = 2, \dots, N$ , and proportional to the number of events, which occurred in that time intervals. This method is widely used in the analysis of financial markets [165, 44, 45] and other large amounts of data, such us the Internet traffic.

Let us introduce a new function  $f_c(t)$ , which counts how many elementary events  $\delta(t - t_k)$  occurred until arbitrary fixed time  $t$ ,

$$f_c(t) = k, \quad (250)$$

where integer number  $k$  should meet the following conditions:

$$\begin{cases} \sum_{l=1}^k \tau_l > t \\ \sum_{l=1}^{k-1} \tau_l < t. \end{cases} \quad (251)$$

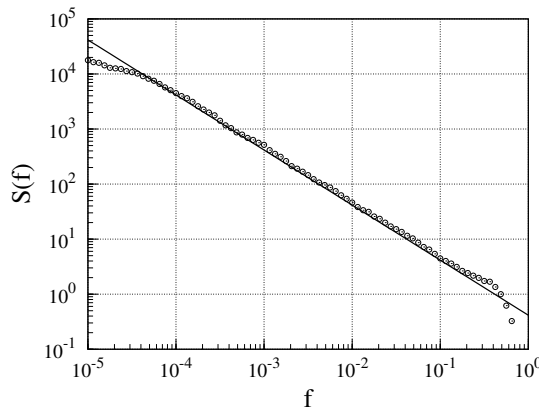


**Figure 16.** Power spectral density of the point process (87), with the parameters  $\bar{\tau} = 1$ ,  $\sigma = 0.01$ , and  $\gamma = 0.0001$ , generated from  $N_\tau = 10^6$  points and averaged over  $n = 100$  realizations, open circles, and the power spectral density of signal (252) generated with  $t_d = 1$ ,  $\bar{a} = 1$  and calculated using Fast Fourier Transform, solid line.

Function  $f_c$  can be easily calculated numerically for every  $t$ , once we have the generated  $\{\tau_k\}$  set. Now we can define the signal as

$$I(t) = \bar{a} \sum_k \{f_c(k\Delta t_d) - f_c([k-1]\Delta t_d)\} f_k([k-1]\Delta t_d, k\Delta t_d), \quad (252)$$

where function  $f_k(t_1, t_2)$  is defined according to Eq. (211).

In Figure 16 we compare power spectral densities of the point process (96) and the signal generated according to (252). We see that the method of counting pulses allows to calculate better spectral density match at high frequencies, because there are no distortions due to the pulse shapes. The figure demonstrates a very good agreement between the two methods of the power spectral density.

## 5.12 Transition from the stochastic signal to the point process

As it has been shown in the previous sections, having a point process we can use a number of different methods to construct a stochastic real time signal from the original point process. Here we will try to go in the opposite direction – from the stochastic signal we will construct a point process (86), described by  $\{t_k\}$  sequence (96) which would have similar power spectral density as the original stochastic process.

First of all, we construct the positive signal,  $I_p(t)$ , for all time interval  $[t_{\min}, t_{\max}]$ . In order to do that, we have to find minimal value,  $I_{\min}$ , of the signal  $I(t)$  and add  $|I_{\min}|$  to the initial signal  $I(t)$ ,

$$I_p(t) = I(t) + |I_{\min}|. \quad (253)$$

Adding a constant to a signal at all points  $t$  will not change the power spectral density of the signal. Then, having a positive at all times  $t$  signal  $I_p(t)$ , we can calculate corresponding  $\{t_k\}$  sequence. If we want to have  $\{t_k\}$  sequence made from  $N$  points, we should require that the integrals of both signals are equal,

$$\int_{t_i}^{t_f} I_p(t) dt = \bar{a} \sum_{k=1}^N \int_{t_i}^{t_f} \delta(t - t_k) dt = \bar{a} N, \quad (254)$$

where  $t_i$  and  $t_f$  is the initial and the final times of the signal. Equation (254) defines  $\bar{a}$  value. Having  $\bar{a}$  value we can numerically integrate the signal  $I_p(t)$  and find  $\{t_k\}$  using the following relations:

$$\begin{aligned} \int_{t_i}^{t_1} I_p(t) dt &= \bar{a}, \\ \int_{t_1}^{t_2} I_p(t) dt &= \bar{a}, \\ &\dots \\ \int_{t_{N-1}}^{t_f} I_p(t) dt &= \bar{a}. \end{aligned} \quad (255)$$

This method is called the integrate-and-fire method [31] and have been used in the spectral analysis of the EKG signals for the predictions of the sudden cardiac death [194]. Once we calculated all  $\{t_k\}$  values, we can use Eq. (87) to calculate the power spectral density of the point process and compare it with the power spectral density of the original signal.

In Figure 17 a) we compare the distribution density (121) of the original point process (96) with the distribution density of the point process, which was numerically

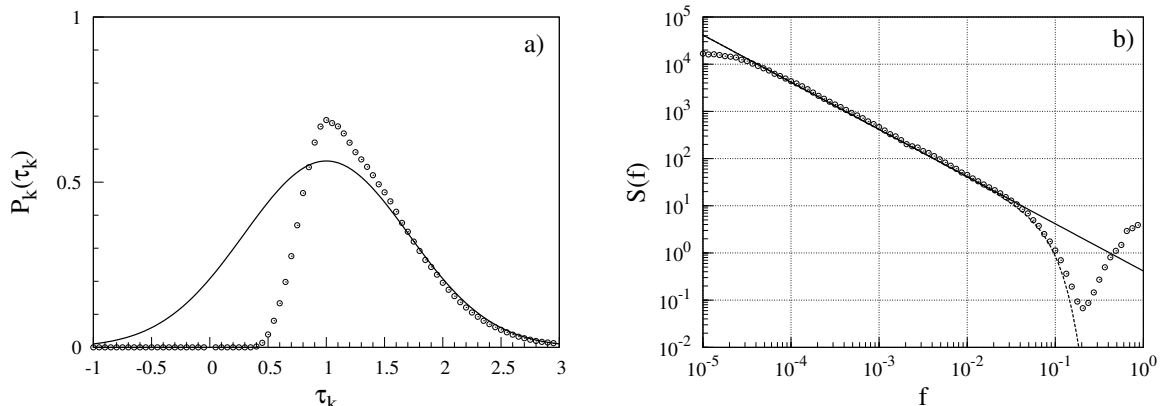


**Figure 17.** a) Distribution density of  $\tau_k$  of the point process, generated according to Eqs. (255) from the stochastic signal, which, on the other hand, was generated using the Gaussian pulses with  $\sigma_p = 2$  and  $N_I = 10^6$  from the original point process (96), with the parameters  $\bar{\tau} = 1$ ,  $\sigma = 0.01$ , and  $\gamma = 0.0001$ , generated from  $N_\tau = 10^6$  points and averaged over  $n = 100$  realizations, open circles, compared with the distribution density (121), solid line; and b) the power spectral density of the point process according to Eqs. (253) – (255), open circles, solid line represents the power spectral density of the original point process (96), calculated by integrating Eq. (113); dashed line shows the power spectral density of stochastic signal, calculated according to Eq. (206).

calculated using Eqs. (255) from the stochastic signal, which, on the other hand, was calculated from the original point process, covered by the Gaussian pulses according to Eq. (204). We can compare distribution density  $P_k(\tau_k)$  with the original point process distribution density, Figure 2. The main difference in distributions is that the distribution density of the integrated point process is shifted to the higher  $\tau_k$  values. This shift can be explained: the Gaussian pulses are not as “sharp” as  $\delta$ -functions, which the original point process is made of, and the influence of one pulse on the signal splits into neighboring area. In Figure 17 b) the power spectral densities of the original point process (96), of the signal, generated using the Gaussian pulses (204), and of the resulting point process (253) – (255) are presented. We see that the Gaussian pulses result in the power spectral density cut-off at higher frequencies. However, by performing integration on the signal, we lose information about the pulses’ shape and, therefore, power spectral density of point process, calculated from the signal at high frequencies approaches power spectral density of the original point process and yields the shot noise.

### 5.13 Signals represented by the fluctuating intensity

In this section the fluctuating signals generated by the stochastic difference equations for the amplitude of the signal will be presented and analyzed.

We can change the point process (96) to avoid the negative interevent times, but leave relaxation rate  $\gamma$  unchanged [195],

$$\tau_k = |\tau_{k-1} - \gamma(\tau_{k-1} - \bar{\tau}) + \sigma \varepsilon_k|. \quad (256)$$

Then we introduce the rate of the signal as  $\nu_k = 1/\tau_k$ . From Eq. (256) we obtain the

recurrent equation for the rate

$$\nu_k = \frac{\nu_{k-1}}{|1 - \gamma(1 - \bar{\nu}^{-1}\nu_{k-1}) + \sigma\nu_{k-1}\varepsilon_k|}. \quad (257)$$

Here  $\bar{\nu} = 1/\bar{\tau}$  and the occurrence time  $t_k$  of the signal  $\nu_k$  should be calculated as

$$t_k = \sum_{l=1}^k \tau_l = \sum_{l=1}^k \nu_l^{-1}. \quad (258)$$

Actual time signal can be calculated using the rectangular pulses as

$$I(t) = \bar{a} \sum_k f_k(t_{k-1}, t_k) \nu_k, \quad (259)$$

where function  $f_k(t_{k-1}, t_k)$  is defined by Eq. (211).

For linearization of Eq. (257) we can use the rule for transformation of the variable in Itô stochastic equation [161]:

$$df[x(t)] = \left\{ h[x(t), t]f'[x(t)] + \frac{1}{2}g[x(t), t]^2 f''[x(t)] \right\} dt + g[x(t), t]f'[x(t)]dW(t), \quad (260)$$

where  $x(t)$  is the solution of stochastic differential equation

$$dx = h(x, t)dt + g(x, t)dW(t), \quad (261)$$

$h(x, t)$  and  $g(x, t)$  are some known functions,  $dW(t) = \xi(t)dt$  is a differential of the Wiener process, and  $\xi(t)$  is  $\delta$ -correlated,  $\langle \xi(t)\xi(t') \rangle = \delta(t - t')$ , white noise. The linearization results in the stochastic difference equation

$$\nu_k = \left| \nu_{k-1} + \gamma\nu_{k-1}(1 - \bar{\nu}^{-1}\nu_{k-1}) + \sigma^2\nu_{k-1}^3 + \sigma\nu_{k-1}^2\varepsilon_k \right|. \quad (262)$$

From Eq. (262) we derive the nonlinear Itô stochastic differential equation for  $\nu(t)$  as a function of the actual time  $t$ , i.e.,

$$\frac{d\nu}{dt} = \gamma\nu^2(1 - \bar{\nu}^{-1}\nu) + \sigma^2\nu^4 + \sigma\nu^{5/2}\xi(t). \quad (263)$$

The intensity of the signal is then  $I(t) = \nu(t)$ .

Therefore, the appropriate nonlinear stochastic differential equation may generate the signal with the  $1/f$  power spectral density, the same as the point process (96) with the fluctuating interevent time.

In Figure 18 a) and b) we present the power spectral densities of signals, generated according to Eqs. (259) and (262), respectively. We can notice that by using this method, we still have  $1/f$  like behavior of power spectral density. As we can see, the power spectral density is about 2 times smaller than the power spectral density, calculated according to Eq. (220). This is due to the reduced effective (averaged) value of the distribution density  $P_k(0)$  as discussed in section 5.5.

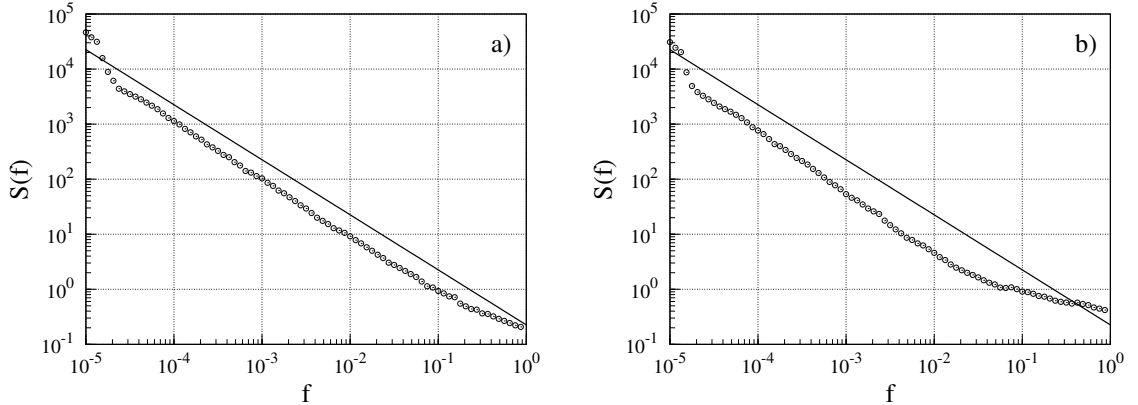


**Figure 18.** a) Power spectral density of the signal (259) generated according to Eq. (257) with parameters  $\bar{\tau} = 1$ ,  $\sigma = 0.01$ , and  $\gamma = 0.0001$  from  $N_\nu = 10^6$  points, converted using rectangular pulses into  $N_I = 10^5$  points real time signal and averaged over  $n = 100$  realizations, open circles. b) Power spectral density generated according to Eq. (262) with mirroring boundary at  $\nu = 10^3$  and the same parameters as in a), open circles. Solid lines represent power spectral density according to Eq. (220).

## 5.14 Stochastic nonlinear differential equation generating $1/f$ noise

In this section we will derive a stochastic differential equation for the signal, the solution of which exhibits  $1/f$  noise. For this purpose, we will investigate the point process case Eq. (86) with no relaxation rate  $\gamma = 0$  [196]. Recurrent equations for the transit time then can be written according to Eq. (96) as

$$t_k = t_{k-1} + \tau_k, \quad (264)$$

$$\tau_k = \tau_{k-1} + \sigma \varepsilon_k \quad (265)$$

with the appropriate boundary conditions, restricting the diffusion of  $\tau_k$  in the finite interval  $[\tau_{\min}, \tau_{\max}]$ . In Eq. (265),  $\varepsilon_k$  are normally distributed uncorrelated random variables with a zero expectation and unit variance, i.e., a white noise, and  $\sigma$  is a standard deviation of the white noise.

The signal (86) generated according to Eqs. (264) and (265), depending on the parameter  $\sigma$  and the interval  $[\tau_{\min}, \tau_{\max}]$ , exhibits  $1/f$  noise in any desirable wide range of frequency. According to the general theory [57, 60, 61, 62, 63], the power spectral density of such point process for  $f \lesssim \tau_{\max}^{-1}$  and  $\tau_{\min} \rightarrow 0$  may be estimated as

$$S(f) \sim \frac{\bar{a}^2}{\tau_{\max}^2} \frac{1}{f}. \quad (266)$$

We rewrite Eq. (265) as a differential Itô stochastic equation, interpreting  $k$  as a continuous variable, i.e.,

$$\frac{d\tau_k}{dk} = \sigma \xi(k). \quad (267)$$

Here  $\xi(k)$  is a Gaussian white noise, satisfying the standard condition

$$\langle \xi(k) \xi(k') \rangle = \delta(k - k'). \quad (268)$$

Then we rewrite Eq. (267), using the occurrence time. Transition from the occurrence number  $k$  to the actual time  $t$  according to the relation  $dt = \tau_k dk$  yields the equation

$$\frac{d\tau}{dt} = \frac{\sigma}{\sqrt{\tau}} \xi(t). \quad (269)$$

The signal averaged over the time interval  $\tau_k$  according to Eq. (86) is

$$x = \frac{\bar{a}}{\tau_k}. \quad (270)$$

In order to transform variables from  $\tau$  to  $x$ , we use the rule for transformation of Itô equation (260). Applying Eq. (261) to Eq. (269) we find functions  $h(x, t) = h(\tau, t) = 0$  and  $g(x, t) = g(\tau, t) = \sigma/\sqrt{\tau}$ . Therefore, Eq. (270) results in the stochastic differential Itô equation

$$\frac{dx}{dt} = \frac{\sigma^2}{\bar{a}^3} x^4 + \frac{\sigma}{\bar{a}^{3/2}} x^{5/2} \xi(t). \quad (271)$$

Equation (271) can be rewritten in a form that does not contain any parameters. Introducing the scaled time

$$t_s = \frac{\sigma^2}{\bar{a}^3} t, \quad (272)$$

we obtain from Eq. (271) an equation

$$\frac{dx}{dt_s} = x^4 + x^{5/2} \xi(t_s). \quad (273)$$

Then we apply the stationary Fokker-Plank equation Eq. (120) and find the steady-state solution with the appropriate reflective boundary conditions and zero flow, obtained from Eq. (273), which is of the power-law form,

$$P(x) = \frac{C}{x^3}, \quad (274)$$

where  $C$  has to be defined from the normalization.

Because of the divergence of the power-law distribution and the requirement of the stationary of the process, the stochastic equation (273) should be analyzed together with the appropriate restrictions of the diffusion in some finite interval  $x_{\min} \lesssim x \lesssim x_{\max}$ . Such restrictions may be introduced as some additional conditions to the iterative solution of the stochastic differential equation. Similar restrictions, however, may be fulfilled by introducing some additional terms into Eq. (273), corresponding to the restriction of the diffusion in some “potential wall”. According to the general theory [161], the exponentially restricted diffusion with the diffusion density

$$P(x) \sim \frac{1}{x^3} \exp \left\{ - \left( \frac{x_{\min}}{x} \right)^m - \left( \frac{x}{x_{\max}} \right)^m \right\} \quad (275)$$

generates the stochastic differential equation

$$\frac{dx}{dt_s} = \frac{m}{2} \left( \frac{x_{\min}^m}{x^{m-4}} - \frac{x^{m+4}}{x_{\max}^m} \right) + x^4 + x^{5/2} \xi(t_s). \quad (276)$$

Here  $m$  is some parameter.

Since the point process Eqs. (86) and (96) gives the signal with  $1/f$  noise, the signal obtained from Eqs. (273) and (276) should also result in  $1/f$  noise in some frequency interval. When  $x_{\max} \rightarrow \infty$ , from Eq. (266) we estimate the power spectral density as

$$S(f) \sim x_{\min}^2 \frac{1}{f}. \quad (277)$$

Such conclusion is confirmed by the numerical solution of Eq. (276).

We solve Eq. (273) and (276) using the method of discretization. When the variable step of integration is  $\Delta t_s = h_i$ , the differential equation (276) transforms to the difference equation

$$x_{i+1} = x_i + \frac{m}{2} \left( \frac{x_{\min}^m}{x_i^{m-4}} - \frac{x_i^{m+4}}{x_{\max}^m} \right) h_i + x_i^4 h_i + x_i^{5/2} \sqrt{h_i} \varepsilon_i. \quad (278)$$

We can solve Eq. (278) numerically with the constant step,  $h_i = \text{const}$ , when  $t_{i+1} = t_i + h$ . However, one of the most effective methods of solution of Eq. (278) is when the change of the variable  $x_i$  in one step is proportional to the value of the variable. We take the integration steps  $h_i$  from the equation  $x_i^{5/2} \sqrt{h_i} = \kappa x_i$ , with  $\kappa \ll 1$  being a small parameter. As a result, we have the system of equations

$$\begin{aligned} x_{i+1} &= x_i + \kappa^2 x_i \left[ 1 + \frac{m}{2} \left( \frac{x_{\min}^m}{x_i^m} - \frac{x_i^m}{x_{\max}^m} \right) \right] + \kappa x_i \varepsilon_i, \\ t_{i+1} &= t_i + \frac{\kappa^2}{x_i^3}. \end{aligned} \quad (279)$$

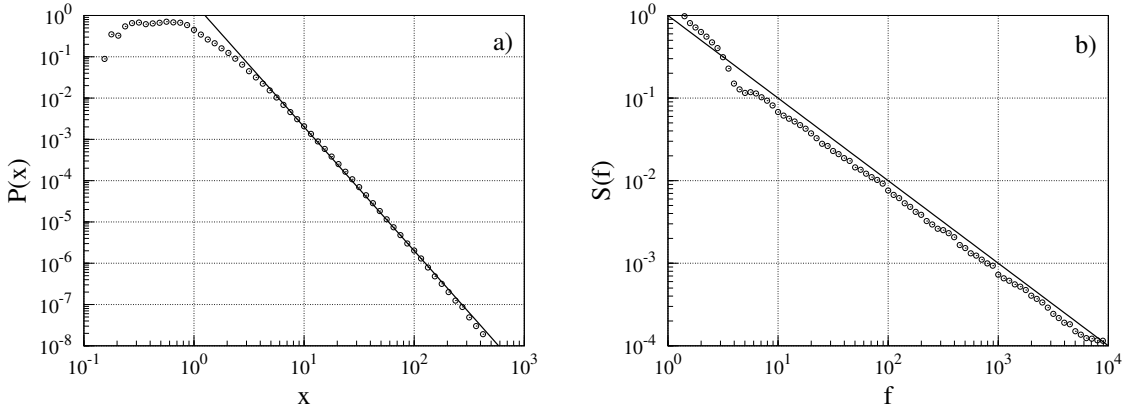


**Figure 19.** a) Distribution density of the variable  $x$ , open circles, compared with Eq. (274), where  $C$  is found from normalization, solid line; and b) power spectral density, obtained from the numerical solution of Eq. (279), open circles. Parameters used are  $x_{\min} = 1$ ,  $x_{\max} = 10^3$ ,  $m = 1$ , and  $\kappa = 0.1$ . Signal was calculated from  $N_x = 10^6$  points and averaged over  $n = 100$  realizations. Solid line in b) represents power spectral density, calculated according to Eq. (277).

The distribution density  $P(x)$  of the variable  $x$ , obtained by numerical simulation of Eq. (279), is shown in Fig. 19 a). We see that our method of solution gives good agreement with the power law distribution (274) in the interval  $x_{\min} \lesssim x \lesssim x_{\max}$ . The power spectral density  $S(f)$  numerically calculated according to Eq. (279) is shown in Fig. 19 b). It shows that Eq. (276) indeed gives a signal, exhibiting  $1/f$  noise in a wide frequency interval.

## 5.15 Generalization for class of stochastic equations

By analogy with the Section 5.14 from the multiplicative equation (147)

$$\tau_{k+1} = \tau_k + \gamma \tau_k^{2\mu-1} + \sigma \tau_k^\mu \varepsilon_k \quad (280)$$

we can obtain the class of the stochastic nonlinear differential equations

$$\frac{dx}{dt} = (\sigma^2 - \gamma) \frac{x^{4-2\mu}}{a^{3-2\mu}} + \frac{\sigma x^{5/2-\mu}}{a^{3/2-\mu}} \xi(t). \quad (281)$$

Introducing the scaled time

$$t_s = \frac{\sigma^2}{\bar{a}^{3-2\mu}} t \quad (282)$$

and the new parameters

$$\eta = \frac{5}{2} - \mu, \quad \Gamma = 1 - \frac{\gamma}{\sigma^2} \quad (283)$$

we obtain the class of equations

$$\frac{dx}{dt_s} = \Gamma x^{2\eta-1} + x^\eta \xi(t_s) \quad (284)$$

which should generate the signals with the power-law distributions of the signal intensity

$$P(x) \sim \frac{1}{x^\lambda}, \quad \lambda = 2(\eta - \Gamma) \quad (285)$$

and  $1/f^\beta$  noise,

$$S(f) \sim \frac{1}{f^\beta}, \quad \beta = 2 - \frac{2\Gamma + 1}{2\eta - 2}. \quad (286)$$

The exponentially restricted diffusion should generate the stochastic differential equation

$$\frac{dx}{dt_s} = \frac{m}{2} \left( \frac{x_{\min}^m}{x^{m+1-2\eta}} - \frac{x^{m-1+2\eta}}{x_{\max}^m} \right) + \Gamma x^{2\eta-1} + x^\eta \xi(t_s), \quad (287)$$

where  $m$  is some parameter.

For the numerical solution of Eq. (287) we can take the integration steps from the equation  $x_i^\eta \sqrt{h_i} = \kappa x_i$ , with  $\kappa \ll 1$  being a small parameter. As a result, we have the system of equations

$$\begin{aligned} x_{i+1} &= x_i + \kappa^2 x_i \left[ \Gamma + \frac{m}{2} \left( \frac{x_{\min}^m}{x_i^m} - \frac{x_i^m}{x_{\max}^m} \right) \right] + \kappa x_i \varepsilon_i, \\ t_{i+1} &= t_i + \frac{\kappa^2}{x_i^{2\eta-2}}. \end{aligned} \quad (288)$$

The distribution densities  $P(x)$  of the variable  $x$ , obtained by numerical simulation of Eq. (288), are shown in Figures 20 a) and c). Power spectral densities  $S(f)$  are shown in Figures 20 b) and d). Numerical simulation of distribution densities and power spectral densities are in good agreement with approximate expressions, Eq. (285) and Eq. (286), respectively. We can compare power spectral densities in Figure 20 b) with Figure 6 a) open circles, and Figure 20 d) with Figure 6 b) open triangles, since the respective point process power spectral densities were simulated using the same parameters as in the corresponding stochastic differential equations. We notice that solution of stochastic differential equation does not result in a shot noise in a high frequency limit.

Generalized differential equation (284) results in power spectral density  $S(f) = 1/f^\beta$  with a different slopes  $\beta$  in a wide frequency interval.

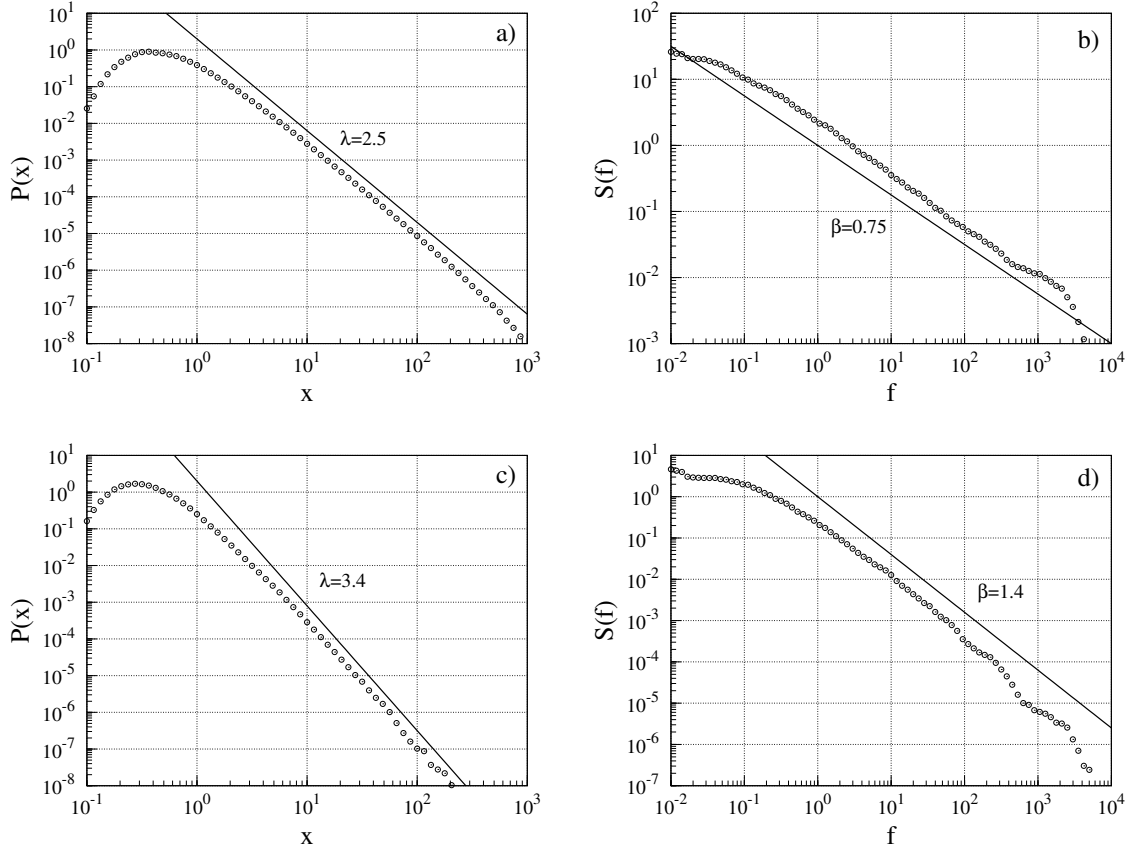


**Figure 20.** a) Numerically simulated distribution density of the variable  $x$ , open circles, compared with expected distribution density, Eq. (285), solid line; and b) power spectral density, obtained from the numerical solution of Eq. (288), open circles. Parameters used are  $x_{\min} = 1$ ,  $x_{\max} = 10^3$ ,  $m = 1$ ,  $\Gamma = 0.75$ ,  $\eta = 2$ , and  $\kappa = 0.1$ . Signal was calculated from  $N_x = 10^6$  points and averaged over  $n = 100$  realizations. Solid line in b) represents power spectral density, calculated according to Eq. (286). c) and d) represent distribution density and power spectral density, respectively, with the parameters  $m = 1$ ,  $\Gamma = -0.2$ ,  $\eta = 1.5$ , and  $\kappa = 0.01$ .

## 6 HAMILTONIAN SYSTEMS AND $1/f$ NOISE

In this section we will try to demonstrate a possibility of occurrence of  $1/f$  noise in the dynamical Hamiltonian systems, exhibiting transition from regular to chaotic dynamics.

### 6.1 Standard map

We will start with the investigation of the oscillator with two degrees of freedom and with a Hamiltonian  $H$  not depending on time [197, 198, 199, 200]. We assume that this system can be integrated and, therefore, we can introduce action-angle variables

$$H(J_1, J_2) = E, \quad (289)$$

where  $E$  is a persisting energy of the system,  $J_1$  and  $J_2$  are the integrals of the motion. Persisting energy lets us to lower phase space dimension from four to three. Persistence of one of the action variables yields decreasing of the phase space dimension to two-dimensional surface in a three-dimensional space of constant energy. Motion on this surface can be written using frequencies, corresponding to both degrees of freedom

$$\begin{aligned} \theta_1 &= \omega_1 t + \theta_{10}, \\ \theta_2 &= \omega_2 t + \theta_{20}, \end{aligned} \quad (290)$$

where angle variables are defined mod  $2\pi$ .

Motion of the given system can be visualized as a motion on a torus in a phase space with actions  $J_1$  and  $J_2$  being the two radius of the torus. Fixing one of the action variable  $J_1$  according to Eq. (289), defines the other action  $J_2$ , as well as defines an invariant surface in the phase space and also the relation

$$\alpha = \frac{\omega_1}{\omega_2}, \quad (291)$$

because  $\omega_1 = \omega_1(J_1, J_2)$  and  $\omega_2 = \omega_2(J_1, J_2)$ . When  $\alpha = r/s$ , where  $r$  and  $s$  are integers, motion on the torus becomes motion along a periodic trajectory, which closes after  $r$  rotations of angle variable  $\theta_1$  and  $s$  rotations of  $\theta_2$ . In a common case  $\alpha$  is an irrational digit and the trajectory covers all surface of the torus.

For investigation of the phase trajectories, especially, in a case of two degrees of freedom, it is very convenient to use the Poincaré maps. For the Hamiltonian (289) we can choose plane  $(J_1, \theta_1)$  ( $\theta_2 = \text{const}$ ) to be the Poincaré surface. Time interval between two successive crossings of the plane  $(J_1, \theta_1)$  is then equal to  $\Delta t = 2\pi/\omega_2$  with  $J_1 = \text{const}$  (motion on the torus). During this time  $\Delta t$  variable  $\theta_1$  increases by  $\omega_1 \Delta t = 2\pi\alpha(J_1)$ , where  $\alpha$  is the number of rotations. Because action  $J_2$  depends only on the energy  $E$  and action  $J_1$ ,  $J_2 = J_2(J_1, E)$ , and energy  $E$  persists, we can consider that  $\alpha$  depends only on  $J_1$ . In the following equation of transition from  $k$  to  $k + 1$  crossing of the plane and in order to simplify the equations we will omit index 1 and the result is a twist mapping

$$\begin{aligned} J_{k+1} &= J_k, \\ \theta_{k+1} &= \theta_k + 2\pi\alpha(J_{k+1}), \end{aligned} \quad (292)$$

where we have written  $\alpha$  to be a function of  $J_{k+1}$  instead of  $J_k$ . This follows from the phase space property that two-dimensional twist mapping should preserve area

$$\frac{\partial(J_{k+1}, \theta_{k+1})}{\partial(J_k, \theta_k)} \equiv [J_{k+1}, \theta_{k+1}] = 1. \quad (293)$$

If  $\alpha$  is an irrational digit, any trajectory continuously covers the circle in the Poincaré plane when  $k \rightarrow \infty$ . On the other hand, if  $\alpha$  is a rational digit  $\alpha = r/s$ , where  $r$  and  $s$  are integers, we will have periodic trajectories with the period of  $s$  iterations.

We will consider a small perturbation on an integrable system with two degrees of freedom (289). In this case Hamiltonian depends on angle variables,

$$H(J_1, J_2, \theta_1, \theta_2) = H_0(J_1, J_2) + \varepsilon H_1(J_1, J_2, \theta_1, \theta_2). \quad (294)$$

On the crossing plane  $\theta_2 = \text{const}$  twist mapping will change to perturbed twist mapping

$$\begin{aligned} J_{k+1} &= J_k + \varepsilon f(J_{k+1}, \theta_k), \\ \theta_{k+1} &= \theta_k + 2\pi\alpha(J_{k+1}) + \varepsilon g(J_{k+1}, \theta_k), \end{aligned} \quad (295)$$

where  $f$  and  $g$  are periodic functions in  $\theta$ . Because this twist map is derived from Hamiltonian equations, it should preserve area (293). We have chosen functions  $f$  and  $g$  depending on  $J_{k+1}$  instead of  $J_k$  in order the area preservation to be written in a very simple form. Indeed, equation (295) then can be derived using generating function

$$F = J_{k+1}\theta_k + 2\pi\mathcal{A}(J_{k+1}) + \varepsilon\mathcal{G}(J_{k+1}, \theta_k), \quad (296)$$

where

$$\begin{aligned} \alpha &= \frac{d\mathcal{A}}{dJ_{k+1}}, \\ f &= -\frac{\partial\mathcal{G}}{\partial\theta_k}, \\ g &= \frac{\partial\mathcal{G}}{\partial J_{k+1}}, \end{aligned} \quad (297)$$

and

$$\frac{\partial f}{\partial J_{k+1}} + \frac{\partial g}{\partial\theta_k} = 0, \quad (298)$$

which leads to the area preservation.

If  $f$  depends on  $J_{k+1}$ , then  $J_{k+1}$  in Eq. (295) can be calculated by using Newton tangent method or using iterations in which new iteration value  $J_{k+1}^{(i)}$  is calculated by putting previous value  $J_{k+1}^{(i-1)}$  into function  $f$ . Both methods result in the fast convergence.

The cases where  $f$  does not depend on  $J$  and  $g \equiv 0$  have been analysed most frequently. We will investigate this particular case more deeply. Eq. (295) then can be written as

$$\begin{aligned} J_{k+1} &= J_k + \varepsilon f(\theta_k), \\ \theta_{k+1} &= \theta_k + 2\pi\alpha(J_{k+1}). \end{aligned} \quad (299)$$

We will linearize second equation in (299) near stable point  $J_{k+1} = J_k = J_0$ , for which  $\alpha(J_0)$  is an integer, i.e.,

$$J_k = J_0 + \Delta J_k. \quad (300)$$

Introducing a new action variable

$$I_k = 2\pi\alpha'\Delta J_k \quad (301)$$

results in the general standard map

$$\begin{aligned} I_{k+1} &= I_k + K f^*(\theta_k), \\ \theta_{k+1} &= \theta_k + I_{k+1}, \end{aligned} \quad (302)$$

where

$$K = 2\pi\alpha'\varepsilon f_{\max} \quad (303)$$

is an indicator of stochastic in the system and  $f^* = f/f_{\max}$  is the change of the angle variable, normalized to unity. In the case where  $f^* = \sin\theta_k$  the general standard map transforms to the standard map, known as Chirikov map,

$$\begin{aligned} I_{k+1} &= I_k + K \sin\theta_k, \\ \theta_{k+1} &= \theta_k + I_{k+1}. \end{aligned} \quad (304)$$

Chirikov [201] and Greene [202] used standard map Eq. (304) to investigate transition from regular to stochastic motion.

## 6.2 Rotor affected by the periodic kicks

One of the simplest systems which shows chaotic behavior in time, is a rotor with a friction, affected by the periodic kicks [203], shown in Figure 21. Equation of motion

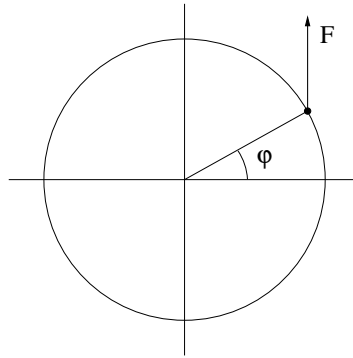


**Figure 21.** Rotor, affected by the periodic force  $F$ , motion of which is described by the differential equation (305).

for the kicked rotor is

$$\ddot{\varphi} + \Gamma\dot{\varphi} = F \equiv K f(\varphi) \sum_{n=0}^{\infty} \delta(t - nT), \quad (305)$$

where dots mean derivatives in time,  $n$  is an integer,  $\Gamma$  is a measure of friction,  $T$  is a period between kicks,  $f$  is the power, striking the rotor and an inertia momentum is considered to be equal to 1. After the following transformation of variables

$$\begin{aligned}x &= \varphi, \\y &= \dot{\varphi}, \\z &= t,\end{aligned}\tag{306}$$

Eq. (305) is transformed to the system of independent non-linear differential equations of the first order

$$\dot{x} = y,\tag{307}$$

$$\dot{y} = -\Gamma y + K f(x) \sum_{n=0}^{\infty} \delta(z - nT),\tag{308}$$

$$\dot{z} = 1.\tag{309}$$

The integration of the equations (307) – (309) results in two-dimensional map for the variables  $(x_k, y_k) = \lim_{\varepsilon \rightarrow 0} [x(kT - \varepsilon), y(kT - \varepsilon)]$ . When  $(k + 1)T - \varepsilon > t > kT - \varepsilon$ , general solution of Eq. (308) is

$$y(t) = y_k e^{-\Gamma(t-kT)} + K \sum_{n=0}^{\infty} f(x_n) \int_{kT-\varepsilon}^t dt' e^{\Gamma(t'-t)} \delta(t' - nT)\tag{310}$$

and

$$y_{k+1} = e^{-\Gamma T} [y_k + K f(x_k)].\tag{311}$$

Integrating Eq. (307) and using Eq. (311) yield

$$x_{k+1} = x_k + \frac{1 - e^{-\Gamma T}}{\Gamma} [y_k + K f(x_k)].\tag{312}$$

Equations (311) and (312) transform initial three-dimensional system of differential equations to the two-dimensional discrete map.

We will investigate in greater detail a special case with no friction ( $\Gamma \rightarrow 0$ ). In this case Eqs. (311) and (312) write as

$$\begin{aligned}y_{k+1} &= y_k + K f(x_k), \\x_{k+1} &= x_k + T y_{k+1}.\end{aligned}\tag{313}$$

Assuming that external power  $f(x_k) = \sin x_k$  and period  $T = 1$ , we obtain

$$\begin{aligned}y_{k+1} &= y_k + K \sin x_k, \\x_{k+1} &= x_k + y_{k+1},\end{aligned}\tag{314}$$

which is a standard map, Eq. (304).

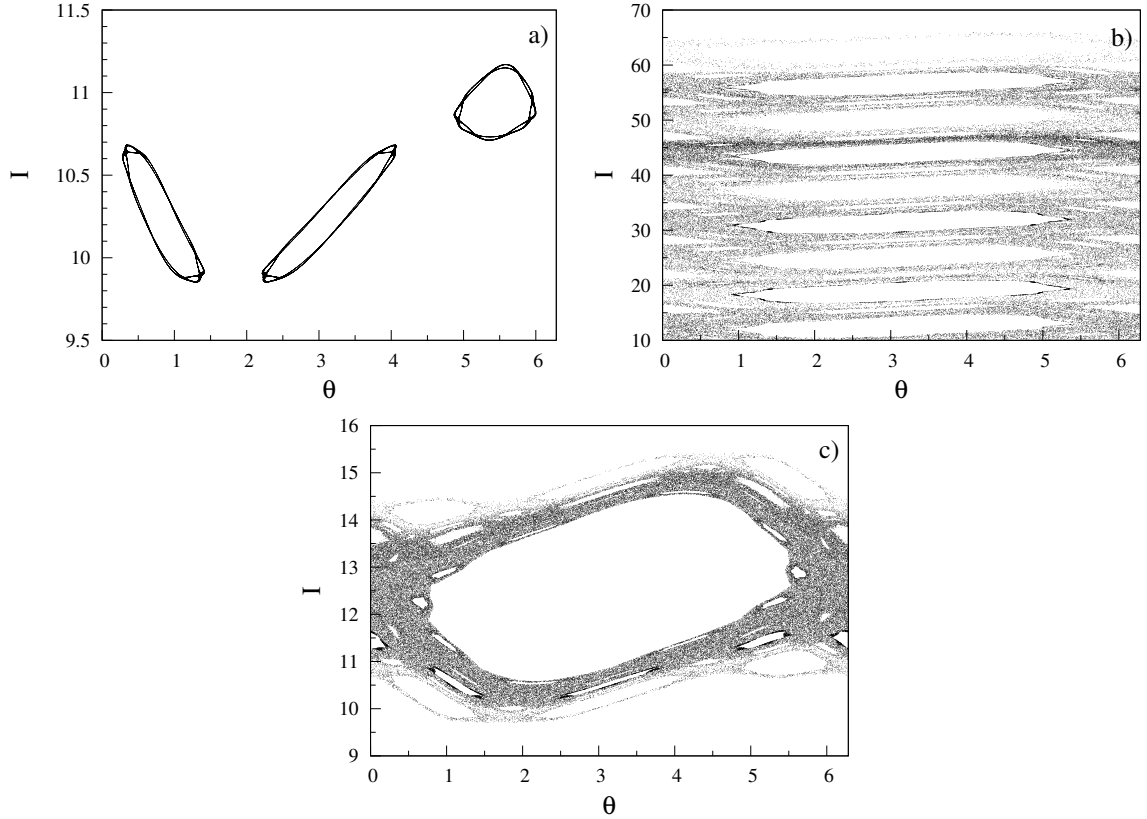


**Figure 22.** Phase spaces of the standard map Eqs. (304) with the parameters a)  $K = 0.96$ , b)  $K = 1.07$ , and  $K = 1.03$ . Initial action-angle values are  $y_0 = 10$  and  $x_0 = 1.302$ ,  $N = 10^5$  iterations are fulfilled.

### 6.3 Numerical simulation of the rotor's dynamics

In this section we present the results of numerical simulations of the standard map, Eq. (304), and investigate appearance of stochasticity in the system. It is a very well investigated transition from the regular to the chaotic motion in the standard map (304) and (314). It occurs at  $K = K_c \approx 1$ . In Figure 22 we present three phase space maps, the first one is for  $K < 1$ , and we see that the motion is deterministic, however, when  $K > 1$ , the second phase space, we see the layers of chaotic motion. In the third figure we see the map for  $K$  close to  $K_c$ , with the intermediate motion between deterministic and chaotic state.

Hamiltonian of the rotor with no friction, Eqs. (305) and (314), can be written as [203]

$$H(x_k, y_k) = \frac{y_k^2}{2} + K \cos(x_k) \sum_{n=0}^{\infty} \delta(t - nT). \quad (315)$$

Angular velocity of the rotor is found from the Hamiltonian equations [198]

$$\omega_k = \frac{\partial H}{\partial y_k} = y_k. \quad (316)$$

Therefore, the period of the rotation after  $n$  strikes

$$T_k = \frac{2\pi}{\omega_k} = \frac{2\pi}{y_k}. \quad (317)$$

In analogy of the heartbeat intervals [143, 144] we construct a signal in  $k$  space, where values of the signal are  $T_k$ .

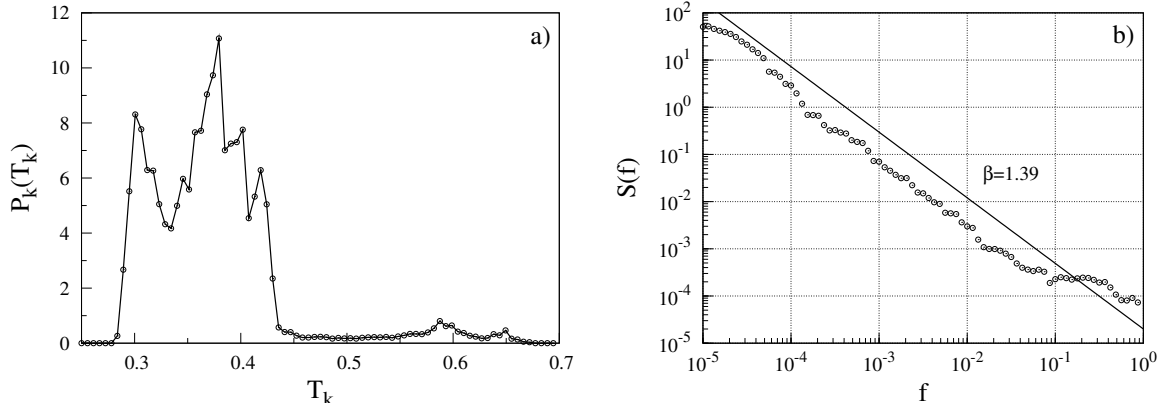


**Figure 23.** a) Signal density and b) power spectral density, calculated using Fast Fourier Transform, for a signal, generated from standard map, Eqs. (304), with the parameter  $K = 1.03$ . Initial action-angle values are  $I = 12.6$  and  $\theta = \pi/6$ ,  $N = 10^6$  iterations are fulfilled. A dashed line shows approximation  $S(f) \sim 1/f^\beta$ .

Signal distribution density and power spectral density of the signal are presented in Figure 23. As we see, the period of the rotor can exhibit  $1/f^\beta$  noise with  $1 \leq \beta \leq 1.5$  when parameter  $K \approx 1$ .

## 6.4 One-dimensional classical hydrogen atom in a monochromatic field

Further we will consider interaction and chaotic dynamics of the classical hydrogen atom in an electromagnetic field.

A classical hydrogen atom in a monochromatic field is one of the simplest real nonlinear systems, whose dynamics may be regular or chaotic [204, 205], depending on the relative field strength and frequency. Even a one-dimensional classical model of a highly excited atom yields results sufficiently close to the experimental findings. For theoretical analysis approximate mapping equations of motion, rather than differential equations, are most convenient [205, 206, 207, 208, 209, 210]. Here a two-dimensional map (for the scaled energy and for relative phase of the field) [206] is generalized for the two-dimensional hydrogen atom, i.e. we calculate energy and angular momentum changes of the atom, interacting with the electromagnetic field.

However, we start from the one-dimensional hydrogen atom in monochromatic field. The Hamiltonian of the classical hydrogen atom in a linearly polarized monochromatic electromagnetic field (in atomic units) is [210, 207, 211]

$$\mathcal{H} = \frac{1}{2} \left( \mathbf{P} + \frac{1}{c} \mathbf{A} \right)^2 - \frac{1}{r}. \quad (318)$$

Here  $\mathbf{P}$  is the generalized momentum,  $c$  is the light velocity,

$$\mathbf{A} = -\frac{c\mathbf{F}}{\omega} \sin(\omega t + \vartheta) \quad (319)$$

is the vector potential of the field,  $\mathbf{F}$ ,  $\omega$  and  $\vartheta$  are the field strength amplitude, field frequency and phase, respectively. The change of the electron energy can be obtained from the Hamiltonian equations of motion [212]

$$\dot{E} = -\dot{\mathbf{r}} \cdot \mathbf{F} \cos(\omega t + \vartheta). \quad (320)$$

One can introduce the scaled energy  $E_s = E/\omega^{2/3}$  and the scaled field strength  $F_s = F/\omega^{4/3}$ . However, it is convenient [205, 206, 210, 209, 208, 207] to introduce the positive scaled energy  $\varepsilon = -2E_s$  and the relative field strength  $F_0 = F_s/\varepsilon_0^2$ , with  $\varepsilon_0$  being the initial scaled energy.

Integration of Eq. (320) over the period of time between two subsequent passages of the electron at the apocenter results in the change of the electron energy [206, 210]

$$\varepsilon_{j+1} = \varepsilon_j - \pi F_0 \varepsilon_0^2 h(\varepsilon_{j+1}) \sin \vartheta_j, \quad (321)$$

where

$$h(\varepsilon_{j+1}) = \frac{4}{\varepsilon_{j+1}} \mathbf{J}'_{s_{j+1}}(s_{j+1}). \quad (322)$$

Here  $s = \varepsilon^{-3/2} = \omega/(-2E)^{3/2}$  is the relative frequency of the field, i.e. the ratio of the field frequency to the electron Kepler orbital frequency and  $\mathbf{J}'_s(s)$  is the Anger function

$$\mathbf{J}_s(z) = \frac{1}{\pi} \int_0^\pi \cos(s\xi - z \sin \xi) d\xi \quad (323)$$

derivative

$$\mathbf{J}'_s(z) = \frac{1}{\pi} \int_0^\pi \sin(s\xi - z \sin \xi) \sin \xi d\xi, \quad (324)$$

when parameter  $s = z$ .

Introducing a generating function  $G(\varepsilon_{j+1}, \vartheta_j)$  [200, 213]

$$G(\varepsilon_{j+1}, \vartheta_j) = \varepsilon_{j+1} \vartheta_j - 4\pi \varepsilon_{j+1}^{-1/2} - \pi F_0 \varepsilon_0^2 h(\varepsilon_{j+1}) \cos \vartheta_j \quad (325)$$

from the equations

$$\begin{aligned} \varepsilon_j &= \frac{\partial G}{\partial \vartheta_j}, \\ \vartheta_{j+1} &= \frac{\partial G}{\partial \varepsilon_{j+1}}, \end{aligned} \quad (326)$$

one can calculate the phase  $\vartheta$  change over the period

$$\vartheta_{j+1} = \vartheta_j + 2\pi \varepsilon_{j+1}^{-3/2} - \pi F_0 \varepsilon_0^2 \eta(\varepsilon_{j+1}) \cos \vartheta_j, \quad (327)$$

where

$$\eta(\varepsilon_{j+1}) = \frac{dh(\varepsilon_{j+1})}{d\varepsilon_{j+1}}. \quad (328)$$

It is easy to show that a generating function, (325), fulfills the requirement to preserve phase space area, Eq. (293), i.e.,

$$\frac{\partial(\varepsilon_{j+1}, \vartheta_{j+1})}{\partial(\varepsilon_j, \vartheta_j)} = 1. \quad (329)$$

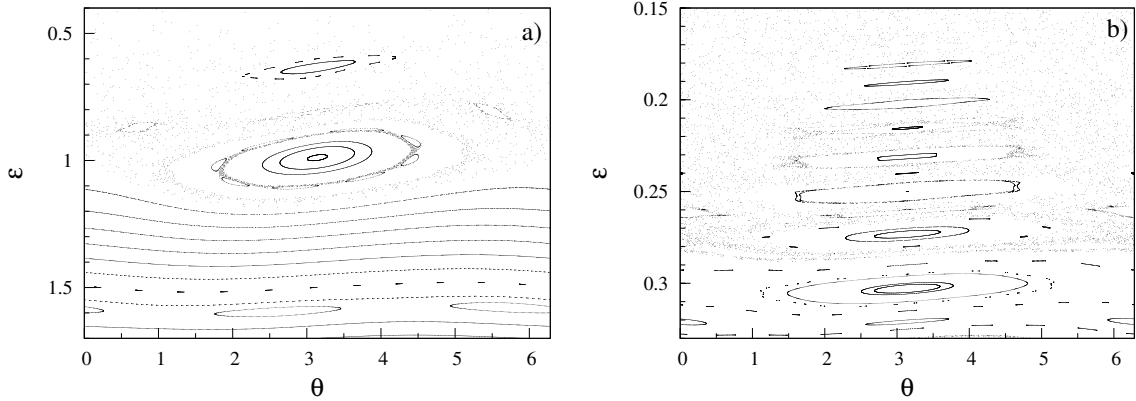


**Figure 24.** Trajectories  $(\varepsilon, \vartheta)$  for the map (321) and (327) with the parameter a)  $\pi F_0 \varepsilon_0^2 = 0.06$  and initial conditions  $\vartheta_0 = \pi$ ,  $\varepsilon_0 = 1.9 - 0.05i$  ( $i = 0, 1, 2, \dots$ ) and b)  $\pi F_0 \varepsilon_0^2 = 0.0035$  and initial conditions  $\vartheta_0 = \pi$ ,  $\varepsilon_0 = 0.35 - 0.003i$  ( $i = 0, 1, 2, \dots$ ).

Equations (321) and (327) describe the changes of the energy and phase in time. This map greatly facilitates numerical investigation of dynamics and ionization process. We use the following expressions for the derivative of Anger function

$$\mathbf{J}'_s(s) = \begin{cases} \frac{1 + \frac{5}{24}s^2}{2\pi(1-s^2)} \sin(\pi s), & s \leq 1 \\ \frac{b}{s^{2/3}} - \frac{a}{5s^{4/3}} - \frac{\sin(\pi s)}{4\pi s^2}, & s \gg 1 \end{cases} \quad (330)$$

where

$$a = \frac{2^{1/3}}{3^{2/3}\Gamma(2/3)} \simeq 0.4473, \quad b = \frac{2^{2/3}}{3^{1/3}\Gamma(1/3)} \simeq 0.41085. \quad (331)$$

Trajectories for the map (321) and (327) are shown in Figure 24 and ionization threshold field dependence on the relative frequency is shown in Figure 25.

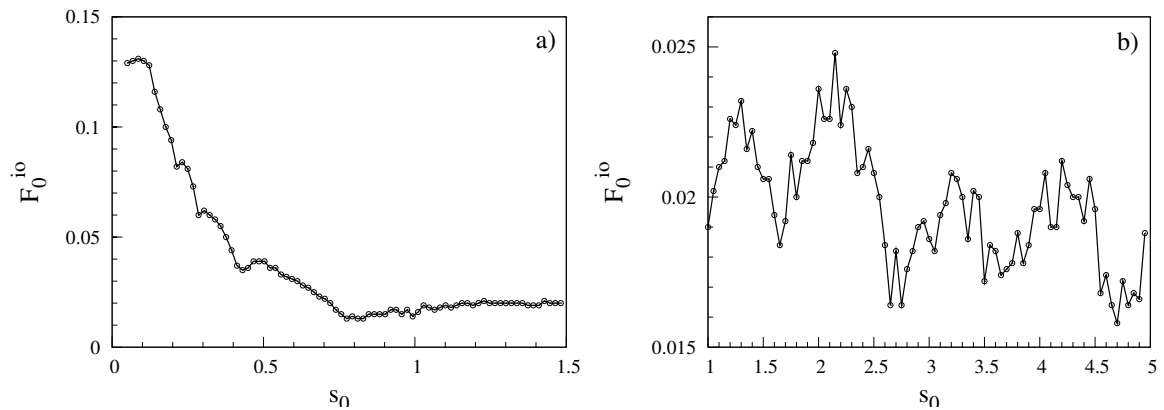


**Figure 25.** Ionization threshold field dependence on the relative frequency for a) small frequencies  $s_0$  and b) for high frequencies, calculated using variation of the initial phase  $\vartheta_0$ .

Period of the electron in atomic units is expressed as [197]

$$T = \pi \sqrt{\frac{1}{2|E|^3}}. \quad (332)$$

After introducing the scaled period  $T_s = \omega T / (2\pi)$  we have

$$T_s = \varepsilon^{-3/2} = s. \quad (333)$$

In Figure 26 we present signal distribution density and power spectral density, calculated for a signal, constructed from  $T_s$  in  $j$ -space. As we can see, it might exhibit  $1/f$  noise.

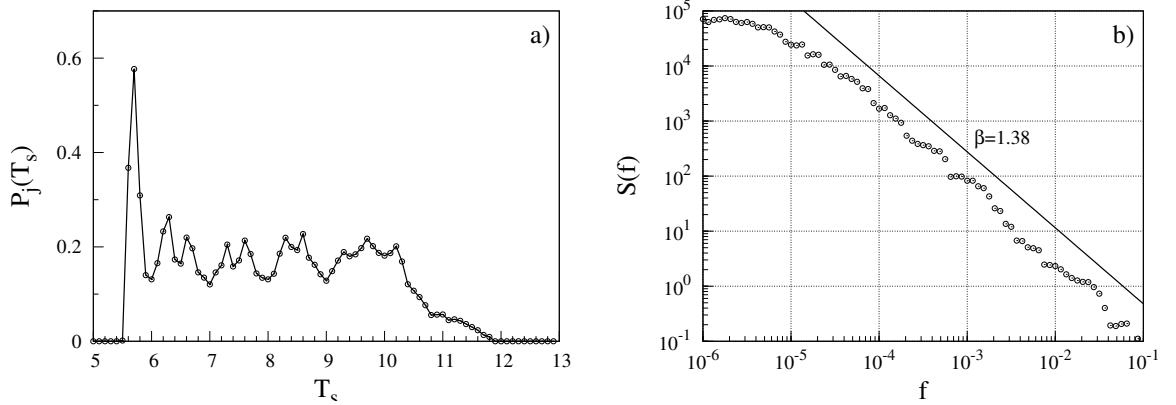


**Figure 26.** a) Signal density and b) power spectral density, calculated using Fast Fourier Transform for a signal generated from map Eqs. (321) and (327) with the parameter  $\pi F_0 \varepsilon_0^2 = 0.0035$  and initial conditions  $\vartheta_0 = \pi$ ,  $\varepsilon_0 = 0.21$ .  $N = 10^6$  iterations are fulfilled. A dashed line shows approximation  $S(f) \sim 1/f^\beta$ .

## 6.5 Two-dimensional atom in a monochromatic field

For the two-dimensional atom in a monochromatic field, Fig. 27, Hamiltonian (318) can be written as

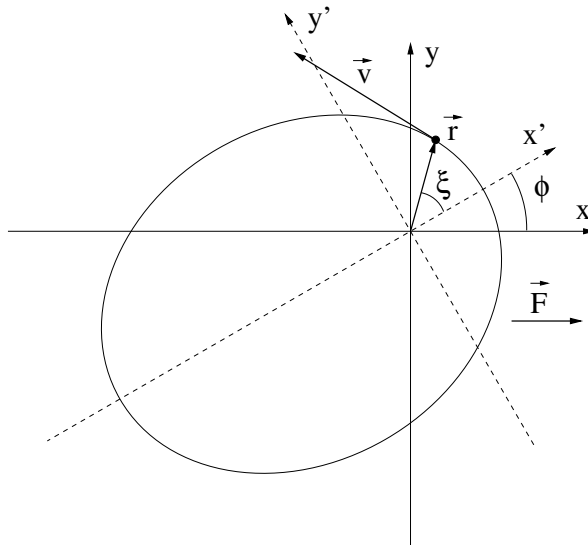


**Figure 27.** Two-dimensional atom in the electromagnetic field.

$$\mathcal{H} = \frac{m}{2} \dot{r}^2 + r^2 \dot{\xi}^2 - rF \cos(\xi + \varphi) \cos(\omega t + \vartheta) - \frac{1}{r}. \quad (334)$$

The change of the electron energy is then equal to

$$\dot{E}_k = -Fv_x \cos(\omega t + \vartheta). \quad (335)$$

For the calculation of the energy change of the arbitrary orientated two-dimensional atom in the electromagnetic field, one should perform the transformation of the coordinates, shown in Fig. 27 [212, 207, 208],

$$\begin{aligned} x &= x' \cos \varphi - y' \sin \varphi, \\ y &= x' \sin \varphi + y' \cos \varphi, \end{aligned} \quad (336)$$

and use elliptic coordinates

$$\begin{aligned} r &= a(1 - e \cos \xi), \\ t &= \sqrt{\frac{ma^3}{\gamma}}(\xi - e \sin \xi), \\ x' &= a(\cos \xi - e), \\ y' &= a\sqrt{1 - e^2} \sin \xi, \end{aligned} \quad (337)$$

where  $\xi$  is a parameter, and going round the ellipsis results in  $2\pi$  change of  $\xi$ ,  $a$  and  $e$  are semi-major axis and eccentricity respectively, and  $\gamma$  describes central field strength, which in atomic units equals to one,  $\gamma = 1$ . We use the following notations

$$s = \omega\sqrt{ma^3}, \quad z = es. \quad (338)$$

During the period when an electron moves from the closest to the nucleus trajectory point, apocenter, to the most distance point, pericenter, the parameter  $\xi$  changes in the interval  $(0, \pi)$ , the energy change can be found by integrating Eq. (335) and applying transformation of the coordinates Eqs. (336) and (337),

$$\begin{aligned} \varepsilon_{j+1} &= \varepsilon_j + \frac{2\pi F_0 \varepsilon_0^2}{\varepsilon_{j+1}} \left\{ -[\mathbf{J}'_s(z) \sin \vartheta_j + \mathbf{E}'_s(z) \cos \vartheta_j] \cos \varphi \right. \\ &\left. + \frac{\sqrt{1 - e^2}}{e} \left[ \left( \mathbf{J}_s(z) - \frac{\sin(s\pi)}{s\pi} \right) \cos \vartheta_j - \left( \mathbf{E}_s(z) - \frac{1 - \cos(s\pi)}{s\pi} \right) \sin \vartheta_j \right] \sin \varphi \right\}, \end{aligned} \quad (339)$$

where  $\mathbf{E}_s(z)$  is a Weber function,

$$\mathbf{E}_s(z) = \frac{1}{\pi} \int_0^\pi \sin(s\xi - z \sin \xi) d\xi, \quad (340)$$

and  $\mathbf{E}'_s(z)$  is its derivative,

$$\mathbf{E}'_s(z) = -\frac{1}{\pi} \int_0^\pi \cos(s\xi - z \sin \xi) \sin \xi d\xi. \quad (341)$$

The change of the angular momentum of the atom follows from the Hamiltonian Eq. (334) and the Hamiltonian equations of motion

$$\dot{M} = -\frac{\partial \mathcal{H}}{\partial \xi} = -rF \sin(\xi + \varphi) \cos(\omega t + \vartheta). \quad (342)$$

By analogy with the scaled energy, we introduce the scaled angular momenta  $M_s = M\omega^{1/3}$  and  $\mu = 2M_s$ . To calculate the change of the scaled angular momentum, we need expressions for the second derivatives of Anger and Weber functions, which can be obtained by differentiating first derivatives, Eqs. (324) and (341) and integrating by parts,

$$\mathbf{J}_s''(z) = \mathbf{J}_s(z) \left[ \frac{1}{e^2} - 1 \right] - \frac{1}{z} \mathbf{J}_s'(z) + \frac{\sin(s\pi)}{\pi z} \left[ 1 - \frac{1}{e} \right], \quad (343)$$

and

$$\mathbf{E}_s''(z) = \mathbf{E}_s(z) \left[ \frac{1}{e^2} - 1 \right] - \frac{1}{z} \mathbf{E}_s'(z) + \frac{1}{\pi z} \left[ \left( \frac{1}{e} - 1 \right) \cos(s\pi) - \left( 1 + \frac{1}{e} \right) \right]. \quad (344)$$

Using expressions (343) and (344) integration of Eq. (342) yields

$$\begin{aligned} \mu_{j+1} = \mu_j + \frac{2\pi F_0 \varepsilon_0^2}{\varepsilon_{j+1}} & \left\{ \frac{\sqrt{1-e^2}}{e} \left[ \left( \mathbf{J}_s(z) - \frac{\sin(s\pi)}{s\pi} \right) \sin \vartheta_j \right. \right. \\ & + \left( \mathbf{E}_s(z) - \frac{1 - \cos(s\pi)}{s\pi} \right) \cos \vartheta_j \left. \right] \cos \varphi + \left[ \left( -\mathbf{J}_s'(z) + (1+e) \frac{\sin(s\pi)}{\pi} \right) \cos \vartheta_j \right. \\ & \left. \left. + \left( \mathbf{E}_s'(z) + (1+e) \frac{\cos(s\pi)}{\pi} + \frac{1-e}{\pi} \right) \sin \vartheta_j \right] \sin \varphi \right\}. \quad (345) \end{aligned}$$

Eqs. (339) and (345) show energy and momentum change while electron travels from apocenter to pericenter. Following the same path, we can find energy and momentum changes while electron moves from pericenter to apocenter. This corresponds to the integration in the interval  $(-\pi, 0)$ ,

$$\begin{aligned} \varepsilon_{j+1} = \varepsilon_j + \frac{2\pi F_0 \varepsilon_0^2}{\varepsilon_{j+1}} & \{ [-\mathbf{J}_s'(z) \sin \vartheta_j + \mathbf{E}_s'(z) \cos \vartheta_j] \cos \varphi \\ & + \frac{\sqrt{1-e^2}}{e} \left[ \left( \mathbf{J}_s(z) - \frac{\sin(s\pi)}{s\pi} \right) \cos \vartheta_j + \left( \mathbf{E}_s(z) - \frac{1 - \cos(s\pi)}{s\pi} \right) \sin \vartheta_j \right] \sin \varphi \}, \quad (346) \end{aligned}$$

and

$$\begin{aligned} \mu_{j+1} = \mu_j + \frac{2\pi F_0 \varepsilon_0^2}{\varepsilon_{j+1}} & \left\{ \frac{\sqrt{1-e^2}}{e} \left[ \left( \mathbf{J}_s(z) - \frac{\sin(s\pi)}{s\pi} \right) \sin \vartheta_j \right. \right. \\ & - \left( \mathbf{E}_s(z) - \frac{1 - \cos(s\pi)}{s\pi} \right) \cos \vartheta_j \left. \right] \cos \varphi + \left[ \left( -\mathbf{J}_s'(z) + (1+e) \frac{\sin(s\pi)}{\pi} \right) \cos \vartheta_j \right. \\ & \left. \left. - \left( \mathbf{E}_s'(z) + (1+e) \frac{\cos(s\pi)}{\pi} + \frac{1-e}{\pi} \right) \sin \vartheta_j \right] \sin \varphi \right\}. \quad (347) \end{aligned}$$

Energy and momentum changes are not periodical, therefore, the changes when the parameter  $\xi$  changes in the interval  $(\pi, 2\pi)$  will not be equal to the changes in the interval  $(-\pi, 0)$ . In order to find changes in the interval  $(\pi, 2\pi)$ , we have to find expressions for second derivatives of Anger and Weber functions with a negative parameter,

$$\mathbf{J}_{-s}''(z) = \mathbf{J}_{-s}(z) \left[ \frac{1}{e^2} - 1 \right] - \frac{1}{z} \mathbf{J}_{-s}'(z) - \frac{\sin(s\pi)}{\pi z} \left[ 1 + \frac{1}{e} \right], \quad (348)$$

$$\mathbf{E}'_{-s}(z) = \mathbf{E}_{-s}(z) \left[ \frac{1}{e^2} - 1 \right] - \frac{1}{z} \mathbf{E}'_{-s}(z) + \frac{1}{\pi z} \left[ \left( \frac{1}{e} + 1 \right) \cos(s\pi) + \left( 1 - \frac{1}{e} \right) \right]. \quad (349)$$

Integration in the interval  $(\pi, 2\pi)$  and the use of expressions (348) and (349) yields the changes of the energy

$$\begin{aligned} \varepsilon_{j+1} = \varepsilon_j + \frac{2\pi F_0 \varepsilon_0^2}{\varepsilon_{j+1}} \left\{ \left[ -\mathbf{J}'_{-s}(z) \sin(s\pi + \vartheta_j) + \mathbf{E}'_{-s}(z) \cos(s\pi + \vartheta_j) \right] \cos \varphi \right. \\ \left. + \frac{\sqrt{1-e^2}}{e} \left[ \left( \mathbf{J}_{-s}(z) - \frac{\sin(s\pi)}{s\pi} \right) \cos(s\pi + \vartheta_j) \right. \right. \\ \left. \left. + \left( \mathbf{E}_{-s}(z) + \frac{1 - \cos(s\pi)}{s\pi} \right) \sin(s\pi + \vartheta_j) \right] \sin \varphi \right\}, \quad (350) \end{aligned}$$

and momentum

$$\begin{aligned} \mu_{j+1} = \mu_j + \frac{2\pi F_0 \varepsilon_0^2}{\varepsilon_{j+1}} \left\{ \frac{\sqrt{1-e^2}}{e} \left[ \left( \mathbf{J}_{-s}(z) - \frac{\sin(s\pi)}{s\pi} \right) \sin(s\pi + \vartheta_j) \right. \right. \\ \left. \left. - \left( \mathbf{E}_{-s}(z) + \frac{1 - \cos(s\pi)}{s\pi} \right) \cos(s\pi + \vartheta_j) \right] \cos \varphi \right. \\ \left. + \left[ \left( -\mathbf{J}'_{-s}(z) + (e-1) \frac{\sin(s\pi)}{\pi} \right) \cos(s\pi + \vartheta_j) \right. \right. \\ \left. \left. + \left( -\mathbf{E}'_{-s}(z) + (e+1+2/e) \frac{\cos(s\pi)}{\pi} - \frac{1}{\pi} (e-1+2/e) \right) \sin(s\pi + \vartheta_j) \right] \sin \varphi \right\}. \quad (351) \end{aligned}$$

Having expressions for the energy and momentum changes in half period, Eqs. (339), (345), (346), and (347), allows us to calculate those changes in the whole period  $(-\pi, \pi)$  when starting point is apocenter,

$$\begin{aligned} \varepsilon_{j+1} = \varepsilon_j + \frac{4\pi F_0 \varepsilon_0^2}{\varepsilon_{j+1}} \left\{ -\mathbf{J}'_s(z) \sin \vartheta_j \cos \varphi \right. \\ \left. + \frac{\sqrt{1-e^2}}{e} \left[ \mathbf{J}_s(z) - \frac{\sin(s\pi)}{s\pi} \right] \cos \vartheta_j \sin \varphi \right\}, \quad (352) \end{aligned}$$

$$\begin{aligned} \mu_{j+1} = \mu_j + \frac{4\pi F_0 \varepsilon_0^2}{\varepsilon_{j+1}} \left\{ \frac{\sqrt{1-e^2}}{e} \left[ \mathbf{J}_s(z) - \frac{\sin(s\pi)}{s\pi} \right] \sin \vartheta_j \cos \varphi \right. \\ \left. + \left[ -\mathbf{J}'_s(z) + (1+e) \frac{\sin(s\pi)}{\pi} \right] \cos \vartheta_j \sin \varphi \right\}. \quad (353) \end{aligned}$$

In order to calculate those changes in the whole period  $(0, 2\pi)$  when a starting point is pericenter, we need expressions for coupling Anger and Weber functions with negative and positive parameters,

$$\mathbf{J}_s(z) = \mathbf{J}_{-s}(z) \cos(s\pi) - \mathbf{E}_{-s}(z) \sin(s\pi), \quad (354)$$

$$\mathbf{E}_s(z) = \mathbf{E}_{-s}(z) \cos(s\pi) + \mathbf{J}_{-s}(z) \sin(s\pi). \quad (355)$$

Using expressions (354) and (355), and Eqs. (346), (347), (350), and (351) we can find energy and momentum changes in the interval  $(0, 2\pi)$ ,

$$\begin{aligned} \varepsilon_{j+1} = \varepsilon_j + \frac{4\pi F_0 \varepsilon_0^2}{\varepsilon_{j+1}} \left\{ -\mathbf{J}'_{-s}(z) \sin(s\pi + \vartheta_j) \cos \varphi \right. \\ \left. + \frac{\sqrt{1-e^2}}{e} \left[ \mathbf{J}_{-s}(z) - \frac{\sin(s\pi)}{s\pi} \right] \cos(s\pi + \vartheta_j) \sin \varphi \right\}, \quad (356) \end{aligned}$$

$$\begin{aligned} \mu_{j+1} = \mu_j + \frac{4\pi F_0 \varepsilon_0^2}{\varepsilon_{j+1}} \left\{ \frac{\sqrt{1-e^2}}{e} \left[ \mathbf{J}_{-s}(z) - \frac{\sin(s\pi)}{s\pi} \right] \sin(s\pi + \vartheta_j) \cos \varphi \right. \\ \left. + \left[ \left( -\mathbf{J}'_{-s}(z) + (e-1) \frac{\sin(s\pi)}{\pi} \right) \cos(s\pi + \vartheta_j) \right. \right. \\ \left. \left. + \frac{(1+1/e) \cos(s\pi) + 1 - 1/e}{\pi} \sin(s\pi + \vartheta_j) \right] \sin \varphi \right\}. \quad (357) \end{aligned}$$

We will investigate thoroughly electron motion between the two passages of the apocenter. Energy change is described by Eq. (352). In analogy with Eq. (325), we introduce a generating function for a two-dimensional hydrogen atom

$$\begin{aligned} G(\varepsilon_{j+1}, \vartheta_j) = \varepsilon_{j+1} \vartheta_j - 4\pi \varepsilon_{j+1}^{-1/2} - \frac{4\pi F_0 \varepsilon_0^2}{\varepsilon_{j+1}} \left\{ \mathbf{J}'_s(z) \cos \vartheta_j \cos \varphi \right. \\ \left. + \frac{\sqrt{1-e^2}}{e} \left[ \mathbf{J}_s(z) - \frac{\sin(s\pi)}{s\pi} \right] \sin \vartheta_j \sin \varphi \right\}. \quad (358) \end{aligned}$$

Eqs. (326) results in the phase change,

$$\begin{aligned} \vartheta_{j+1} = \vartheta_j + 2\pi \varepsilon_{j+1}^{-3/2} - 4\pi F_0 \varepsilon_0^2 \frac{\partial}{\partial \varepsilon_{j+1}} \left( \frac{1}{\varepsilon_{j+1}} \left\{ \mathbf{J}'_s(z) \cos \vartheta_j \cos \varphi \right. \right. \\ \left. \left. + \frac{\sqrt{1-e^2}}{e} \left[ \mathbf{J}_s(z) - \frac{\sin(s\pi)}{s\pi} \right] \sin \vartheta_j \sin \varphi \right\} \right). \quad (359) \end{aligned}$$

### 6.5.1 Approximation for high relative frequency $s$

When  $s \gg 1$  and  $(1-e) \ll 1$  we can use approximations [207]

$$\begin{aligned} \mathbf{J}_s(se) &= \mathbf{J}_s(s) - s(1-e)\mathbf{J}'_s(s) + o((1-e)^2), \\ \mathbf{J}'_s(se) &= \mathbf{J}'_s(s) + (1-e)\mathbf{J}'_s(s) + o((1-e)^2). \end{aligned} \quad (360)$$

Asymptotic form of the Anger function when  $s \gg 1$  is

$$\mathbf{J}_s(s) = \frac{a}{s^{1/3}} + \frac{\sin(s\pi)}{2\pi s} - \frac{b}{70s^{5/3}}. \quad (361)$$

The asymptotic form of the derivative of the Anger function and constants  $a$  and  $b$  are defined by Eqs. (330) and (331).

Substituting asymptotic forms (330) and (361) into approximations (360) and these approximations into energy and phase expressions (352) and (359), respectively, yields mapping equations for the energy

$$\begin{aligned} \varepsilon_{j+1} = \varepsilon_j + \pi F_0 \varepsilon_0^2 \left\{ (e-2) \left[ 4b - \frac{4a}{5} \varepsilon_{j+1} - \frac{\sin(\varepsilon_{j+1}^{-3/2} \pi)}{\pi} \varepsilon_{j+1}^2 \right] \sin \vartheta_j \cos \varphi \right. \\ \left. + \frac{\sqrt{1-e^2}}{e} \left[ 4a \varepsilon_{j+1}^{-1/2} - \frac{2 \sin(\varepsilon_{j+1}^{-3/2} \pi)}{\pi} \varepsilon_{j+1}^{1/2} - \frac{2b}{35} \varepsilon_{j+1}^{3/2} \right. \right. \\ \left. \left. + (e-1) \left( 4b \varepsilon_{j+1}^{-3/2} - \frac{4a}{5} \varepsilon_{j+1}^{-1/2} - \frac{\sin(\varepsilon_{j+1}^{-3/2} \pi)}{\pi} \varepsilon_{j+1}^{1/2} \right) \right] \cos \vartheta_j \sin \varphi \right\} \quad (362) \end{aligned}$$

and phase

$$\begin{aligned} \vartheta_{j+1} = \vartheta_j + 2\pi \varepsilon_{j+1}^{-3/2} + \pi F_0 \varepsilon_0^2 \left\{ (2-e) \left[ \frac{4a}{5} - \frac{3 \cos(\varepsilon_{j+1}^{-3/2} \pi)}{2} \varepsilon_{j+1}^{-1/2} \right. \right. \\ \left. \left. + \frac{2 \sin(\varepsilon_{j+1}^{-3/2} \pi)}{\pi} \varepsilon_{j+1} \right] \cos \vartheta_j \cos \varphi + \frac{\sqrt{1-e^2}}{e} \left[ 2a \varepsilon_{j+1}^{-3/2} - 3 \cos(\varepsilon_{j+1}^{-3/2} \pi) \varepsilon_{j+1}^{-2} \right. \right. \\ \left. \left. + \frac{\sin(\varepsilon_{j+1}^{-3/2} \pi)}{\pi} \varepsilon_{j+1}^{-1/2} + \frac{3b}{35} \varepsilon_{j+1}^{1/2} + (e-1) \left( 6b \varepsilon_{j+1}^{-5/2} \right. \right. \right. \\ \left. \left. \left. - 2a \varepsilon_{j+1}^{-3/2} - \frac{3 \cos(\varepsilon_{j+1}^{-3/2} \pi)}{2} \varepsilon_{j+1}^{-2} + \frac{\sin(\varepsilon_{j+1}^{-3/2} \pi)}{2\pi} \varepsilon_{j+1}^{-1/2} \right) \right] \sin \vartheta_j \sin \varphi \right\} \quad (363) \end{aligned}$$

for motion between two apocenters.

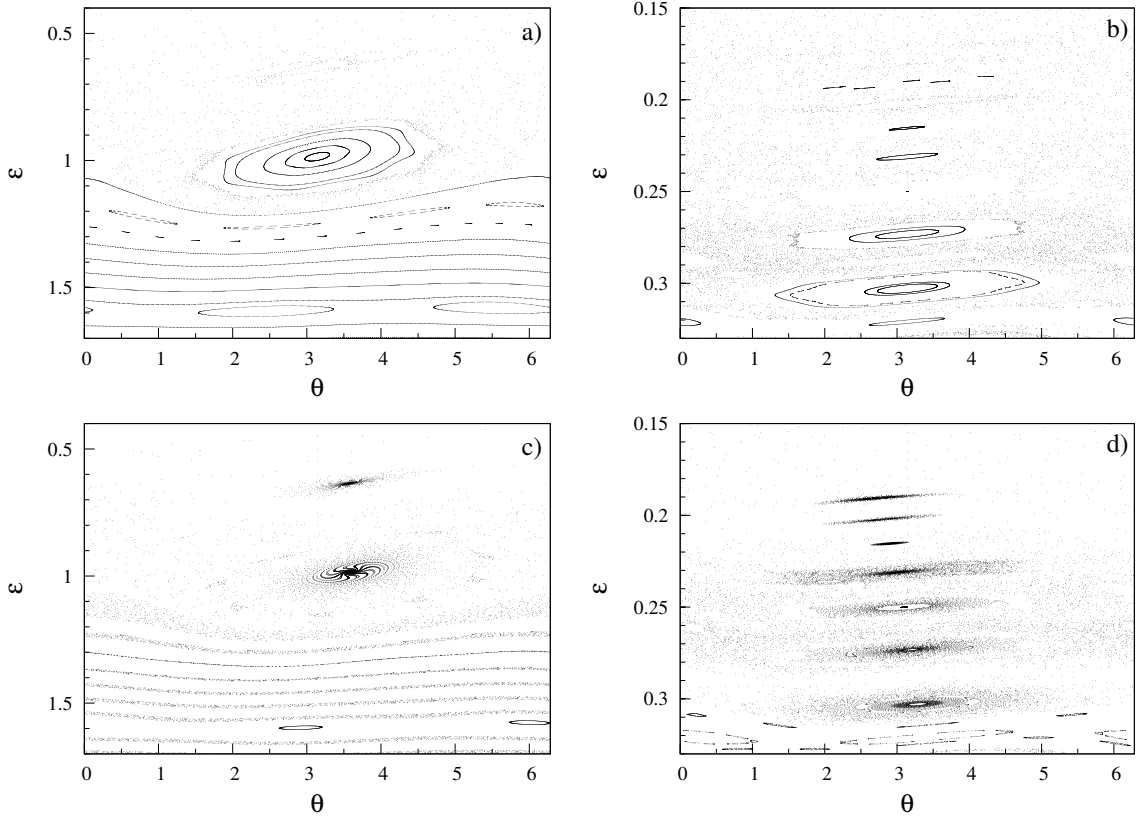
In Figure 28  $(\varepsilon, \vartheta)$  maps are shown for the two-dimensional hydrogen atom, calculated according to Eqs. (362) and (363) with different parameters  $\pi F_0 \varepsilon_0^2$  and different values of orientation angle  $\varphi$ . We can compare maps a) and b) with the corresponding one-dimensional hydrogen maps in Figure 24 a) and b), plotted with the same initial conditions  $\varepsilon_0, \vartheta_0$ , and the same parameters  $\pi F_0 \varepsilon_0^2$  and notice that in a two-dimensional case phase trajectories are similar. However, introduction of an orientation angle between vector potential of the field and the ellipsis major axis results in distortion of continuous phase trajectories and increasing of the chaotic region.

Figure 29 shows ionization threshold field dependence on the relative frequency for different angles  $\varphi$ . We see that increasing orientation angle results in increasing of the ionization threshold field.

Power spectral densities of the two-dimensional hydrogen atom for different orientation angles are shown in Figure 30. Figure 28 shows that an increase of orientation angle results in an increase of chaotic region, which, on the other hand, results in an increase of power spectral density slope.

### 6.5.2 Approximation for very extended orbits

Further we investigate the energy and momentum changes of the hydrogen atom in a monochromatic field in the period, when starting point of motion is apocenter and  $e \approx 1$ . In the limit  $e \rightarrow 1$  we should recover results for one-dimensional atom. We approximate



**Figure 28.** Trajectories  $(\varepsilon, \vartheta)$  for the two-dimensional hydrogen atom map (362) and (363) with the parameters a)  $\pi F_0 \varepsilon_0^2 = 0.06$ ,  $e = 0.7$ ,  $\varphi = 0$ , and initial conditions  $\vartheta_0 = \pi$ ,  $\varepsilon_0 = 1.9 - 0.05i$  ( $i = 0, 1, 2, \dots$ ) and b)  $\pi F_0 \varepsilon_0^2 = 0.0035$ ,  $e = 0.7$ ,  $\varphi = 0$ , and initial conditions  $\vartheta_0 = \pi$ ,  $\varepsilon_0 = 0.35 - 0.003i$  ( $i = 0, 1, 2, \dots$ ). Maps c) and d) are plotted with the same parameters as a) and b), accordingly, but the angle between vector potential of the field and the major axis of the ellipse is  $\varphi = \pi/6$ .

equations for energy and momentum (352) and (353) in the power of  $\beta = \sqrt{1 - e^2}$ ,

$$\varepsilon_{j+1} = \varepsilon_j + \frac{4\pi F_0 \varepsilon_0^2}{\varepsilon_{j+1}} \left\{ - (1 + \beta^2) \mathbf{J}'_s(s) \sin \vartheta_j \cos \varphi + \beta \left[ \mathbf{J}_s(s) - \frac{\sin(s\pi)}{s\pi} \right] \cos \vartheta_j \sin \varphi \right\}, \quad (364)$$

$$\mu_{j+1} = \mu_j + \frac{4\pi F_0 \varepsilon_0^2}{\varepsilon_{j+1}} \left\{ \beta \left[ \mathbf{J}_s(s) - \frac{\sin(s\pi)}{s\pi} \right] \sin \vartheta_j \cos \varphi + \left[ - (1 + \beta^2) \mathbf{J}'_s(s) + (2 - \beta^2) \frac{\sin(s\pi)}{\pi} \right] \cos \vartheta_j \sin \varphi \right\} \quad (365)$$

From the equation (364) we can notice that in the limit  $\beta \rightarrow 0$  we recover results for one-dimensional hydrogen atom, Eq. (321).

### 6.5.3 Approximation for almost circular orbits

When eccentricity  $e = 0$  we will obtain a circular orbit. We will find energy and momentum change when  $e \approx 0$ . To accomplish this, we should approximate Eqs. (352)

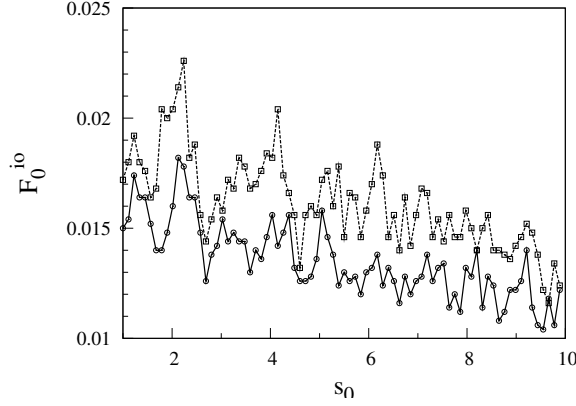


**Figure 29.** Ionization threshold field dependence on the relative frequency  $s_0$  for a two-dimensional hydrogen atom with the eccentricity  $e = 0.7$  and orientation angle  $\varphi = 0$ , solid line, and  $\varphi = \pi/6$ , dashed line, calculated using variation of the initial phase  $\vartheta_0$ .

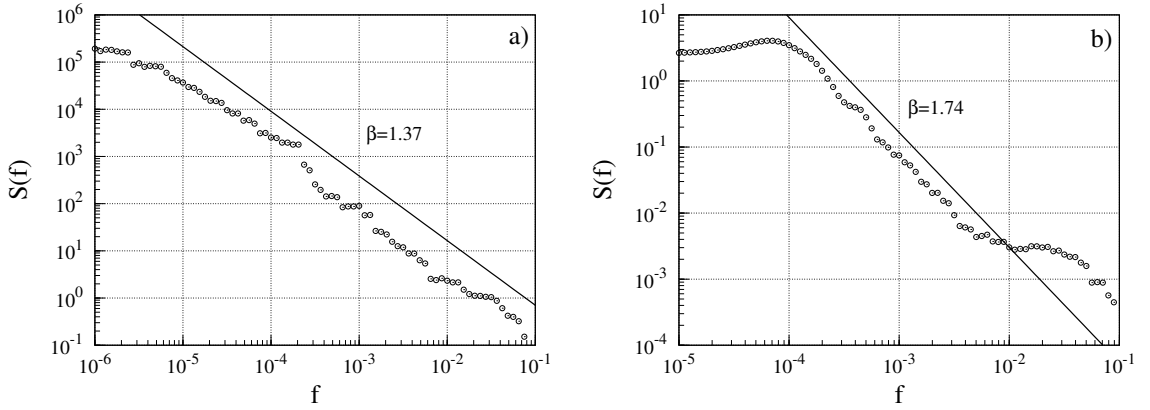


**Figure 30.** Power spectral density calculated using Fast Fourier Transform for a signal generated from the map Eqs. (362) and (363) with the parameter  $\pi F_0 \varepsilon_0^2 = 0.0035$  and initial conditions  $\vartheta_0 = \pi$ ,  $\varepsilon_0 = 0.21$ , and a)  $\varphi = 0$ , b)  $\varphi = \pi/6$ .  $N = 10^6$  iterations are fulfilled. Solid lines show approximation  $S(f) \sim 1/f^\beta$ .

and (353) in the power of  $e$ , but we cannot calculate derivatives in the point  $e = 0$ , because a denominator turns into zero. Therefore, for each term we should integrate equations (335) and (342), but before that, we should differentiate them and substitute  $e = 0$ . After some algebra we obtain

$$\varepsilon_{j+1} = \varepsilon_j + \frac{4F_0 \varepsilon_0^2 \sin(s\pi)}{\varepsilon_{j+1}} \left\{ \left[ \frac{e}{2} + \frac{\frac{3}{4}e^2 s^2 - 1}{1 - s^2} + \frac{\frac{1}{2}e s^2}{4 - s^2} - \frac{\frac{3}{4}e^2 s^2}{9 - s^2} \right] \sin \vartheta_j \cos \varphi \right. \\ \left. + s \left[ \frac{1 - \frac{1}{4}e^2 (s^2 - 4)}{1 - s^2} - \frac{e}{4 - s^2} + \frac{\frac{1}{4}e^2 s^2}{9 - s^2} \right] \cos \vartheta_j \sin \varphi \right\}, \quad (366)$$

$$\begin{aligned}
\mu_{j+1} = \mu_j + \frac{4F_0\varepsilon_0^2 \sin(s\pi)}{\varepsilon_{j+1}} \\
\times \left\{ s \left[ -\frac{e}{2} + \frac{1 - e^2(1 + \frac{1}{4}s^2)}{1 - s^2} + \frac{e(1 - \frac{1}{2}s^2)}{4 - s^2} + \frac{\frac{1}{4}e^2s^2}{9 - s^2} \right] \sin \vartheta_j \cos \varphi \right. \\
\left. + \left[ \frac{3e}{2} + \frac{s^2(\frac{1}{2}e^2(1 + \frac{1}{2}s^2) - 1)}{1 - s^2} - \frac{\frac{1}{2}es^2}{4 - s^2} + \frac{\frac{1}{2}e^2s^2(3 - \frac{1}{2}s^2)}{9 - s^2} \right] \cos \vartheta_j \sin \varphi \right\}. \quad (367)
\end{aligned}$$

Equations (366) and (367) are not valid in the points, where  $s = 1, 2, 3$ .

## 6.6 Two-dimensional atom in a circular polarized field

In the case when a two-dimensional hydrogen atom is placed in a circular polarized electromagnetic field, differential equation (320) can be written as

$$\dot{E} = -eF (v_x \cos(\omega t + \vartheta) \pm v_y \sin(\omega t + \vartheta)), \quad (368)$$

where signs  $\pm$  corresponds to the left and right circular polarizations, respectively.

Using similar calculations as in monochromatic field, after some algebra we find the energy and momentum changes between two apocenters when  $\xi$  changes in the interval  $(-\pi, \pi)$ ,

$$\varepsilon_{j+1} = \varepsilon_j + \frac{4\pi F_0\varepsilon_0^2}{\varepsilon_{j+1}} \left\{ -\mathbf{J}'_s(z) \mp \frac{\sqrt{1 - e^2}}{e} \left[ \mathbf{J}_s(z) - \frac{\sin(s\pi)}{s\pi} \right] \right\} \sin(\vartheta_j \mp \varphi), \quad (369)$$

$$\begin{aligned}
\mu_{j+1} = \mu_j + \frac{4\pi F_0\varepsilon_0^2}{\varepsilon_{j+1}} \left\{ \frac{\sqrt{1 - e^2}}{e} \left[ \mathbf{J}_s(z) - \frac{\sin(s\pi)}{s\pi} \right] \right. \\
\left. \mp \left[ -\mathbf{J}'_s(z) + (1 + e) \frac{\sin(s\pi)}{\pi} \right] \right\} \sin(\vartheta_j \mp \varphi), \quad (370)
\end{aligned}$$

and two pericenters when  $\xi$  changes in the interval  $(0, 2\pi)$ ,

$$\varepsilon_{j+1} = \varepsilon_j + \frac{4\pi F_0\varepsilon_0^2}{\varepsilon_{j+1}} \left\{ -\mathbf{J}'_{-s}(z) \mp \frac{\sqrt{1 - e^2}}{e} \left[ \mathbf{J}_{-s}(z) - \frac{\sin(s\pi)}{s\pi} \right] \right\} \sin(s\pi + \vartheta_j \mp \varphi), \quad (371)$$

$$\begin{aligned}
\mu_{j+1} = \mu_j + \frac{4\pi F_0\varepsilon_0^2}{\varepsilon_{j+1}} \left\{ \left[ \frac{\sqrt{1 - e^2}}{e} \left( \mathbf{J}_{-s}(z) - \frac{\sin(s\pi)}{s\pi} \right) \right. \right. \\
\left. \mp \left( -\mathbf{J}'_{-s}(z) + (e - 1) \frac{\sin(s\pi)}{\pi} \right) \right] \sin(s\pi + \vartheta_j \mp \varphi) \\
\left. \pm \frac{(1 + 1/e) \cos(s\pi) + 1 - 1/e}{\pi} \cos(s\pi + \vartheta_j \mp \varphi) \right\}. \quad (372)
\end{aligned}$$

It should be noted, that expression in the curly brackets in Eq. (371) coincides with the expression in the quasi-classical radial dipole matrix element in the velocity representation [208]

$$D_p^\pm = \frac{1}{s} \left\{ \mathbf{J}'_{-s}(z) \pm \frac{\sqrt{1 - e^2}}{e} \left[ \mathbf{J}_{-s}(z) - \frac{\sin(s\pi)}{s\pi} \right] \right\}. \quad (373)$$

This correspondence, however, takes place only for the interaction of the hydrogen atom with the circularly polarized microwave field and for the integration of the equations of motion between the two subsequent pericenters. In general, the energy [206,207] and angular momentum changes depend on the integration interval. So, for the motion of the electron between two subsequent apocenters, i.e., the most distant from the nucleus points, where the electron's energy change is minimal, the energy change is described by the expression similar to Eq. (371) but instead of  $\mathbf{J}_{-s}(es)$  and  $\mathbf{J}'_{-s}(es)$  we have the Anger function and its derivative of the positive order,  $\mathbf{J}_s(es)$  and  $\mathbf{J}'_s(es)$ . This interval has been used in [206,209,210] for the derivation of the Kepler map for a one-dimensional hydrogen atom.

Therefore, analytical expressions for the energy and angular momentum changes of the two-dimensional hydrogen atom in linearly and circularly polarized electromagnetic fields are derived. It should be noted that in general the expressions are rather complicated. The approximate expressions for limiting cases of the parameters are more convenient for analytical and numerical analysis of the dynamics.

The derived expressions are suitable for a three-dimension hydrogen atom as well, and may be generalized for the analysis of the chaotic motion (due to the Jupiter perturbations) of comets and asteroids in the solar system.

## 7 PROGRAMS FOR NUMERICAL SIMULATIONS AND CALCULATIONS

All numerical simulations in the framework of this research have been performed using a set of programs, which were written in C++ programming language and were executed under Linux operating system. In particular, GNU C++ compiler g++ version 3.2.2 was used to compile and link different parts of the code. The source code of the programs has been written in a platform independent way and can be easily moved and compiled under different platforms and different C++ compilers.

Random number generation for the point processes and signals as well as Fast Fourier Transform, used to calculate power spectral density from the signals, were accomplished by linking programs to GNU Scientific Library (GSL). GSL provides a well-defined C language Applications Programming Interface (API) for common numerical functions, while allowing wrappers to be written for very high level languages. The routines have been written from scratch by the GSL team in ANSI C. Using of GSL random number generators allows us to overcome shortcomings of random number generators, which usually persist in C compilers. We can “seed” initial state of the generator and we can get random numbers, distributed according various predefined distributions.

Programs are written in a strict Object Orientated Programming (OOP) manner. For example, to calculate interevent times for point processes, we use “Distribution” parent class, which defines only variables and methods (functions), common for different calculation algorithms. Here we present a header file of “Distribution” class:

```
#ifndef _DISTRIBUTION_H_
#define _DISTRIBUTION_H_

#include <valarray>
#include <iostream>
#include <fstream>
#include <ctime>
#include <gsl/gsl_randist.h>
#include <gsl/gsl_histogram.h>

/*****
/** class Distribution
/**
/** Parent class. Makes recurrent times sequence distributed according
/** different distributions. Needs children classes.
/**
/**
/*****
class Distribution
{
public:

    std::valarray<double> *sequence;

    Distribution();
    Distribution(long ln);
    Distribution(long ln, long lsorted, double lsigma, double lgamma,
```

```

        double lbeta);
    virtual ~Distribution();
    void Mirroring_Boundary(double ltau_min, double ltau_min);
    void Cutoff_Boundary(double ltau_min);
    void Module_Boundary();
    void Build_Recurrent_Sequence();
    void Add_Constant_Tau(double ltau_c);
    void Change_To_Taus();
    void Out(char *filename);
    void Taus_Out(char *filename);

protected:

    long n;
    double sigma;
    double gamma;
    double beta; /* extra parameter */
    double tau_first;
    gsl_rng* r;

    double (Distribution::*Boundary_Function)(double tau);
    void Set_Tau_First(double ltau_first);

private:

    long sorted;

    double tau_min;
    double tau_max;
        /* Different tau distributions defined in child classes */
    virtual double Recurrent_Function(double tau_old) = 0;
        /* Boundary conditions */

    double Remain_Tau(double tau);
    double Mirroring_Boundary_Function(double tau);
    double Cutoff_Boundary_Function(double tau);
    double Module_Boundary_Function(double tau);
};

#endif /* _DISTRIBUTION_H_ */

```

This approach allows us to have different child classes, which correspond to different point processes interevent time distributions and extend parent *Distribution* class to include additional features. Here follows the example of header file of *AdditiveDistribution* child class, derived from parent *Distribution* class.

```

#ifndef _ADDITIVE_H_
#define _ADDITIVE_H_

#include "distribution.h"

```

```

/*****

```

```

/** class AdditiveDistribution : public Distribution          **/
/**                                                         **/
/** Children class. Makes recurrent times sequence with tau distributed **/
/** according additive iterations.                          **/
/**                                                         **/
/*****
class AdditiveDistribution : public Distribution
{
public:

    AdditiveDistribution(long ln, long lsorted, double lsigma, double lgamma,
                        double ltau_mean);
    AdditiveDistribution(long ln, long lsorted, double lsigma, double lgamma,
                        double ltau_mean, double lupper_restriction);

private:

    double tau_mean;
        /* Different recurrent function when this parameter is 1 */
    double upper_restriction;

    double Recurrent_Function(double tau_old);
};

#endif /* _ADDITIVE_H_ */

```

Virtual functions, as given in the example above, allow us easily to overload some methods of the program, without changing the existent structure. This might seem to be complicated, but, on the contrary, this allows us to maintain the logical structure of the algorithm as simple as possible.

Programming in OOP approach makes it easy to modularize a code writing process. We write different, independent parent classes for point processes, signals generation, distribution density, power spectral density calculation, then it is easy to expand by adding child classes with different methods and properties. Code, written in OOP is easier to debug and find the exact place of the error in case such error occurs.

Number of points in point processes or signal length in case of signals, which can handle computer, are completely defined by the random access memory (RAM) of the computer. We have used personal computer with 256Mb of RAM and this allowed us to generate sequences of up to ten millions of numbers without computer crash.

Programs, used in numerical simulations, are easily portable into other systems and can be compiled and linked using common Makefile.

## 8 SUMMARY OF THE RESULTS AND CONCLUSIONS

1. We present a simple point process model of  $1/f^\beta$  noise, covering different values of the exponent  $\beta$ . The interevent times of the signal stochastically diffuse in some interval, resulting in the power-law distribution. The model is free from the requirement of a wide distribution of relaxation times and from the power-law forms of the pulses. It contains only one relaxation rate and yields  $1/f^\beta$  power spectral density in a wide range of frequency.
2. We investigate McWhorter model, representing the signals as a superposition of the uncorrelated components, and show that a signal, consisting of the superposition of signals with the linear relaxation rates  $\gamma$ , distributed according to the power-law, results in  $1/f^\beta$  power spectral density with different slopes  $\beta$ . We analyse the relation of the point process model with the McWhorter model. The point processes are multifractal, whereas those of the McWhorter model are monofractal.
3. We show that a point process, consisting of discrete set of Dirac delta functions, can be transformed, using different shapes of the pulses into a continuous signal and back to the point process, while preserving initial power spectral density at low frequencies.
4. We present a model where a signal, represented as the sequences of random pulses of fixed area with random duration, distributed uniformly in a wide interval, produces  $1/f$  behavior of the power spectral density in a wide range of frequency.
5. The interrelation between the point process signals, shown as consisting of pulses and stochastic signals and represented by the fluctuating intensity, is analysed. It is demonstrated how one type of the signal may be transformed into another type of the signal with the same power spectral density at low frequencies.
6. We derive a stochastic nonlinear difference and differential equation for the signal, exhibiting  $1/f^\beta$  noise in any desirable wide range of frequency. The solutions of the equations exhibit the power-law distribution of the signal intensity.
7. We show that the period of motion of a rotor without a friction, affected by the periodic strikes, exhibits  $1/f^\beta$  noise in transition from regular to chaotic motion.
8. One-dimensional classical hydrogen atom in a linearly polarized monochromatic electromagnetic field and a two-dimensional atom in monochromatic field exhibit stochastic motion and can result in  $1/f^\beta$  noise.
9. The expressions for energy and angular momentum changes of the hydrogen atom due to the interaction with the electromagnetic field during the period and halves of the period of the electron motion in the Coulomb field are derived. It is shown that it is only energy change for the motion between two subsequent passings of the pericenter that is related to the quasi-classical dipole matrix element for transitions between the excited states.

10. During the research process various programs, generating different stochastic point processes and signals of various distributions, calculating power spectral densities of different processes and analysing statistics of the signals were written, tested and applied.

## 9 LIST OF PUBLICATIONS

### 9.1 Publications

1. M. Alaburda, V. Gontis, and B. Kaulakys, Interaction and chaotic dynamics of the classical hydrogen atom in an electromagnetic field, *Lithuanian J. Phys.* **40** (4), p. 242–247 (2000).
2. J. Ruseckas, B. Kaulakys, and M. Alaburda, Modelling of  $1/f$  noise by sequences of stochastic pulses of different duration, *Lithuanian J. Phys.* **43** (4), p. 223–228 (2003).
3. M. Alaburda and B. Kaulakys,  $1/f$  noise in point processes and its modelling by stochastic difference equations, *Lithuanian J. Phys.* **43** (6), p. 415–418 (2003).
4. B. Kaulakys and M. Alaburda,  $1/f$  noise as a Brownian motion of interevent time and as a superposition of Lorentzians, In: *Noise and Fluctuations*, Proc. 17<sup>th</sup> Intern. Conf., Aug. 18–22, 2003, Prague, p. 59–62 (2003).
5. B. Kaulakys, M. Alaburda, V. Gontis, and T. Meškauskas Modeling and estimation of  $1/f$  noise of the signals represented by pulses and by fluctuating amplitude, *ibid*, p. 679–682 (2003).
6. V. Gontis, B. Kaulakys, M. Alaburda, and J. Ruseckas, Evolution of complex systems and  $1/f$  noise: From physics to financial markets, *Solid State Phenomena* **97-98**, p. 65–70 (2004).
7. B. Kaulakys, V. Gontis, and M. Alaburda, Point process model of  $1/f$  noise vs a sum of Lorentzians, *Phys. Rev. E* **71**, 051105 (11 pp.) (2005); cond-mat/0504025.

### 9.2 Presentations at Conferences

1. M. Alaburda, V. Gontis, B. Kaulakys, Klasikinio vandenilio atomo trikdymas ir chaotinė dinamika elektromagnetiniame lauke, 33-ioji Lietuvos nacionalinė fizikos konferencija, Vilnius, 1999 m. rugsėjo 16–18 d. Tezės, p. 292–293 (1999).
2. M. Alaburda, V. Gontis, and B. Kaulakys, Energy change of the classical hydrogen atom in an electromagnetic field, *Europhysics Conference 32<sup>nd</sup> EGAS*, Vilnius, 4–7 July 2000, p. 187–188 (2000).
3. M. Alaburda, B. Kaulakys,  $1/f$  triukšmo, modeliuojamo signalo impulsais ir amplitudės fliktuacijomis, analizė, 34-oji Lietuvos nacionalinė fizikos konferencija, Vilnius, 2001 m. birželio 14–16 d. Tezės, p. 165 (2001).
4. M. Alaburda, B. Kaulakys,  $1/f$  triukšmas taškiniuose vyksmuose ir jo modeliavimas stochastinėmis skirtuminėmis lygtimis, 35-oji jubiliejinė Lietuvos nacionalinė fizikos konferencija, Vilnius, 2003 m. birželio 12–14 d. Tezės, p. 236 (2003)
5. V. Gontis, B. Kaulakys, M. Alaburda, Taškinių vyksmų modelis, generuojantis įvairaus polinkio  $1/f$  triukšmą, *ibid*, p. 237 (2003)

6. J. Ruseckas, B. Kaulakys, M. Alaburda,  $1/f$  triukšmo modeliavimas įvairaus ilgio stochastiniais impulsais, *ibid*, p. 240 (2003)
7. B. Kaulakys and M. Alaburda,  $1/f$  noise as a Brownian motion of interevent time and as a superposition of Lorentzians, 17<sup>th</sup> Intern. Conf. on Noise and Fluctuations, Aug. 18–22, 2003, Prague (2003).
8. B. Kaulakys, M. Alaburda, V. Gontis, and T. Meškauskas, Modeling and estimation of  $1/f$  noise of the signals represented by pulses and by fluctuating amplitude, *ibid* (2003)
9. V. Gontis, B. Kaulakys, M. Alaburda, and J. Ruseckas, Evolution of complex systems and  $1/f$  noise: From physics to financial markets, 6<sup>th</sup> Intern. Conf. Self-formation Theory and Applications, Vilnius, Nov. 26–28, 2003. Abstracts p. 73–74 (2003).

## ACKNOWLEDGMENTS

The author would like to express his sincere appreciation to his scientific supervisor, Prof. Habil. Dr. Bronislovas Kaulakys, for his patient, friendly, and unfailing guidance and support over the past five years.

The author would like to extend his gratitude to Institute of Theoretical Physics and Astronomy of Vilnius University and especially to staff of Department of the Theory of Processes and Structures for their encouragements and valuable suggestions.

## References

- [1] C. A. Hartmann, *Ann. der Phys.* **65**, 51 (1921).
- [2] W. Schottky, *Ann. der Phys.* **57**, 541 (1918).
- [3] J. B. Johnson, *Phys. Rev.* **26** (1), 71 (1925).
- [4] W. Schottky, *Phys. Rev.* **28** (1), 74 (1926).
- [5] B. B. Mandelbrot, *Fractals: Form, Chance and Dimension*, W. H. Freeman and Co. (1977).
- [6] M. Gardner, *Sci. Am.* **238** (4), 16 (1978).
- [7] R. F. Voss and J. Clarke, *Nature* **258**, 317 (1975).
- [8] R. F. Voss and J. Clarke, *J. Acoust. Soc. Am.* **63**, 258 (1978).
- [9] А. К. Нарышкин and А. С. Врачев, *Теория низкочастотных шумов*, Энергия, Москва (1972).
- [10] С. М. Рыжов, *Введение в статистическую радиофизику*, Наука, Москва (1979).
- [11] А. ван дер Зил, *Шумы при измерениях*, Мир, Москва (1979).
- [12] D.R. Cox, *Point Processes*, Chapman & Hall (1980).
- [13] F. N. Hooge, T. G. M. Kleinpenning, and L. K. J. Vandamme, *Rep. Prog. Phys.* **44** (5), 479 (1981).
- [14] P. Dutta and P. M. Horn, *Rev. Mod. Phys.* **53** (3), 497 (1981).
- [15] М. Букингом, *Шумы в электронных приборах и системах*, Мир, Москва (1986).
- [16] M. B. Weissman, *Rev. Mod. Phys.* **60** (2), 537 (1988).
- [17] G. P. Zhigalskii, *Usp. Fiz. Nauk* **167** (6), 623 (1997).
- [18] J. Davidsen and H. G. Schuster, *Phys. Rev. E* **62** (5), 6111 (2000).
- [19] J. Davidsen and R. Kapral, *Phys. Rev. E* **66**, 055202 (2002).
- [20] J. Davidsen, I. Z. Kiss, J. L. Hudson, and R. Kapral, *Phys. Rev. E* **68**, 026217 (2003).
- [21] D. L. Gilden, T. Thornton, and M. W. Mallon, *Science* **267** (5205), 1837 (1995).
- [22] J. Davidsen and H. G. Schuster, *Phys. Rev. E* **65**, 026120 (2002).
- [23] J. B. Gao, *Med. Biolog. Eng. Comp.* **42** (3), 345 (2004).
- [24] J. Davidsen and M. Paczuski, *Phys. Rev. E* **66**, 050101 (2002).

- [25] W. Müller, R. Blender, and K. Fraedrich, *Nonlin. Proc. Geophys.* **9** (1), 37 (2002).
- [26] K. Fraedrich, U. Luksch, and R. Blender, *Phys. Rev. E* **70**, 037301 (2004).
- [27] W. W. Tung, M. W. Moncrieff, and J. B. Gao, *J. Climate* **17** (14), 2736 (2004).
- [28] W. H. Press, *Comm. Astrophys.* **7**, 103 (1978).
- [29] S. UeNo, S. Mineshige, H. Negoro, K. Shibata, and H. S. Hudson, *Astrophys. J.* **484** (2), 920 (1997).
- [30] D. Maino, C. Burigana, K. M. Górskiand, N. Mandolesi, and M. Bersanelli, *Astron. Astrophys.* **387** (1), 356 (2002).
- [31] S. Thurner, S. B. Lowen, M. C. Feurstain, C. Heneghan, H. G. Feichtinger, and M. C. Teich, *Fractals* **5** (4), 565 (1997).
- [32] B. B. Mandelbrot, *Multifractals and 1/f Noise*, Springer-Verlag (1999).
- [33] M. Takayasua, H. Takayasu, and T. Sato, *Physica A* **233** (3–4), 824 (1996).
- [34] P. Abry and D. Veitch, *IEEE Trans. Inf. Theor.* **44** (1), 2 (1998).
- [35] I. Rubin J. Gao, *Intern. J. Commun. Syst.* **14** (8), 783 (2001).
- [36] C. W. J. Granger, *Econometrica* **34**, 150 (1966).
- [37] V. Palenskis, K. Maknys, and A. Stadalnikas, in *Proc. of the 13th Inter. Conf. on Noise in Physical Systems and 1/f Fluctuations, Palanga, Lithuania, 29 May - 3 June 1995*, edited by V. Bareikis and R. Katilius, World Scientific, Singapore (1995), p. 285.
- [38] B. B. Mandelbrot, *Fractals and Scaling In Finance*, Springer-Verlag (1997).
- [39] R. N. Mantegna and H. E. Stanley, *An Introduction to Econophysics: Correlations and Complexity in Finance*, Cambridge University Press (1999).
- [40] P. Gopikrishnan, V. Plerou, X. Gabaix, and H. E. Stanley, *Phys. Rev. E* **62** (4), R4493 (2000).
- [41] B. J. W. Fleming, D. Yu, R. G. Harrison, and D. Jubb, *Eur. Phys. J. B* **20** (4), 543 (2001).
- [42] V. Gontis, *Lith. J. Phys.* **41** (4–6), 551 (2001).
- [43] X. Gabaix, P. Gopikrishnan, V. Plerou, and H. E. Stanley, *Nature* **423**, 267 (2003).
- [44] V. Gontis and B. Kaulakys, *Physica A* **343**, 505 (2004).
- [45] V. Gontis and B. Kaulakys, *Physica A* **344**, 128 (2004).
- [46] V. Bareikis, R. Šaltis, and J. Požela, *Liet. fiz. rink.* **6**, 103 (1966).
- [47] V. A. Bareikis and J. S. Liberis, *Liet. fiz. rink.* **13**, 881 (1973).

- [48] S. V. Gantsevich, V. L. Gurevich, and R. Katilius, Riv. Nuovo Cimento **2** (5), 1 (1979).
- [49] S. V. Gantsevich, V. D. Kogan, and R. Katilius, ZETF **80**, 1827 (1981).
- [50] S. V. Gantsevich, V. D. Kogan, and R. Katilius, Liet. fiz. rink. **14** (2), 42 (1984).
- [51] V. Palenskis, J. Laučius, and H. Mykolaitis, Liet. fiz. rink. **24** (2), 32 (1984).
- [52] A. Belazaras, P. Serapinas, and P. Šimkus, J. Phys. D **18** (7), 1353 (1985).
- [53] V. Palenskis, Liet. fiz. rink. **30** (2), 107 (1990).
- [54] L. Ren and J. S. Liberis, Physica B **183** (1–2), 40 (1993).
- [55] P. Serapinas, Accred. Qual. Assur. **3** (4), 145 (1993).
- [56] X. Y. Chen, P. M. Koenraad, F. N. Hooge, , J. H. Wolter, and V. Aninkevičius, Phys. Rev. B **55** (8), 5290 (1997).
- [57] B. Kaulakys and T. Meškauskas, Phys. Rev. E **58** (6), 7013 (1998).
- [58] J. Berntgen, K. Heime, W. Daumann, U. Auer, F.-J. Tegude, and A. Matulionis, IEEE Trans. Electron. Dev. **46** (1), 194 (1999).
- [59] A. Lisauskas, S. I. Khartsev, and A. M. Grishin, J. Low Temp. Phys. **117** (5–6), 1647 (1999).
- [60] B. Kaulakys, Phys. Lett. A **257** (1–2), 37 (1999).
- [61] B. Kaulakys and T. Meškauskas, Microelectron. Reliab. **40** (11), 1781 (2000).
- [62] B. Kaulakys, Microelectron. Reliab. **40** (11), 1787 (2000).
- [63] B. Kaulakys, Lith. J. Phys. **40** (1–3), 281 (2000).
- [64] H. L. Hartnagel, R. Katilius, and A. Matulionis, *Microwave Noise in Semiconductor Devices*, Wiley-Interscience, New York (2001).
- [65] K. Staliūnas, Intern. J. Bifurc. Chaos **11** (11), 2845 (2001).
- [66] K. Staliūnas, Advan. Compl. Syst. **6** (2), 251 (2003).
- [67] R. Katilius, Phys. Rev. B **69**, 245315 (2004).
- [68] J. Bernamont, Ann. Phys. **7**, 71 (1937).
- [69] M. Surdin, J. Phys. Radium **10** (7), 188 (1939).
- [70] F. K. Du Pré, Phys. Rev. **78** (5), 615 (1950).
- [71] A. Van Der Ziel, Physica **16** (4), 359 (1950).
- [72] A. L. McWhorter, in *Semiconductor Surface Physics*, edited by R. H. Kingston, Univ. Penn. Press, Philadelphia (1957), p. 207.

- [73] B. Kaulakys and T. Meškauskas, in *Proc. of the 14th Inter. Conf. on Noise in Physical Systems and 1/f Fluctuations, Leuven, Belgium, 14 - 18 July 1997*, edited by C. Claeys and E. Simoen, World Scientific, Singapore (1997), p. 126.
- [74] A. R. Butz, *J. Stat. Phys.* **4**, 199 (1972).
- [75] A. van der Ziel, *Adv. Electronics Electron Phys.* **49**, 225 (1979).
- [76] B. Pelligrini, R. Salleti, P. Terreni, and M. Prudenziati, *Phys. Rev. B* **27** (2), 1233 (1983).
- [77] M. A. Caloyannides, *J. Appl. Phys.* **45** (1), 307 (1974).
- [78] I. Flinn, *Nature* **219**, 1356 (1968).
- [79] Ю. И. Грибанов and В. П. Мальков, *Спектральный анализ случайных процессов*, Энергия, Москва (1979).
- [80] M. B. Priestley, *Spectral Analysis and Time Series (Probability and Mathematical Statistics)*, Academic Press (1981).
- [81] M. B. Priestley, *Spectral Estimation and Time Series*, Academic Press, San Diego (1989).
- [82] С. Л. Марпл-мл., *Цифровой спектральный анализ и его положение*, Мир, Москва (1990).
- [83] F. N. Hooge and P. A. Bobbert, *Physica B* **239** (3–4), 223 (1997).
- [84] C. M. Van Vliet, *Physica A* **303** (3–4), 421 (2002).
- [85] P. Lévy, *Calcul des Probabilités*, Gauthier-Villars, Paris (1925).
- [86] P. Lévy, *Théorie de l'Addition des Variables Aléatoires*, Gauthier-Villars, Paris (1954).
- [87] W. Feller, *An Introduction to Probability Theory and Its Applications, Volume 1*, Wiley (1968).
- [88] W. Feller, *An Introduction to Probability Theory and Its Applications, Volume 2*, Wiley (1971).
- [89] J.-P. Bouchaud and M. Potters, *Theory of Financial Risk: From Statistical Physics to Risk Management*, Cambridge University Press (2000).
- [90] H. Kantz and T. Schreiber, *Nonlinear Time Series Analysis*, Cambridge University Press (2003).
- [91] S. B. Lowen and M. C. Teich, *Phys. Rev. E* **47** (2), 992 (1993).
- [92] A. Papoulis, *Probability, Random Variables, and Stochastic Processes*, McGraw-Hill Companies, New York (1984).
- [93] D. R. Cox and P. A. W. Lewis, *The Statistical Analysis of Series of Events*, Chapman & Hall (1966).

- [94] T. Geisel, A. Zacherl, and G. Radons, *Phys. Rev. Lett.* **59** (22), 2503 (1987).
- [95] E. N. Lorentz, *J. Atm. Sci.* **20** (2), 130 (1963).
- [96] R. M. May, *Nature* **261**, 459 (1976).
- [97] P. Manneville and Y. Pomeau, *Phys. Lett. A* **75** (1–2), 1 (1979).
- [98] P. Manneville, *J. de Physique* **41** (11), 1235 (1980).
- [99] J. E. Hirsch, B. A. Huberman, and D. J. Scalapino, *Phys. Rev. A* **25** (1), 519 (1982).
- [100] F. Rödelsperger, A. Čenys, and H. Benner, *Phys. Rev. Lett.* **75** (13), 2594 (1995).
- [101] A. Čenys and H. Lustfeld, *J. Phys. A* **29** (1), 11 (1996).
- [102] A. Čenys, J. Ulbikas, A. N. Anagnostopoulos, and G. L. Bleris, *Intern. J. Bifurc. Chaos* **9** (2), 355 (1999).
- [103] M. J. Feigenbaum, *Physica D* **7** (1–3), 16 (1983).
- [104] I. Procaccia and H. Shuster, *Phys. Rev. A* **28** (2), 1210 (1983).
- [105] A. Ben-Mizrachi, I. Procaccia, N. Rosenberg, A. Schmidt, and H. G. Schuster, *Phys. Rev. A* **31** (3), 1830 (1985).
- [106] P. Bak, C. Tang, and K. Wiesenfeld, *Phys. Rev. Lett.* **59** (4), 381 (1987).
- [107] P. Bak, C. Tang, and K. Wiesenfeld, *Phys. Rev. A* **38** (1), 364 (1988).
- [108] S. Brown and G. Grüner, *Sci. Am.* **270** (4), 28 (1994).
- [109] R. E. Thorne, *Phys. Today* **49** (5), 42 (1996).
- [110] G. Grüner, *Rev. Mod. Phys.* **60** (4), 1129 (1988).
- [111] B. Drossel and F. Schwabl, *Phys. Rev. Lett.* **69** (11), 1629 (1992).
- [112] J. de Boer, B. Derrida, H. Flyvbjerg, A. D. Jackson, and T. Wettig, *Phys. Rev. Lett.* **73** (6), 906 (1994).
- [113] J. Davidsen and N. Lüthje, *Phys. Rev. E* **63**, 063101 (2001).
- [114] D. Dhar, *Physica A* **263** (1–4), 4 (1999).
- [115] K. P. O'Brien and M. B. Weissman, *Phys. Rev. A* **46** (8), R4475 (1992).
- [116] H. M. Jaeger, C. Liu, and S. R. Nagel, *Phys. Rev. Lett.* **62** (1), 40 (1989).
- [117] S. R. Nagel, *Rev. Mod. Phys.* **64** (1), 321 (1992).
- [118] H. J. Jensen, K. Christensen, and H. C. Fogedby, *Phys. Rev. B* **40** (10), 7425 (1989).

- [119] P. Helander, S. C. Chapman, R. O. Dendy, G. Rowlands, and N. W. Watkins, *Phys. Rev. E* **59** (6), 6356 (1999).
- [120] F. Dalton and D. Corcoran, *Phys. Rev. E* **63**, 061312 (2001).
- [121] B. H. Скоков and B. П. Коверда, *Писма а ЖТФ* **26** (20), 13 (2000).
- [122] D. Dhar, *Phys. Rev. Lett.* **64** (14), 1613 (1990).
- [123] G. Pruessner, *Phys. Rev. E* **67**, 030301 (2003).
- [124] C. B. Yang, *J. Phys. A* **37** (42), L523 (2004).
- [125] B. Gutenberg and C. F. Richter, *Seismicity of the Earth and Associated Phenomena*, Hafner Pub. Co., New York (1965).
- [126] R. Burridge and L. Knopoff, *Bull. Seism. Soc. Am.* **57**, 341 (1967).
- [127] B. G. Levi, *Phys. Today* **43** (11), 17 (1990).
- [128] J. M. Carlson and J. S. Langer, *Phys. Rev. A* **40** (11), 6470 (1989).
- [129] J. M. Carlson, *Rev. Mod. Phys.* **66** (2), 657 (1994).
- [130] E. Milotti, arXiv: physics/0204033 (2002).
- [131] H. Kanamori and E. E. Brodsky, *Phys. Today* **54** (6), 34 (2001).
- [132] L. Telesca, V. Cuomo, V. Lapenna, and M. Macchiato, *Fluct. Noise Lett.* **2** (4), L357 (2002).
- [133] J.-I. Yano, K. Fraedrich, and R. Blender, *J. Climate* **14** (17), 3608 (2001).
- [134] J.-I. Yano, R. Blender, C. Zhang, and K. Fraedrich, *J. R. Met. Soc.* **130** (600), 1697 (2004).
- [135] J.-I. Yano, M. W. Moncrieff, X. Wu, and M. Yamada, *J. Atm. Sci.* **58** (8), 850 (2001).
- [136] J.-I. Yano, M. W. Moncrieff, X. Wu, and M. Yamada, *J. Atm. Sci.* **58** (8), 868 (2001).
- [137] T. Musha and H. Higuchi, *Jap. J. Appl. Phys.* **15** (7), 1271 (1976).
- [138] H. Greenberg, *Operations Res.* **7**, 79 (1959).
- [139] M. Peyrard, *Phys. Rev. E* **64**, 011109 (2001).
- [140] G. Careri and G. Consolini, *Phys. Rev. E* **62** (3), 4454 (2000).
- [141] M. Takano, T. Takahashi, and K. Nagayama, *Phys. Rev. Lett.* **80** (25), 5691 (1998).
- [142] M. Kobayashi and T. Musha, *IEEE Transaction of Biomed. Engin.* **29**, 456 (1982).

- [143] C.-K. Peng, J. Mietus, J. M. Hausdorff, S. Havlin, H. E. Stanley, and A. L. Goldberger, *Phys. Rev. Lett.* **70** (9), 1343 (1993).
- [144] P. Ch. Ivanov, L. A. N. Amaral, A. L. Goldberger, S. Havlin, M. G. Rosenblum, H. E. Stanley, and Z. R. Struzik, *Chaos* **11** (3), 641 (2001).
- [145] M. C. Teich, *Proc. Int. Conf. IEEE Eng. Med. Biol. Soc.* **18**, 1128 (1996).
- [146] Y. Liu, P. Gopikrishnan, P. Cizeau, M. Meyer, C.-K. Peng, and H. E. Stanley, *Phys. Rev. E* **60** (2), 1390 (1999).
- [147] A. Erramilli, O. Narayan, and W. Willinger, *IEEE/ACM Transactions on Networking* **4** (2), 209 (1996).
- [148] A. J. Field, U. Harder, and P. G. Harrison, *IEE Proceedings-Communications* **151** (4), 355 (2004).
- [149] I Csabai, *J. Phys. A* **27** (12), L417 (1994).
- [150] T. Lukes, *Proc. Phys. Soc.* **78** (2), 153 (1961).
- [151] C. Heiden, *Phys. Rev.* **188** (1), 319 (1969).
- [152] K. L. Schick and A. A. Verveen, *Nature* **251**, 599 (1974).
- [153] F. Grüneis, *Physica A* **123** (1), 149 (1984).
- [154] T. Musha and K. Shimizu, *Jap. J. Appl. Phys.* **26** (12), 2022 (1987).
- [155] M. Y. Choi and H. Y. Lee, *Phys. Rev. E* **52** (6), 5979 (1995).
- [156] F. Grüneis, *Fluct. Noise Lett.* **1** (2), R119 (2001).
- [157] J. M. Halley and P. Inchausti, *Fluct. Noise Lett.* **4** (2), R1 (2004).
- [158] J. Timmer and M. Konig, *Astron. Astrophys.* **300**, 707 (1995).
- [159] P. Stoica and R. L. Moses, *Introduction to Spectral Analysis*, Prentice Hall (1997).
- [160] H. Risken, *The Fokker-Planck Equation: Methods of Solution and Applications*, Springer-Verlag (1989).
- [161] C. W. Gardiner, *Handbook of Stochastic Methods for Physics, Chemistry, and the Natural Sciences*, Springer-Verlag (1983).
- [162] C. Guidorzi, F. Frontera, E. Montanari, M. Feroci, L. Amati, E. Costa, and M. Orlandini, *Astron. Astrophys.* **416** (1), 297 (2004).
- [163] M. Agu, H. Akabane, and T. Saito, *J. Phys. Soc. Jap.* **70** (9), 2798 (2001).
- [164] M. Celasco and R. Eggenhöfner, *Eur. Phys. J. B* **23** (4), 415 (2001).
- [165] V. Gontis, B. Kaulakys, M. Alaburda, and J. Ruseckas, *Solid State Phen.* **97–98**, 65 (2004).

- [166] A. Coza and V. V. Morariu, *Physica A* **320**, 449 (2003).
- [167] D. Delignières, L. Lemoine, and K. Torre, *Human Mov. Sc.* **23** (2), 87 (2004).
- [168] P. Meakin, *Fractals, Scaling and Growth Far From Equilibrium*, Cambridge University Press (1998).
- [169] E. Bacry, J. Delour, and J. F. Muzy, *Phys. Rev. E* **64**, 026103 (2001).
- [170] D.R. Bickel, *Fractals* **11** (3), 245 (2003).
- [171] J. W. Lee, K. E. Lee, and P. A. Rikvold, arXiv: nlin/0412038 (2004).
- [172] U. Frisch, *Turbulence: The Legacy of A. N. Kolmogorov*, Cambridge University Press (1995).
- [173] J.-P. Bouchaud and M. Potters, *Theory of Financial Risk and Derivative Pricing*, Cambridge University Press (1999).
- [174] P. C. Ivanov, M. G. Rosenblum, L. A. N. Amaral, Z. R. Struzik, S. Havlin, A. L. Goldberger, and H. E. Stanley, *Nature* **399**, 461 (1999).
- [175] B. J. West, M. Latka, M. Glaubic-Latka, and D. Latka, *Physica A* **318**, 453 (2003).
- [176] W. Willinger, M. S. Taqqu, R. Sherman, and D. V. Wilson, *IEEE/ACM Trans. Networking* **5** (1), 71 (1997).
- [177] S. Cohen and M. S. Taqqu, *Methodol. Comput. Appl. Probabil.* **6** (4), 363 (2004).
- [178] L. A. N. Amaral, A. Díaz-Guilera, A. A. Moreira, A. L. Goldberger, and L. A. Lipsitz, *Proc. Natl. Acad. Sci. USA* **101** (44), 15551 (2004).
- [179] A.-H. Sato, H. Takayasu, and Y. Sawada, *Phys. Rev. E* **61** (2), 1081 (2000).
- [180] Z.-F. Huang and S. Solomon, *Physica A* **306**, 412 (2002).
- [181] B. B. Mandelbrot, *J. Business* **36**, 394 (1963).
- [182] I. McHardy and B. Czerny, *Nature* **325**, 696 (1987).
- [183] P. Bak, K. Christensen, L. Danon, and T. Scanlon, *Phys. Rev. Lett.* **88**, 178501 (2002).
- [184] L. Giraitis, P. Kokoszka, R. Leipus, and G. Teyssière, *Acta Applicandae Mathematicae* **78** (1–3), 285 (2003).
- [185] P. Gopikrishnan, M. Meyer, L. A.N. Amaral, and H. E. Stanley, *Eur. Phys. J. B* **3** (10), 139 (1998).
- [186] William J. Reed and Barry D. Hughes, *Phys. Rev. E* **66**, 067103 (2002).
- [187] N. Scafetta and B. J. West, *Phys. Rev. Lett.* **92**, 138501 (2004).

- [188] L. A. N. Amaral, D. J. B. Soares, L. R. da Silva, L. S. Lucena, M. Saito, H. Kumano, N. Aoyagi, and Y. Yamamoto, *Europhys. Lett.* **66** (3), 448 (2004).
- [189] A. Fujihara, T. Ohtsuki, and H. Yamamoto, *Phys. Rev. E* **70**, 031106 (2004).
- [190] F. N. Hooge, *IEEE Trans. Electron. Dev.* **41** (11), 1926 (1994).
- [191] F. N. Hooge, *Physica B* **311** (3–4), 238 (2002).
- [192] F. N. Hooge, *Physica B* **336** (3–4), 236 (2003).
- [193] J. Ruseckas, B. Kaulakys, and M. Alaburda, *Lith. J. Phys.* **43** (4), 223 (2003).
- [194] T. Meškauskas, R. Vaišnys, A. Matiukas, M. Tamošiūnaitė, I. Blužaitė, G. Urbonavičienė, and J. Blužas, *Lith. J. Cardiol.* **7**, 8 (2000).
- [195] M. Alaburda and B. Kaulakys, *Lith. J. Phys.* **43** (6), 415 (2003).
- [196] B. Kaulakys and J. Ruseckas, *Phys. Rev. E* **70**, 020101 (2004).
- [197] Л. Д. Ландау and Е. М. Лифшиц, *Механика*, Наука, Москва (1973).
- [198] H. Goldstein, *Classical Mechanics*, Addison-Wesley Longman, Incorporated (1950).
- [199] E. T. Whittaker, *A Treatise on the Analytical Dynamics of Particles and Rigid Bodies*, Cambridge University Press (1964).
- [200] A. J. Lichtenberg and M. A. Leiberman, *Regular and Stochastic Motion*, Springer-Verlag (1982).
- [201] B. V. Chirikov, *Phys. Rep.* **52** (5), 263 (1979).
- [202] J. M. Greene, *J. Math. Phys.* **20** (6), 1183 (1979).
- [203] H. G. Schuster, *Deterministic Chaos*, Physik-Verlag Weinheim (1984).
- [204] N. B. Delone, V. P. Krainov, and D. L. Shepelyansky, *Usp. Fiz. Nauk* **140**, 355 (1983).
- [205] P. M. Koch and K. A. H. van Leeuwen, *Phys. Rep.* **255** (5–6), 289 (1995).
- [206] V. Gontis and B. Kaulakys, *J. Phys. B* **20** (19), 5051 (1987).
- [207] B. Kaulakys, *J. Phys. B* **24** (3), 571 (1991).
- [208] B. Kaulakys, *J. Phys. B* **28** (23), 4963 (1995).
- [209] B. Kaulakys, D. Graužinis, and G. Vilutis, *Europhys. Lett.* **43** (2), 123 (1998).
- [210] B. Kaulakys and G. Vilutis, *Physica Scripta* **59** (4), 251 (1999).
- [211] M. Alaburda, V. Gontis, and B. Kaulakys, *Lith. J. Phys.* **40** (4), 242 (2000).
- [212] Л. Д. Ландау and Е. М. Лифшиц, *Теория поля*, Наука, Москва (1973).
- [213] Г. М. Заславский, *Стохастичность динамических систем*, Наука, Москва (1974).